

ABSTRACT

Title of dissertation: THE INTERPLAY OF SUBSTRATE, PROTEIN AND ITS COFACTOR IN CONTROLLING THE CATALYTIC PROPERTIES OF HUMAN IODOTYROSINE DEIODINASE

Jimin Hu, Doctor of Philosophy, 2014

Dissertation directed by: Professor Steven E. Rokita
Department of Chemistry and Biochemistry

Human iodotyrosine deiodinase (hIYD) belongs to nitro-FMN reductase superfamily and is responsible for recycling iodine from the I-Tyr (monoiodotyrosine) and I₂-Tyr (diiodotyrosine) formed as byproducts of thyroid hormone synthesis. Heterologous expression of hIYD lacking its membrane domain in *E. coli* provided large quantities of highly pure hIYD that allowed for its physical and biochemical studies. Its kinetic parameters, binding constants and crystal structure were characterized. Substrate was able to induced dramatic effects on FMN coordination in hIYD, including the zwitterionic region of I-Tyr interacts with the N3 and O4 of the FMN, the OH of Thr239 moved close to N⁵ of FMN (from 4.8 Å to 3.1Å) and allowed the formation of a hydrogen bond. The aromatic ring of I-Tyr additionally stacks above the FMN. Accumulation of the neutral semiquinone was observed during the reduction of hIYD in the presence

of substrate analogue 3-fluoro-L-tyrosine (F-Tyr). In the absence of ligand, only the oxidized and two-electron reduced forms of FMN were observed. Among all of the interactions to FMN in hIYD, H-bonding at the N5 FMN was identified as most important to control the redox of flavin. Mutagenesis of Thr239 to Ala removed this H-bonding as confirmed by the crystal structure of hIYDT239A•F-Tyr. As a result, no semiquinone was detected during the titration of hIYDT239A in the presence of F-Tyr. The deiodination activity of T239A was also dramatically decreased (10-fold).

The zwitterion region of the substrate was found critical for binding to enzyme. Modifications of the zwitterion region resulted in at least a 500-fold increase in K_D . The catalytic activity was unlikely determined by the zwitterion region since all of the modified substrates exhibited similar initial rates as the native substrate under conditions in which their concentration equaled their K_D . The pH dependence of hIYD binding indicated that the phenolic group of I₂-Tyr is also critical for binding and the hIYD prefers binding to the phenolate form of substrate. All the results presented in this thesis support the current proposed catalytic mechanism of IYD involving a stepwise electron transfer process.

THE INTERPLAY OF SUBSTRATE, PROTEIN AND ITS COFACTOR IN
CONTROLLING THE CATALYTIC PROPERTIES OF HUMAN
IODOTYROSINE DEIODINASE

By

Jimin Hu

Dissertation submitted to the Faculty of the Graduate School of the
University of Maryland, College Park, in partial fulfillment
of the requirements for the degree of
Doctor of Philosophy
2014

Advisory Committee:

Professor Douglas Julin, Chair
Professor Steven Rokita
Professor Caren Chang
Professor Paul Paukstelis
Professor Nicole LeRonde_LeBlanc

Copyright by

Jimin Hu

2014

Dedication

To my family for your endless support

Acknowledgements

I would like to express my appreciation to my advisor Professor Steve Rokita for his endless support and encouragement. You are the best mentor in my student life and I feel so lucky for doing my Ph.D studies under your supervision. After 5 years of studying in your lab, I have become a much better researcher.

I would like to express my sincerely gratitude to my committee members, Professor Douglas Julin, Paul Paukstelis, Nicole LeRonde_LeBlanc, Caren Chang for their advice and support for my research and dissertation. Professor Paul Paukstelis, also thank you for your valuable help with my independent proposal.

Thank you to Professor Jamie Schlessman and Dr. Watchalee Chuenchor for help with the crystallography study of my enzyme.

Thank you to all the past and present members of Rokita lab. You are so friendly and helpful since I join the lab. Thanks to Dr. Jen Buss, Dr. Kostyantyn Bobyk, Dr. Arnab Mukherjee and Dr. Fazel Fakhari for your advice and discussion about my research. Thanks to Dr. Michael McCrane, Dr. Yang Liu, Dr. Chengyun Huang, Petrina Boucher, Abhishek Phatarphekar, Shalini Saha, Blessing Deeyaa, Nattha Ingavat and Mark Hutchinson for being great labmates. Thank you all for your help in my research and practice talk. I wish everyone a great future ahead.

I would like to thank my parents. Thank you for your continuous support for all these years. I can hardly express how grateful I am to have you as my parents.

Finally, thank you to my husband and my daughters. Thank you for making my life happy and colorful. I love you all.

Table of Contents

Dedication	ii
Acknowledgements.....	iii
List of Tables	ix
List of Figures	x
Chapter 1: Introduction	1
1.1 The function of IYD.....	1
1.1.1 Iodine is an essential element required for thyroid hormones.	1
1.1.2 Iodine deficiency.....	1
1.1.3 Iodotyrosine deiodinase is critical for iodine recycling.....	2
1.1.4 Molecular level analysis on IYD deficiency.....	4
1.1.5 Screening for ITDD	5
1.1.6 Function of IYD beyond thyroid hormone synthesis.....	6
1.2 The flavoenzyme.....	6
1.2.1 IYD is an unusual flavoprotein	6
1.2.2 Flavoprotein in human	7
1.2.3 The redox states of flavoproteins	9
1.2.4 Redox control of Flavin	10
1.3 IYD represents a new subclass within the nitro-FMN reductase superfamily	13
1.3.1 IYD belongs to nitro-FMN reductase superfamily	13
1.3.2 Highly conserved key residues in IYD homologue	14
1.3.3 IYD and BluB represent a new subfamily	16
1.3.4 Proposed mechanism of deiodination by IYD.....	17
1.4 Specific aims.....	19
Chapter 2: General characterization of hIYD	20

2.1 Introduction.....	20
2.2 Experimental.....	23
2.2.1 Materials	23
2.2.2 General methods	23
2.2.3 Cloning, protein expression and purification.....	24
2.2.4 Circular Dichroism.....	26
2.2.5 Deiodinase activity.....	27
2.2.6 Fluorescence titration for measuring binding affinity	28
2.2.7 pH dependent assay.....	29
2.3 Results and Discussion	29
2.3.1 Expression and Purification	29
2.3.2 Circular dichroism spectroscopy analysis.....	31
2.3.3 Deiodination activity.....	33
2.3.4 Affinity of hIYD for 3-Halotyrosines	34
2.3.5 pH dependence of I ₂ -Tyr's binding with hIYD	35
2.3.6 pH dependence of I ₂ -Tyr deiodination by hIYD.....	38
2.4 Conclusion	39
Chapter 3: The influence of substrate binding on redox property and structure ..	40
3.1 Introduction.....	40
3.2 Materials and Methods.....	42
3.2.1 General methods and materials	42
3.2.2 Protein crystallization, structure determination and refinement.	43
3.2.3 Anaerobic Titration.....	44
3.3 Results and Discussion	46
3.3.1 Structural determination of hIYD	46
3.3.2 The effect of substrate binding on the reduction of hIYD.	50
3.3.3 The effect of substrate on the redox potential of FMN in hIYD	52
3.3.4 A comparison of the redox properties of hIYD with other flavoprotein	56
3.4 Conclusion	57

Chapter 4: The role of H-bonding to FMN N5 in hIYD for redox control and deiodination.....	59
4.1 Introduction.....	59
4.2 Materials and Methods.....	62
4.2.1 General methods	62
4.2.2 Site-directed Mutagenesis.....	62
4.2.3 Crystallization of hIYDT239A•F-Tyr.....	63
4.3 Results and Discussion	65
4.3.1 Influence of N5 H-bond on ligand binding property	65
4.3.2 Crystal structure determination of hIYDT239A•F-Tyr	66
4.3.3 Influence of mutation on redox property of FMN	69
4.3.4 Influence of an H-bond to FMN N5 on deiodination activity	76
4.4 Conclusion	77
 Chapter 5: Importance of the zwitterion region of I-Tyr for recognition and catalysis by hIYD.....	 78
5.1 Introduction.....	78
5.2 Materials and Methods.....	82
5.2.1 Materials	82
5.2.2 General methods	82
5.2.3 Kinetic characterization of hIYD with I-Tyr or I-Tyr analogs by HPLC	83
5.3 Results and Discussion	84
5.3.1 Importance of the zwitterion region of I-Tyr for its binding affinity to hIYD	84
5.3.2 Zwitterion requirement for IYD catalysis.....	88
5.3.3 Redox chemistry of IYD affected by the of H-bond interactions between the zwitterion region of substrates and N3 and O4 of FMN ring ...	98
5.4 Conclusion	101
 Chapter 6: Conclusion.....	 103

Appendices.....	107
References.....	115

List of Tables

Chapter 2

Table 2-1. Catalytic properties of iodotyrosine deiodinase homologs.	33
Table 2-2. hIYD affinity for halotyrosines.	35

Chapter 3

Table 3-1. Data collection and refinement statistics for hIYD.	44
---	----

Chapter 4

Table 4-1. The N5 H-bonding of FMN in nitro-FMN reductase superfamily.	61
Table 4-2. Data collection and refinement statistics for hIYDT239A.	64
Table 4-3. Characterization of mutants T239S and T239A.	65

Chapter 5

Table 5-1. The binding properties of substrate analogs to hIYD.	88
Table 5-2. Initial catalytic rates of hIYD with native and modified substrate. ...	97

List of Figures

Chapter 1

Figure 1-1. Thyroid hormones (T3 and T4) and the byproducts I-Tyr and I ₂ -Tyr during hormones synthesis.	2
Figure 1-2. Iodide metabolism process in thyroid follicular cells.	4
Figure 1-3. The catalytic reaction of IYD.	7
Figure 1-4. Structure of FMN.	8
Figure 1-5. The redox states of flavin.	10
Figure 1-6. The crystal structure of mIYD and mIYD•I-Tyr.	14
Figure 1-7. Multiple sequence alignment of the catalytic domains of IYD homologs.....	15
Figure 1-8. FMN coordination in mIYD, BluB and FRP.	17
Figure 1-9. The proposed one electron transfer mechanism of IYD.	18

Chapter 2

Figure 2-1. The active site of mIYD•I-Tyr.	22
Figure 2-2. hIYD consists of three domains.	30
Figure 2-3. SDS-PAGE characterization of expression and purification of hIYD from <i>E. coli</i>	31
Figure 2-4. Far-UV CD spectra of hIYD.	32
Figure 2-5. Visible CD spectra of hIYD.	32
Figure 2-6. The pH dependence of substrate binding to hIYD.	35
Figure 2-7. Stepwise one-electron transfer catalytic mechanism of IYD.	37
Figure 2-8. The pH dependence for deiodination of I ₂ -Tyr by hIYD.	38

Chapter 3

Figure 3-1. Interactions to the isoalloxazine ring of FMN in mIYD•I-Tyr.	40
Figure 3-2. Comparison between structures of hIYD and hIYD•I-Tyr.	47
Figure 3-3. The active site lid shields the substrate and FMN from solvent.	48
Figure 3-4. Details of the active site interactions around FMN.	49

Figure 3-5. Comparison between structures of hIYD and mIYD with bound I-Tyr.	50
Figure 3-6. Anaerobic reduction of hIYD by xanthine and xanthine oxidase as observed by UV/VIS.	51
Figure 3-7. Selected spectra for the reduction of hIYD flavin in the presence of AQDS by the xanthine/xanthine oxidase.	53
Figure 3-8. Selected spectra showing the reduction of hIYD in the presence of substrate analogue F-Tyr and NB by xanthine/xanthine oxidase.	54
Figure 3-9. Reduction of FMNsq to FMNhq in hIYD in the presence of F-Tyr and SFO by xanthine/xanthine oxidase.	55
Figure 3-10. Aromatic stacking between I-Tyr and FMN observed in structure of hIYD•I-Tyr.	57

Chapter 4

Figure 4-1. Substrate binding induces the movement of Thr239 toward N5 of FMN.	60
Figure 4-2. Structural comparison of hIYDT239A•F-Tyr and hIYD•I-Tyr.	67
Figure 4-3. FMN coordination in hIYDT239A•F-Tyr and hIYD•I-Tyr.	68
Figure 4-4. Reduction of FMN bound to hIYDT239S and the reference dye AQS by xanthine/xanthine oxidase.	70
Figure 4-5. Reduction of hIYDT239A and the reference dye AQS by xanthine/xanthine oxidase.	71
Figure 4-6. Reduction of hIYD, hIYDT239A and hIYDT239S in the presence of F-Tyr by xanthine/xanthine oxidase.	73
Figure 4-7. Reduction of hIYDT239A in the presence of F-Tyr and the dye SFO by xanthine/xanthine oxidase.	74
Figure 4-8. Reduction of hIYDT239S in the presence of F-Tyr and the dye PSF by xanthine/xanthine oxidase.	75

Chapter 5

Figure 5-1. Interactions between the zwitterion region of I-Tyr and FMN in hIYD.	81
Figure 5-2. Modifications on the zwitterion region of substrate I-Tyr and F-Tyr.	83
Figure 5-3. Equilibrium binding curves of hIYD with different ligands.	87
Figure 5-4. Analysis of hIYD's activity with I-tyrosinamide by HPLC.	89

Figure 5-5. Mass spectra of the product of I-tyrosinamide catalyzed by hIYD...	91
Figure 5-6. Analysis of hIYD's activity with I-tyramine by HPLC.	92
Figure 5-7. Mass spectra of the product of I-tyramine catalyzed by hIYD.	93
Figure 5-8. Analysis of hIYD's activity with I-HPPA by HPLC.	94
Figure 5-9. Mass spectra of the product of I-HPPA catalyzed by hIYD.	95
Figure 5-10. Michaelis-Menten curve of I-Tyr deiodination by hIYD.	97
Figure 5-11. Anaerobic reduction of hIYD in the presence of I-tyrosinamide by xanthine/xanthine oxidase.	98
Figure 5-12. Selected spectra for the reduction of hIYD in the presence of I-tyrosinamide by xanthine/xanthine oxidase.	98
Figure 5-13. Reduction of hIYD in the presence of 1mM I-tyramine by xanthine/xanthine oxidase.	100
Figure 5-14. Redox titration of hIYD in the presence of 1mM I-HPPA by xanthine/xanthine oxidase.	101

List of Abbreviations

AQS	anthraquinone-2-sulfonate
AQDS	anthraquinone-2,6-disulfonate
Br-Tyr	3-monobromotyrosine
CD	circular dichroism
Cl-Tyr	3-monochlorotyrosine
CV	column volume
E_m	midpoint redox potential
FAD	flavin adenine dinucleotide
FMN	flavin mononucleotide
FMN_{ox}	flavin mononucleotide oxidized species
FMN_{sq}	flavin mononucleotide semiquinone species
FMN_{hq}	flavin mononucleotide hydroquinone species
FRP	flavin reductase P
F-Tyr	3-monofluorotyrosine
F-HPPA	4-hydroxy-3-fluorophenyl propionic acid
F-tyramine	3-fluorotyramine
F-tyrosinamide	3-fluorotyrosinamide

HEK293	human embryonic kidney293
IDD	iodine deficiency disorders
I-HPPA	4-hydroxy-3-iodophenyl propionic acid
IQ	intelligence quotient
ITDD	iodotyrosine deiodinase deficiency
I-Tyr	3-monoiodotyrosine
I ₂ -Tyr	3,5-diiiodotyrosine
I-tyrosinamide	3-iodotyrosinamide
I-tyramine	3-iodotyramine
IYD	iodotyrosine deiodinase
k _{cat}	catalytic constant
K _D	dissociation constant
K _m	Michaelis constant
Me-Tyr	3-methyltyrosine
NADH	nicotinamide adenine dinucleotide
NADPH	nicotinamide adenine dinucleotide phosphate
NB	nile blue
NOX	NADH oxidase
NTR	nitroreductase

P2O	pyranose-2-oxidase
PSF	phenosafranine
RF	response factor
RMSD	root-mean-square deviation
SFO	safranin O
UV/VIS	ultraviolet-visible spectroscopy
V_m	maximum reaction velocity

Chapter 1: Introduction

1.1 The function of IYD

1.1.1 Iodine is an essential element required for thyroid hormones.

The thyroid hormones, triiodothyronine (T_3) and thyroxine (T_4) made by the thyroid gland are important for regulation of the body, including the rate of our metabolism, the speed of our heartbeat, our body temperature, muscle strength and the rate of replacing dying cells (1, 2). Iodine is an essential element required for the synthesis of T_3 and T_4 (Figure 1-1). Iodine is relative scarce in the topsoil of the earth. Most iodine (as iodide) is stored in ocean. Iodine from the seawater evaporates into the atmosphere and returns to the soil and groundwater by rain. The cycle of iodine in inland regions and mountainous areas is slow and incomplete. Population depending on food from these areas have insufficient iodine intake. Around 2 billion individuals live in iodine deficient areas, such as south Asia and sub-Saharan Africa (3).

1.1.2 Iodine deficiency

Iodine deficiency has multiple adverse effects on growth and development in human termed iodine deficiency disorders (IDD). Goiter and hypothyroidism can occur of all ages and are the classic of iodine deficiency. Severe iodine deficiency during pregnancy causes serious damage to the fetus and may result in abortion, mental retardation, stillbirths and congenital abnormalities (3). For child

and adolescent, IDD is reported as impaired mental function and delayed physical development. The intelligence quotient (IQ) of children suffering severe iodine deficiency was reported to be 12 points on average lower than children from iodine-sufficient areas (4-6). Moderate iodine deficiency in adults may lead to reduce work productivity resulting in impaired social and economic development (6). The prevalence of severe iodine deficiency was reduced during the past 25 years by introducing iodized salt. Thirty countries remain iodine-deficient (9 are moderately and 21 are mildly) until 2013 (7).

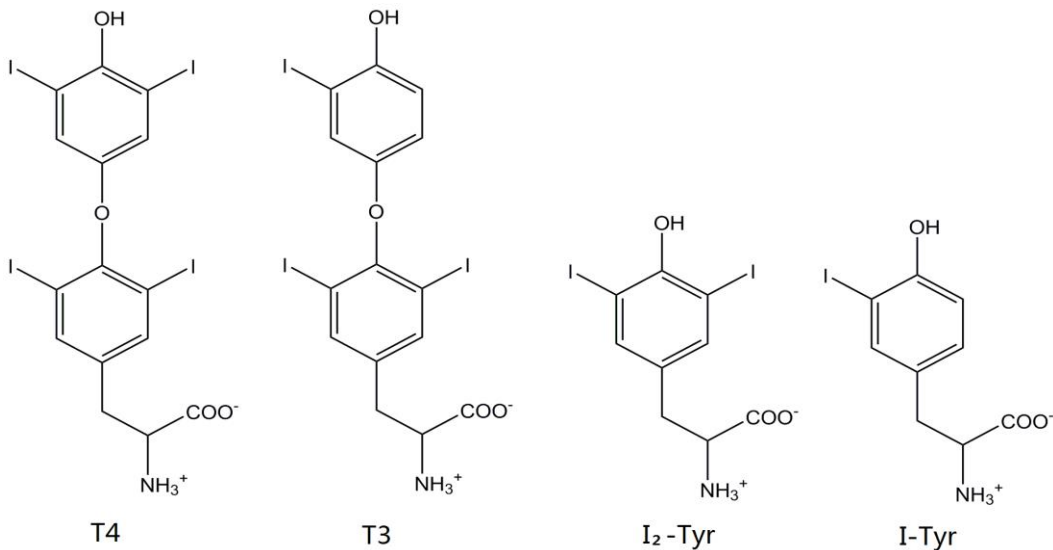


Figure 1-1. Thyroid hormones (T3 and T4) and the byproducts monoiodotyrosine (I-Tyr) and diiodotyrosine (I₂-Tyr) during hormones synthesis.

1.1.3 Iodotyrosine deiodinase is critical for iodine recycling

Adequate production of thyroid hormones is not only depended on the daily ingestion of iodine, it also requires the efficient recycling of iodine from I-Tyr and I₂-Tyr produced during thyroid hormones synthesis. Iodide is transported into the thyroid follicular cell by the Na⁺/I⁻ symporter (Figure 1-2) (8). Iodide is

then oxidized and coupled to tyrosyl residues of thyroglobulin in colloid by thyroid peroxidase. The resulting mono- and diiodinated tyrosyl residues of thyroglobulin undergo further coupling to form T_3 , T_4 and forming byproducts I-Tyr and I_2 -Tyr (9). Approximately seven I-Tyr and six I_2 -Tyr are formed for every T_4 synthesis (10). Release of T_3/T_4 into the plasma is under the regulation of thyroid-stimulating hormone. T_3 is 10-fold more active than T_4 in regulating metabolism (11). A thioredoxin superfamily protein-iodothyronine deiodinase is responsible for converting T_4 to T_3 , which also contributes to iodide recycling. However, the primary mechanism for iodide recycling is salvaging the iodide from the excess I-Tyr and I_2 -Tyr catalyzed by iodotyrosine deiodinase (IYD). Failure of IYD's activity termed as iodotyrosine deiodinase deficiency (ITDD) causes excess I-Tyr and I_2 -Tyr to be released into the bloodstream that finally leads to severe loss of iodide. The first type of ITDD was recognized in 1953, when patients shown spontaneous release of iodotyrosines from the gland after uptake ¹³¹Iodide (12, 13). Stanbury et al later detected an abnormal increase of iodotyrosines from patient with congenital goiter and hypothyroidism in 1955 (14). Until 2014, ITDD has been identified in more than 25 family pedigrees with various conditions range from simple goiter to severe hypothyroidism with mental retardation and strongly suggested as a recessive inheritance disease (15).

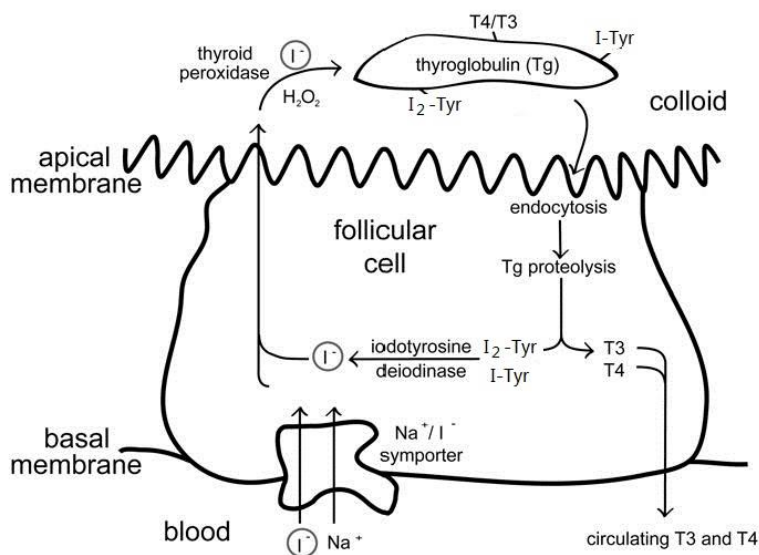


Figure 1-2. Iodide metabolism process in thyroid follicular cells (9).

1.1.4 Molecular level analysis on IYD deficiency

In 2002, serial analysis of gene expression to human thyroid tissue identified the hIYD gene *DEHAL1*, which is organized in six exons spanning over 35 kb on human chromosome 6p24, up-regulated by TSH-stimulated cAMP and down-regulated by iodide (16, 17). Alternative splicing of exon 5 results in several isoforms of *DEHAL1*, the most abundant isoform in thyroid is isoform A encoding active IYD. Isoforms B and C from the inclusion of exon 5 and a 3'-extension of exon 5 were inactive (18). The N-terminal domains of the three isoforms are similar. However, the C-terminal domain, which is critical for the deiodination activity, is different. Most hIYD is present in the thyroid. Other organs, liver, kidney and trachea also have low levels of hIYD (9, 17).

Identification of *DEHAL1* leads to the evolution of ITDD screening to molecular level. hIYD mutations were reported in 2008 in patients with severe

goitrous hypothyroidism and abnormal I₂-Tyr level from unrelated families living in different countries (19). These mutations include mutants R101W and I116T and a deletion of three residues F105-I106L. An additional mutant A220T was also reported in two consanguineous families from Morocco with severe hypothyroidism and goiter (20). Further analysis on these patients indicates that the severity of ITDD also depend on environmental factors (iodine intake).

1.1.5 Screening for ITDD

The prevalence of ITDD may be more common than thought since patients harboring IYD defects may be undetected by current screening programs for congenital hypothyroidism due to the lack of biochemical expression of the disease at the early age of life. Delayed diagnosis of ITDD may lead to severe mental retardation later in life. Using I-Tyr/I₂-Tyr as biomarkers gives the potential to improve the pre-clinical detection of IYDD during the neonatal time. Radio-immunoassay was shown capable to determine I₂-Tyr in serum and urine (19). A new generation of sensitive antibodies against IYD and a defined population-based reference may be required for development of this method for ITDD detection. Another useful technique, HPLC-MS, accurately distinguished normal from elevated I-Tyr/I₂-Tyr serum/urine levels although this technique is highly cost and poor in clinical settings (20, 21).

1.1.6 Function of IYD beyond thyroid hormone synthesis

IYD appears in a wide range of organism, including honeybee, lancelet, daphnia, zebrafish, sea anemone and bacteria, and all behave as reductive deiodinases for I₂-Tyr (22). The function of iodide derivatives in lower organisms is still unknown. The physiological role of IYD in diverse organisms not associated with iodide digestion may imply a function of IYD beyond iodide recycling for hormones synthesis. A recent investigation on the expression pattern of IYD during chick ontogeny indicates that IYD present in different components of the chick embryo, suggesting IYD might be involved in regulating cell specific deiodination of I-Tyr and I₂-Tyr prior to the formation of functional thyroid (23). The *Caenorhabditis elegans* IYD ortholog was suggested important for the metabolic state of muscle cells by using NADH as a coenzyme to activate the K⁺ channel associated with muscle membranes (24).

1.2 The flavoenzyme

1.2.1 IYD is an unusual flavoprotein

In 1969, Rosenberg and Ahn investigated the effects of flavins (FAD, FMN and riboflavin) on the I₂-Tyr deiodination activity of IYD and found that IYD's activity is largely depended on flavin, suggesting IYD as a flavoprotein (25) (Figure 1-3). 10 years later, IYD from bovine thyroid was partially purified and flavin mononucleotide (FMN) as its cofactor was identified (Figure 1-3) (26, 27). Flavoproteins serve a wide range of biological and chemical process, including

electron transfer, bioluminescence, reduction and oxidation, halogenation, photosynthesis and more (28, 29). However, dehalogenation has only been reported in few flavoprotein. Anaerobic organisms commonly adopt reductive dehalogenation. Based on our current knowledge, only two other enzymes, iodothyronine deiodinases D1 and tetrachlorohydroquinone dehalogenase were suggested catalyzing reductive dehalogenation (9). A flavoprotein performing reductive dehalogenation under aerobic conditions is very unusual.

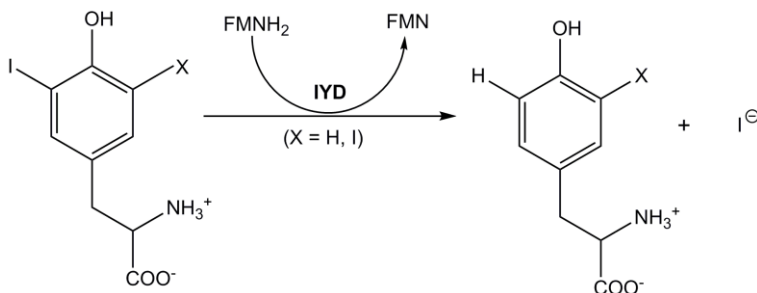


Figure 1-3. The catalytic reaction of IYD.

1.2.2 Flavoprotein in human

According to a recent analysis, 90 genes within the human genome encode flavin-dependent proteins using either FMN (12) or flavin adenine dinucleotide FAD (64) or both (5) (30). 90 % of the human flavoproteins non-covalently bind to FMN or FAD. Others may covalently bind between the 8- α -methyl of flavin and His or Cys residue of protein. More than half of the human flavoproteins structures have been solved. The structures of many membrane-associated human flavoproteins are still unavailable. The majority of human flavoenzymes involved in cofactor biogenesis and metabolism, including folate and cobalamin metabolism, biosynthesis of heme, pyridoxal 5'-phosphate, Coenzyme A,

Coenzyme Q, steroid, thyroxine and iodine salvage. Flavoproteins also partner with other flavoproteins. For example, two FAD-dependent proteins, ACAD9 and FOXRED1 have been shown to be critical for the assembly and activity of complex I responsible for human respiratory electron transport (31). Flavoenzymes are also closely associated with certain human diseases. According to the records in OMIM, around 60 % of human flavin-dependent proteins have been reported associated with human disorders, including dysfunctions in mitochondrial processes and abnormal metabolic pathways (30). Considering the important roles of flavoproteins in human, determination of their structures as well as fully characterization of their catalytic mechanisms is certainly encouraged.

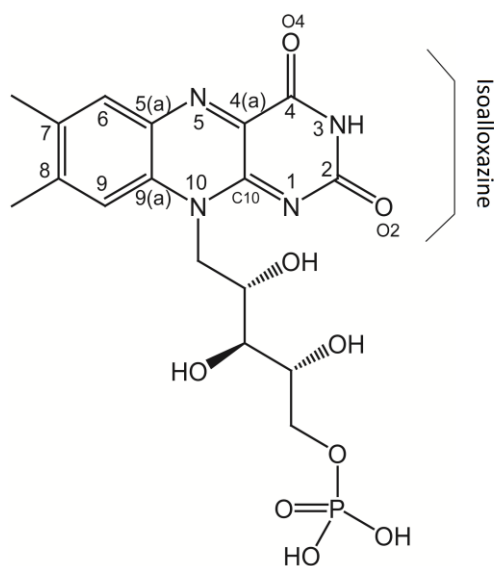


Figure 1-4. Structure of FMN. Atoms in the isoalloxazine ring are labeled.

1.2.3 The redox states of flavoproteins

The biochemical function of flavoprotein is largely depended on its FMN or FAD. By adding hydrogen atoms to the nitrogen atoms on the isoalloxazine ring (Figure 1-4), oxidized FMN or FAD can be reduced to its one-electron-reduced state (semiquinone) or fully reduced state (hydroquinone) via one-electron reduction or two-electron reduction (Figure 1-5) (29, 32). They can easily be distinguished by optical spectroscopy. The oxidized flavin is yellow and exhibits a maximum absorbance around 450 nm. The pKa of N1 and N3 of oxidized isoalloxazine ring are 0 and 10, respectively (28). Once reduced to the semiquinone form, the protonating/deprotonating at the N5 atom result in two different semiquinone forms due to the pKa at N5 is ~ 8.3 (33). The protonated neutral semiquinone is blue and has an absorbance around 590 nm. In contrast, the deprotonated anionic semiquinone is red and show maximum absorbance around 390-410 nm and 480 nm. The fully reduced hydroquinone form is colorless and can also exist in neutral or anionic forms under physiological conditions since the pKa of N1 is ~6.6 (34).

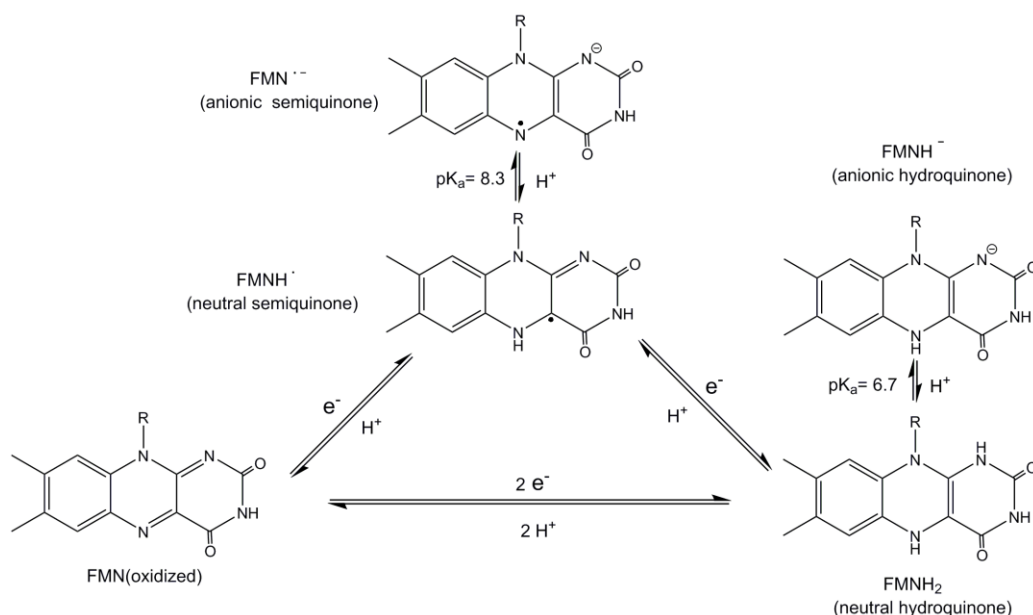


Figure 1-5. The redox states of flavin.

1.2.4 Redox control of Flavin

In flavoproteins, an input signal will cause the redox change of flavin followed by a new functional output of the flavoprotein. Substrate binding, electron transfer or light-mediated reductions represent the primary input signal. In the active site of flavoproteins, the redox control can be realized by H-bonding to N5 atoms, H-bonding between protein and N1, N3, O2, and O4 of flavin, aromatic stacking, bending of the isoalloxazine ring along N5-N10 axis and conformational changes of ribityl chain of flavin as discussed below.

1.2.4.1 Redox dependent change in the bending angle of isoalloxazine ring

According to a recent analysis on the crystal structure in PDB (34), for oxidized flavins in protein, their isoalloxazine rings mainly adopt planar

conformation. However, fully reduced flavins in proteins are likely bend along the N5-N10 axis by range from 0° to 34° (34). For most flavoproteins, the bending angles are less than 10° . Thioredoxin reductase was observed with the largest bending angle of 34° (35). The conformational change of isoalloxazine ring may cause by crystal packing instead of redox state change because all the structure was in crystal form. Quantum chemical analysis provides support to the observation that bending of isoalloxazine ring is redox depended (36). However, the conformation change of FMN may largely affected by the interactions of neighboring groups since NMR analysis suggested that the fully reduced flavin is intrinsically planar in water (36). Moreover, some oxidized flavoprotein, such as monoamine oxidases, polyamine oxidase and cholesterol oxidase, are also reported with bent isoalloxazine ring (34). In some flavoprotein, altering the direction of bond connecting the N10 atom and the ribityl chain will result in an accumulation of mechanical tension (37). To release the tension, the ribityl chain will adopt a conformational change, causing the rearrangement of the hydrogen bonding between its three hydroxyl groups and protein.

1.2.4.2 H-bonding with the N5 atom

The redox control of flavin frequently involves the N5 position since this atom can behave as hydrogen bond donor or acceptor based on its redox state. As a redox control, N5 atom could behave in three different types. In first type, a H-bond forms between the oxidized flavin N5 atom and protein. Reducing the flavin results in breaking of this H-bond and induces further conformational changes on

protein. For example, breaking of the H-bond between Lys53 and N5 of FAD in bacterial ferredoxin reductase was observed under reduced condition and was suggested necessary for forming high binding affinity with its partner protein (34, 38). The second type of N5 redox control was found in flavodoxin. There is no H-bond for its oxidized state, however, reduction of flavin in flavodoxin induces the flip of a peptide bond and enables the H-bonding between the protonated N5 and the carbonyl oxygen of the flipped peptide (39). The third type includes the rearrangement of H-bond network at N5 and O4 atoms upon light activation, which is critical for catalysis.

1.2.4.3 Aromatic stacking

Aromatic stacking between the isoalloxazine ring of FMN and aromatic residues of the proteins is also important for the redox control of flavoprotein. In the flavodoxin, the isoalloxazine ring of FMN is flanked by at least one aromatic amino acid residue, such as Tyr 98 of the *Desulfovibrio vulgaris flavodoxin* (40). Elimination of the π - π stacking by mutation of Tyr 98 to Ala produces substantially shift on the one-electron reduction potentials, particularly for the FMN_{sq/hq} couple. Similarly, Trp1046 in cytochrome P450 reductase BM3 stacks over the isoalloxazine ring and an equivalent Trp is conserved across the P450 superfamily (41). In wild type, a stable blue semiquinone species was observed during reductive titration. However, no semiquinone species was detected during the titration of W1046H and W1046A mutant (42). Redox potential analysis also indicated significant elevation on the redox potential of FMN_{sq/hq} couple.

As a flavoprotein, the electron transfer process as well as the redox property of flavin in IYD is still not clear. Recent progress on IYD as described below improved the understanding on the coordination of FMN and provided a structural base for understanding the redox property as well as the redox control of FMN in IYD.

1.3 IYD represents a new subclass within the nitro-FMN reductase superfamily

1.3.1 IYD belongs to nitro-FMN reductase superfamily

Sequence analysis of mIYD indicates that IYD consists of three domains, N-terminal membrane domain (residues 1-24), intermediate domain (residues 25-85) and C-terminal catalytic domain (residues 86-289) that belongs to the nitro-FMN reductase superfamily (43). The N-terminal domain was a trans-membrane anchor. The structure and function of the intermediate domain is still unknown. Deletion of the first 33 amino acid of mouse IYD and expressing the remaining gene in Sf9 cells result in pure soluble mIYD (44). The truncated mouse IYD retains the deiodination activity with dithionite as reducing reagent. Crystal structures of this truncated mIYD with or without substrate I-Tyr were solved (44). This protein contains a α - β fold structure typical to nitro-FMN reductase superfamily. Two FMN bind the interface of the two swap monomers (Figure 1-6). Interestingly, substrate binding induces the formation of a helix-turn-helix active site lid that covers the FMN and I-Tyr binding site and sequesters the active site from solvent (Figure 1-6). The aromatic ring of substrate I-Tyr stacks on the

isoalloxazine ring of FMN. The zwitterion region of I-Tyr form H-bonds to the N3 and O4 atom of FMN. In the presence of I-Tyr, the OH group of Thr235 in mouse IYD moves close to the FMN and form H-bond to the N5 atom of FMN (Figure 1-8). The rearrangement of H-bond network of FMN induced by substrate binding may significantly influence the redox property of FMN in IYD.

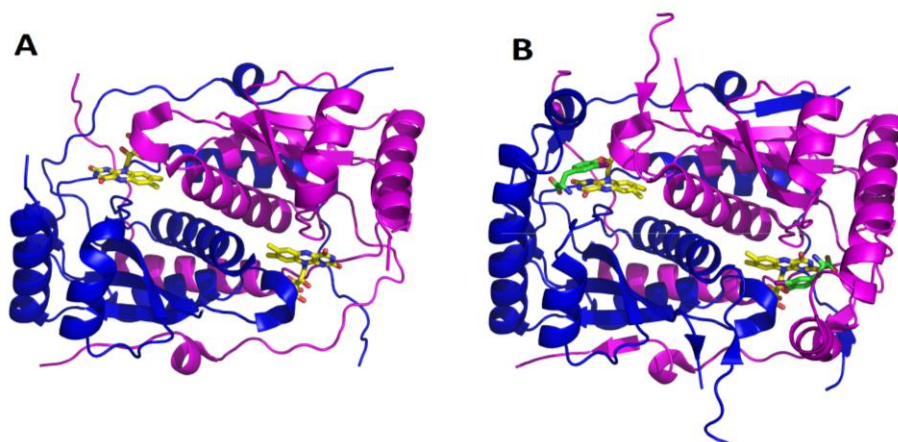


Figure 1-6. The crystal structure of mIYD (A) and mIYD•I-Tyr (B). Two monomers are shown in magenta and blue. Substrate I-Tyr is shown as green stick. FMN is shown in yellow (44).

1.3.2 Highly conserved key residues in IYD homologue

Successfully expression of the truncated soluble IYD accelerates the study of IYD homologous. The IYD homologous from a variety of organism were purified and exhibited comparable deiodination activity (within a single order of magnitude) with mouse IYD (45). The key residues involved in the substrate binding are highly conserved (Figure 1-7), including E153, Y157 and K178, which directly interact with the zwitterion region of I-Tyr, and A126, which provides interaction to the OH group of I-Tyr (46). Residues responsible for the

FMN coordination in IYD are found also highly conserved, such as Thr235 that forms interaction with N5 of FMN and Arg 96, Arg 97, Arg 100 and Arg 275 that form interaction with the O₂ and ribityl chain of FMN. Slightly variation between Ser and Thr was found on Ser98, which also involves in ribityl chain interactions (45). This finding suggests those key residues may be important for the deiodination of IYD.

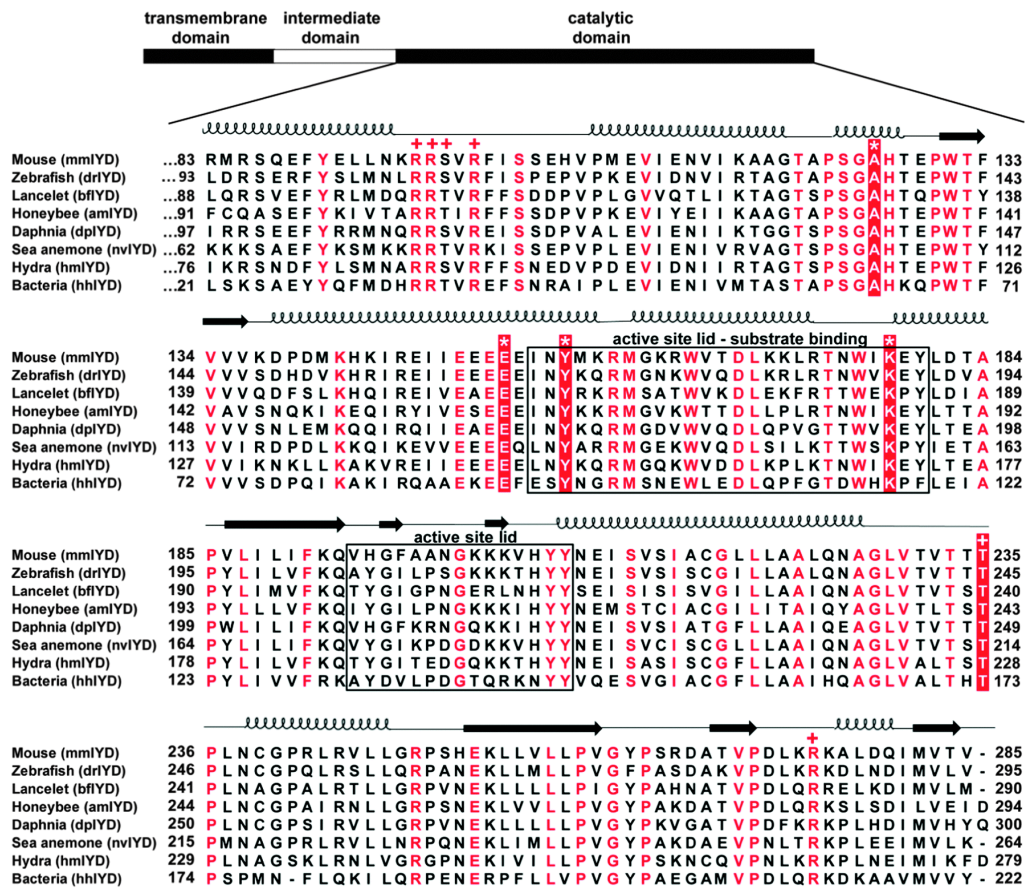


Figure 1-7. Multiple sequence alignment of the catalytic domains of IYD homologs. Residues in red (or white) are fully conserved. Key residues coordinating to substrate and FMN are indicated with an (*) and (+), respectively. Sequences forming the active site lids are indicated with a box (45).

1.3.3 IYD and BluB represent a new subfamily

Within nitro-FMN reductase superfamily, IYD share the most structural similarity with a bacterial flavin destructase (BluB, an enzyme using FMN as substrate for vitamin B₁₂ synthesis) despite only 19 % sequence identity (44, 47). The positions of their active site lid sequence for IYD and BluB are very distinct with the other two subfamilies representatives NADH oxidase (NOX) from *Thermus thermophiles* and flavin reductase P (FRP) from *Vibrio harveyi* (48, 49). For IYD and BluB, a region close to the N-terminal forms the active site lid. In contrast, the lid for NOX is positioned within the central region of whole polypeptide and the lid for FRP is from the C-terminal extension region. This difference led to the proposal that IYD and BluB may represent a new subfamily of nitro-FMN reductase superfamily (44). The flavin coordination in IYD and BluB are also very different with NOX and FRP (Figure 1-8). There are fewer interactions between the pyrimidine ring of FMN and active site residues in BluB and IYD (44). H-bond to the N5 atom of FMN in IYD and BluB is derived from the side chain hydroxyl group of Thr235 and Ser167, respectively, however, the H-bond to N5 position for other superfamily members are commonly from the backbone or side chain N-H bonds. As described above, the H-bond network of flavin is very important for the redox control as well as the reduction process. Thus, the similar H-bond network of isoalloxazine of flavin in IYD and BluB may imply that IYD and BluB have the similar redox process.

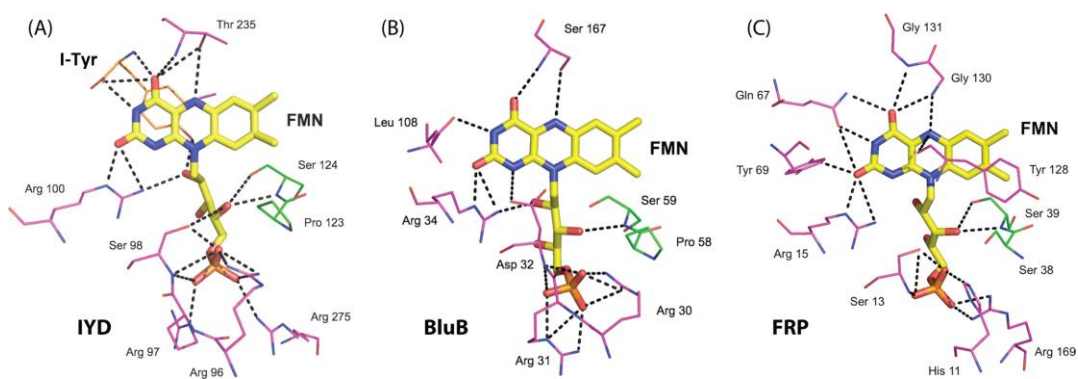


Figure 1-8. FMN coordination in mIYD, BluB and FRP (44).

1.3.4 Proposed mechanism of deiodination by IYD

The electron transfer of FMN in IYD may proceed through two single-electron transfer processes with stabilization of the flavin semiquinone or via a single two-electron transfer process. The nitroreductase described in nitro-FMN reductase superfamily are O_2 insensitive and unable to promote single electron transfer to reduce O_2 (50). In general, they perform two-electron transfer from NAD(P)H to the nitro group of nitroaromatic compounds using ping-pong, bi-bi kinetic mechanism, and the FMN cycles between oxidized and reduced form by two-electron reduction (50). As a member of this superfamily, it was suggested that IYD's mechanism might involve a two-electron transfer process. Especially, the catalytic mechanism of two other reductive dehalogenase-tetrachlorohydroquinone dehalogenase and ID involves a substrate tautomerization, keto intermediates formation and subsequent nucleophilic reaction by the said chain of Cys or Ser (51, 52). Based on analysis of the mechanism of those reductive dehalogenase, the early two-electron transfer mechanism for IYD was proposed (53). In this proposal, a sulfenyl iodide will be

generated after active site Cys reacts with the tautomeric keto substrate, followed by further reducing by flavin and iodide releasing. However, later site-direct mutagenesis and structural analysis indicated that Cys residues in IYD are not involved in IYD catalysis (54). Moreover, no other amino acids in the active site is appropriate for a nucleophilic reaction such as that supported by Cys (46). Therefore, the two-electron transfer deiodination proposal for IYD is not supported by current evidence.

In contrast, the neutral flavin semiquinone radical was detected during the oxidation of reduced FMN within IYD, although its lifetime of this semiquinone (days) is not consistent with the enzyme reaction (44). Observation of semiquinone may imply a stepwise single-electron transfer process of FMN in IYD. Moreover, BluB, exhibiting the most similarity in FMN coordination with IYD in nitro-FMN reductase superfamily, promotes one electron transfer process involving O₂-dependent degradation of its bound FMN (47). The current proposal for IYD's mechanism involving a stepwise single electron reduction may or may not involve the substrate tautomerization as illustrated in Figure 1-9 (9). Fully understanding the catalytic mechanism of hIYD waits more direct evidence.

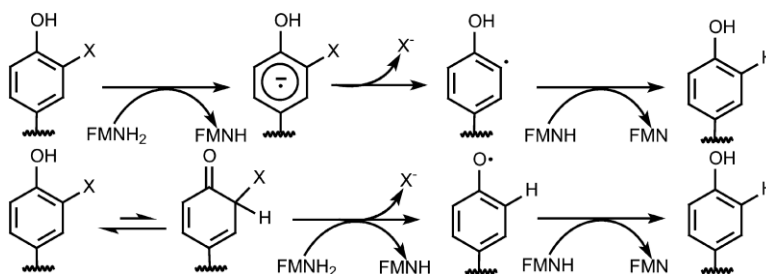


Figure 1-9. The proposed one electron transfer mechanism of IYD (9).

1.4 Specific aims

IYD from human remains poorly characterized. Over the past decade, significant progress have been made on IYD from other organisms providing a platform for understanding the redox property as well as deiodination mechanism of IYD. The goal of my research was to investigate the catalytic process using IYD from human as the model. This dissertation describes the following:

- 1) Obtaining highly pure hIYD in large scale by convenient *E.coli* expression for biochemical and biophysical characterization,
- 2) Elucidating the possible ionization of residues critical for catalysis and binding by pH dependent studies,
- 3) Demonstrating the influence of substrate binding to the structure and redox properties of IYD by X-ray crystallography and redox titration,
- 4) Investigating the role of H-bonding between OH group of Thr239 and N5 of FMN in control of FMN redox and deiodination in hIYD by generating T239A and T239S mutants and characterizing their structural, redox and kinetic properties,
- 5) Illustrating the importance of the zwitterion region of substrate for its binding, catalysis and redox control of hIYD by measuring the K_D and activity of hIYD with modified substrate analogues.

Chapter 2: General characterization of hIYD

2.1 Introduction

hIYD is still poorly characterized although cDNA that encodes human IYD had been discovered 10 years ago (16). Previous investigation on hIYD had been limited to its expression in human embryonic kidney (HEK) 293 cells in 2004 (17). The fraction of expression identified with hIYD by western blot analysis was used for initial biochemical characterization (17). The hIYD fraction was shown to require NADPH for deiodination (17). The V_m of deiodination with I-Tyr was found 6 times higher than I₂-Tyr (0.53 nmol/100 µg/10 min). The K_m of I₂-Tyr was reported as 2.67 µM, which is around two-fold larger than that of I-Tyr (1.35 µM) (17). No further kinetic or structure characterization on hIYD has been reported after 2004. Considering the importance of hIYD for iodide recycling, investigation the hIYD is advantageous for understanding of hIYD related disease.

Sequence analysis allow the identification of the N-terminal trans-membrane anchor of IYD (43). Truncation of the N-terminal domain of the gene from mouse provided a soluble enzyme when expressed in sf9 and *P.pastoris* (44, 54). The ability for NADPH to drive catalysis is lost once IYD is removed from its native membrane and consequently dithionite is used as reducing reagent for most studies in vitro (54). This truncated IYD exhibited similar rate constants to that of the wild-type enzyme with dithionite (54).

Recently, pure soluble IYD from 7 different organisms has been

successfully obtained after fusion to a SUMO tag and expression in *E.coli* (45, 46). Sumo is an 11 kDa ubiquitin-like protein (55). Fusion of protein to sumo can largely improve the solubility of the recombinant protein (56-58). Cleavage of sumo tag depends on the recognition of the tertiary structure by sumo protein protease Ulp1 (59). The digestion is very specific, resulting in production of the target protein with no extra residues. Successful expression of IYDs from other organisms by using sumo fusion tag and bacterial expression system provided a great platform for obtaining a large amount of pure protein for further study on IYD from human.

Success in heterologous expression allows many experiments on the catalytic properties of mIYD. The binding property and reactivity of mIYD with several substrate analogs such as, 3-monobromotyrosine (Br-Tyr), 3-monochlorotyrosine (Cl-Tyr), 3-monofluorotyrosine (F-Tyr), Tyr and 3-methyltyrosine (Me-Tyr) were investigated to understand the role of the 3-position substituent in substrate specificity (44). Interestingly, the mIYD was also found to promote dehalogenation of Br-Tyr and Cl-Tyr. However, no turnover was observed with F-Tyr. The K_D for Br-Tyr and Cl-Tyr are almost equivalent to I-Tyr, demonstrating very tight binding to IYD. The K_D for F-Tyr is slightly higher (10 fold) than I-Tyr, but still in μM range. The decreased binding affinity for F-Tyr seems not correlated with fluorine's decreased sterics since Me-Tyr, which is larger than fluoro substituent, exhibited very poor affinity (K_D is over 1.5 mM). Similar to Me-Tyr, Tyr also shows poor affinity (60). The phenolic pKa of Me-Tyr and Tyr are ~ 10 , which is 2 units higher than other halo-tyrosine

derivatives with $pK_a \sim 8$ (61). This result seems consistent with the hypothesis described by Green that Tyr derivatives with lower pK_a 's binds more tightly to IYD (62). Lower pK_a means a greater equilibrium concentration of the phenoxide anion. Confirmation that the phenolate preferentially binds awaits analysis on the dependence of substrate's binding affinity with pH.

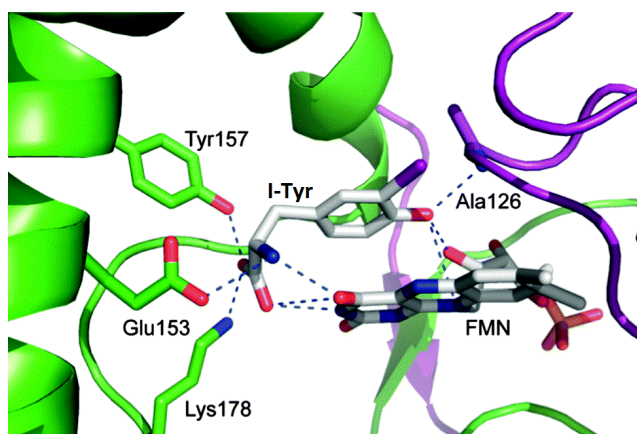


Figure 2-1. The active site of mIYD•I-Tyr (PDB ID 3GFD). Two monomers are shown in green and purple (45).

X-ray crystallographic studies on mIYD revealed that the IYD active site residues (Tyr157, Lys178, Glu153, Ala126) directly interact with substrate and FMN (Figure 2-1) (44, 45). Their ionizable groups may be critical for binding as well as catalytic activity and worth for further investigation. From the pH dependence of enzyme catalyzed reaction, it is possible to determine the ionizable groups involved in catalysis and may yield a great deal of information on catalytic mechanism.

In this chapter, we first time investigated the expression of truncated IYD from human by *E.coli* system. Successful purification of hIYD on a large scale allowed the further characterization of the kinetic behavior of hIYD. To

investigate the hIYD's substrate binding specificity and to rationalize the relationship of ligand's pKa and binding affinity with hIYD, binding affinities of hIYD to tyrosine derivatives is measured. pH-rate profile and pH vs K_D profile is also created to investigate the variations of activity and binding affinity with pH to illustrate the ionizable groups that are critical for binding affinity and catalysis.

2.2 Experimental

2.2.1 Materials

DNA primers were obtained from Intergrated DNA Technologies (Coralville, IA). OneShot Top10 *E.coli* was purchased from Invitrogen (Carlsbad, CA). Rosetta 2 (DE3) *E. coli* was from Novagen (San Diego, CA). The pET28-SUMO vector was obtained from Dr Christopher Lima. Other pET plasmids and antibodies were purchased from Novagen. All enzymes were from New England Biolabs. All other biochemical reagents were obtained at the highest grade and used without further purification unless specified.

2.2.2 General methods

PCR reactions were performed in Eppendorf Mastercycler. The amplified product and pET28-SUMO vector were digested with BamHI and XhoI. The vector was dephosphorylated with Antarctic alkaline phosphatase. The insert and vector were then ligated using T4 DNA ligase following the manufacturer's instructions. Transformations were performed with an Eppendorf Electroporator 2510 (1700 V, 1 mm gap cuvet). Plasmid DNA was isolated from colonies

resistant to Kanamycin monosulfate using a GeneJET plasmid miniprep kit (Fermentas, Glen Burnie, MD). Agarose gel electrophoresis was performed using 1 % agarose at 125 V according to Ausubel (63). Plasmids exhibiting the expected digestion pattern after enzyme digestion and gel electrophoresis were sequenced (University of Maryland Biotechnology Institute) to verify the sequence. The SDS-PAGE gels with 12 % acrylamide resolving and 5 % stacking and Laemmli running buffer were prepared according to standard procedures (64). The running protocol was following the previous published protocol by Ausubel at 200 V using a mini protean 3 gel system (Bio-Rad, Hercules, CA). Coomassie Brilliant Blue was used to stain all the protein gels. UV measurements were performed with a Hewlett-Packard 8453 spectrophotometer (Palo Alto, CA). Fluorescence measurements were made with a Hitachi F-4500 fluorescence spectrophotometer.

2.2.3 Cloning, protein expression and purification.

The *Homo sapiens* iodotyrosine dehalogenase protein gene (GeneBank: AY259176.1) was amplified by PCR using the following primers to generate a derivative lacking codons for amino acids 1-31 and gaining a C-terminal His₆ tag, 5'-AAGCTTAAGCTTGGATCCGCCACCATGGCTCAAGTTCAGCCC-3' and 5'CTCGAGCTCGAGCTAATGGTGATGGTGATGGTGACTGTCACCATGATC-3'. The amplified PCR was digested with BamHI and XhoI and inserted into pET28-SUMO vector, in which a SUMO fusion tag was added to the N-terminal to improve the solubility. The resulting plasmid pET28JH1 containing the hIYD

gene was transformed into *E. coli* Rosetta 2 (DE3) (Novagen). Cells were grown in LB media with kanamycin and chloramphenicol at 37 °C until an OD₆₀₀ of 0.6~0.8, expression was then induced with 0.2 mM IPTG and incubated at 18 °C for 4 hours. Cells were harvested by centrifugation and were resuspended in buffer N (50 mM sodium phosphate (pH 8.0), 500 mM NaCl and 10 % glycerol). The cells were flash frozen and stored at – 80 °C until use.

To isolate the deiodinase, the cells were thawed and subsequently lysed by three passages through a French press at 1000 psi. Cell debris was removed by centrifugation at 40,000×g at 4 °C for 2 h. The supernatant was fractionated with nickel ion affinity chromatography (HispurTM Ni-NTA resin, Thermo Scientific) that was equilibrated with buffer N. Successive washes used increasing concentrations of imidazole (20 mM for five column volumes (CV), 60 mM for 5 CV, 80 mM for 2 CV and 100 mM CV) in buffer N. The SUMO fusion of hIYD was finally eluted with 350 mM imidazole in buffer N and digested with Ulp1 protease (1:200 w/w) to release hIYD from SUMO. The resulting solution was concentrated to 3 ml and passed through a gel filtration column (Sephacryl S-200 HR, GE Healthcare) equilibrated with 50 mM sodium phosphate pH 7.4, 100 mM NaCl, 1 mM DTT and 10 % glycerol. Fractions containing hIYD were pooled and the concentration of hIYD was determined by the A₂₈₀ after correcting for the contribution from bound FMN ($A_{280}/A_{450} = 1.57$) (45) and an extinction coefficient ($\epsilon_{280} = 37,930 \text{ M}^{-1} \text{ cm}^{-1}$) estimated by ExPASy ProtParam tool (65). The concentration of FMN was determined by its A₄₅₀ ($\epsilon_{450} = 12,500 \text{ M}^{-1} \text{ cm}^{-1}$)

(66). The purified hIYD was concentrated to 10 mg/ml by using Amicon[®] Ultra centrifugal filters prior to storage at 4 °C.

2.2.4 Circular Dichroism

CD data were collected by using a JASCO-810 at 25 °C. For far UV CD (190 nm-250 nm), the protein concentration is 4.1 μM in buffer (20 mM sodium phosphate, 0.1mM DTT, pH 7.4), cell path length is 1mm and scan speed is 50 nm/min with response time 4 sec. The scanning of the cuvette with buffer has been set as baseline. After ten times scanning, the average data has been calculated. Equation 2-1 was used to convert the data from mdeg to mean residue ellipticity (degree cm² dmol⁻¹) (67). [E] is protein concentration, L is the path length, N is the number of residue. For visible CD (300 nm-500 nm), the protein concentration was increased to at least 60 μM in 20 mM sodium phosphate, 0.1 mM DTT, pH 7.4 buffer with or without I-Tyr. Cuvette pathlength is 1mm and six times scanning for each sample at a speed of 20 nm/min and response time 16 sec. The baseline was set by scanning of the cuvette with buffer. The data then have been averaged for each sample after subtracted the baseline. After converting the mdeg to molar elicity by Equation 2-2 (67), [E] is protein concentration, L is the pass length, and data was then graphed by Origin 7.

$$\text{Equation 2-1.} \quad \text{Mean residue elicityity} = \frac{100 \times \theta(\text{m deg}) \times 0.001}{[E](M) \times L(\text{cm}) \times (N - 1)}$$

$$\text{Equation 2-2.} \quad \text{Molar elicityity} = \frac{100 \times \theta(\text{m deg}) \times 0.001}{[E](M) \times L(\text{cm})}$$

2.2.5 Deiodinase activity

The deiodination activity of hIYD was measured by detecting the release of ^{125}I from [^{125}I]-I₂-Tyr as reported previously (26). The assay was performed by adding 100 μl of hIYD (0.8 μM) to 300 μl solution 2 (1.66 mM methimidazole, 166 mM 2-mercaptoethanol, 666 mM KCl, 333 mM potassium phosphate pH 7.4), varied amounts of I₂-Tyr (from 10 μM to 100 μM), water and 100 μl [^{125}I]-diiodotyrosine (I₂-Tyr) to make the total volume 900 μl . Reactions were initiated by 100 μl of 10 % dithionite in 5 % sodium bicarbonate. Samples were incubated at 20 °C for 10 min and quenched by addition of 100 μl of 0.1 % I₂-Tyr in 0.1 M NaOH. Aliquots of 250 μl (S) were immediately added to 4.75 ml 10 % acetic acid to determine the total radioactivity for each assay. The remaining 850 μl was then loaded onto a cation exchange column (3.5 ml, AG50W-X8 resin), washed with 4.15 ml 10 % acetic acid and the eluent was labeled as A. The column was then washed with 5 ml of 10 % acetic acid and collected as B. Radioactive I release was quantified using a Packard 1600 TR liquid scintillation analyzer after adding 25 ml scintillation fluid to each S, A and B,.

Using Equation 2-3 to calculate the percent of iodide released (F) from each assay, the rate of iodide release ($\mu\text{M}/\text{h}$) was then calculated using Equation 2-4. F_0 is the background radioactivity obtained without adding protein. [S] is the substrate concentration in each sample. x is the reaction time. The product formation could be calculated by using Equation 2-5. Assays were performed in triplicate. The data set that not shown substrate inhibition were fit to Michaelis–

Menton kinetics using Origin 7.0. The k_{cat} value was calculated based on the protein concentration.

$$\text{Equation 2-3.} \quad F = \frac{\frac{dpmA + dpmB}{0.85}}{\frac{dpmS}{0.25}}$$

$$\text{Equation 2-4.} \quad V = (F - F_0) \times \frac{\frac{60min}{x min}}{h} \times [S](\mu M) \times 2$$

$$\text{Equation 2-5.} \quad P = (F - F_0) \times [S] \times 2$$

2.2.6 Fluorescence titration for measuring binding affinity

Fluorescence quenching of the enzyme bound FMN ($\lambda_{ex} = 450$ nm and $\lambda_{em} = 527$ nm) was measured to determine ligand binding as described previously (68). Briefly, hIYD was titrated with the Tyr derivatives (I-Tyr, Br-Tyr, Cl-Tyr, and F-Tyr) over a range of concentrations centered at that necessary for a 50 % quenching of the emission signal. Fluorescence intensities were normalized by dividing the initial fluorescence (F_0) (obtained without adding substrate) and plotted against the ligand concentration using Origin 7. Dissociation constants (K_D) were obtained from the nonlinear fitting to the Equation 2-6 (51).

$$\text{Equation 2-6.} \quad F = F_0 + \Delta F \times \left(\frac{(K_D + [E] + [S]) - \sqrt{(K_D + [E] + [S])^2 - 4[E][S]}}{2[E]} \right)$$

2.2.7 pH dependence assay

To assess the role of acid/base chemistry in the hIYD enzymatic reaction, apparent steady-state kinetics constants were determined using the standard deiodinase assay at pH 6.0 – 7.5 (100 mM potassium phosphate (Kpi)) and pH 7.5 – 8.5 (100 mM Tris-HCl). All the reactions were performed under the same enzyme concentration ($[E] = 0.08 \mu\text{M}$). The V_{\max} and V_{\max}/K_M for each pH were obtained as the average of the three times repeat. The $\log V_{\max}$ and $\log V_{\max}/K_M$ were plotted against pH. The pH-rate profiles were fitted to Equation 2-7 (69).

$$\text{Equation 2-7.} \quad \log(y) = \log(y)_{\max} - \log(1 + 10^{pH-pK_a})$$

$$\text{Equation 2-8.} \quad \log(y) = \log(y)_{\max} - \log(1 + 10^{pK_a-pH})$$

The K_D vs pH was measured at pH 6.0 – 8.0 (100 mM Kpi) and pH 8.0 – 9.0 (100 mM Tris-HCl) by fluorescence titration assay as described above. The K_D values were obtained from the average of three independent repetitions at each pH. The $\log K_D$ was plotted against pH, and fitted to Equation 2-7 and Equation 2-8 (69).

2.3 Results and Discussion

2.3.1 Expression and Purification

Removal of the transmembrane domain from mIYD generates a soluble, stable and active derivative of the deiodinase (54, 60). An equivalent truncation was performed on hIYD. The gene encoding hIYD but lacking the first (1-31)

amino acids (Figure 2-2) was inserted into the pET28-SUMO vector and expressed in *E. coli*.

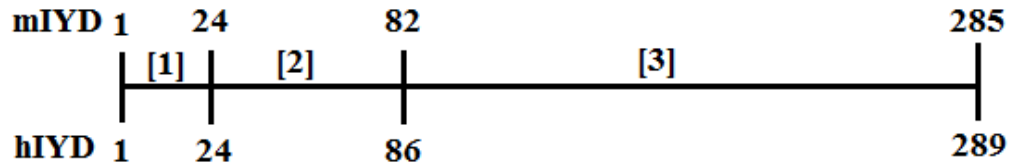


Figure 2-2. hIYD consists of three domains. A transmembrane domain [1] (residues 1-23), an intermediate domain [2] (residues mIYD (24-82), hIYD (24-86)), and catalytic domain [3] (residues mIYD (82-285), hIYD (86-289)).

The soluble fraction of the fusion protein (~ 50 %) was isolated by nickel-based affinity chromatography. The SUMO tag was then removed by the protease Ulp1 and hIYD was isolated by size exclusion chromatography in a yield of ~10~20 mg /1 L culture. Native protein assembles as a homodimer and was isolated with the expected FMN to monomer ratio of 1.9 ~ 2.1 as determined by A_{280} and A_{450} . The purity of hIYD approached 97 % as estimated by SDS-PAGE, Coomassie staining and analysis by ImageQuant TL. The desired protein migrates similar to the 30-kDa marker as expected for a monomer of 30.5 kDa as calculated by Expasy (Figure 2-3) (65).

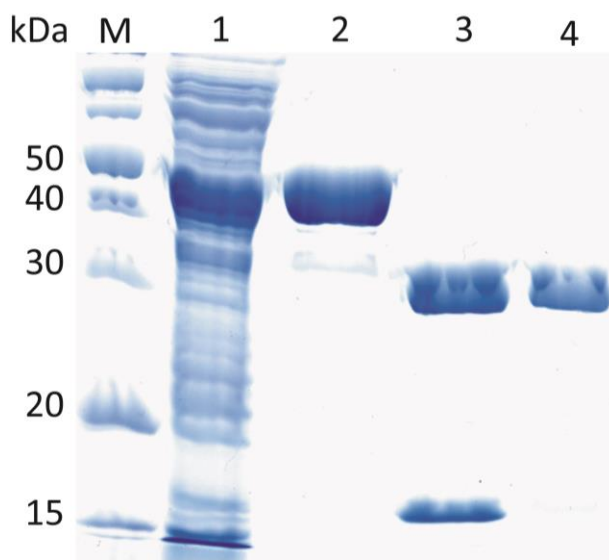


Figure 2-3. SDS-PAGE characterization of expression and purification of hIYD from *E. coli*. M illustrates the molecular weight markers. Lanes 1 refers to the soluble fraction of the whole-cell extracts of *E. coli* cultures. Lane 2 shows protein after purification by HisTrap column. Lane 3 shows protein after Ulp1 digestion to remove the Sumo fusion. Lane 4 refers to pure hIYD after size-exclusion chromatography.

2.3.2 Circular dichroism spectroscopy analysis

CD measures the difference between the absorbance of left and right circularly polarized light caused by the asymmetry of the solute. It has a wide range of applications, such as determining whether a protein is folded and whether protein-ligand interactions alter the conformation of the protein. Information can also be learned on the environments of protein's cofactor (67). The difference between far-UV CD of hIYD and hIYD in the presence of I-Tyr illustrates the change of secondary structure caused by I-Tyr binding (Figure 2-4). The CD are consistent with the prior observations made from substrate-bound

crystal structure of mIYD (44). Substrate I-Tyr induces the formation of additional α -helix and β -sheet, which represent the lid of the active site.

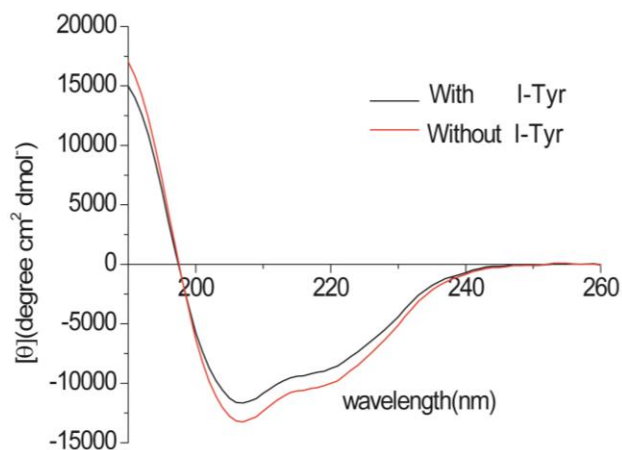


Figure 2-4. Far-UV CD spectra of hIYD. In the presence of I-Tyr (black line); without I-Tyr (red line), in 20 mM sodium phosphate, 0.1mM DTT, pH 7.4.

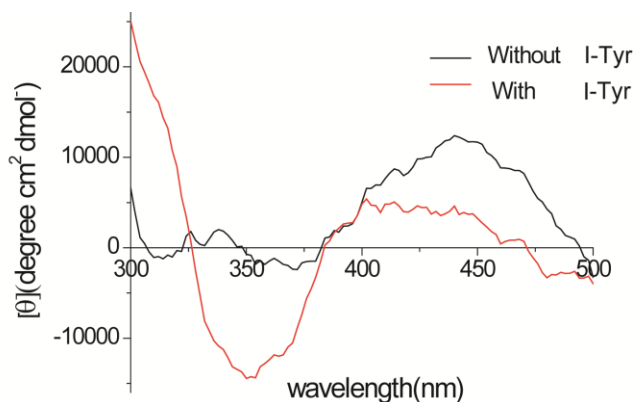


Figure 2-5. Visible CD spectra of hIYD. hIYD with I-Tyr is shown in red line; hIYD is shown in black line. Buffer - 20 mM sodium phosphate, 0.1mM DTT, pH 7.4.

Distinct change in the visible range CD spectra was observed when I-Tyr was added to hIYD (Figure 2-5). The development of a negative CD signal around 350 nm and a weak positive CD signal in the longer wavelength range reveal the change of coordination of FMN upon substrate binding. These data are consistent with observations made from mIYD crystal structure. Upon I-Tyr

binding, the I-Tyr stacks on the top of FMN ring and its zwitterion region forms H-bonds to N3 and O4 of FMN.

2.3.3 Deiodination activity

The standard [¹²⁵I]-iodide release assay was used for characterization of hIYD expressed in *E. coli*. A K_M of $31 \pm 6 \mu\text{M}$ and a k_{cat} of $12.5 \pm 1 \text{ min}^{-1}$ were measured using I₂-Tyr as substrate (See Appendices A) and the resulting k_{cat}/K_M of $0.40 \text{ min}^{-1}\mu\text{M}^{-1}$ is close to that reported for mIYD ($0.95 \text{ min}^{-1}\mu\text{M}^{-1}$) also lacking its N-terminal transmembrane region (54).

Table 2-1. Catalytic properties of iodotyrosine deiodinase homologs.

Organism	K_M (μM)	k_{cat} (min^{-1})	$\frac{k_{\text{cat}}}{K_M}$ ($\text{min}^{-1}\mu\text{M}^{-1}$)
Honeybee ^a	29 ± 7	8 ± 1	0.28 ± 0.07
Sea anemone ^a	105 ± 26	32 ± 4	0.30 ± 0.08
Human	31 ± 6	12.5 ± 1	0.40 ± 0.05
Zebrafish ^a	8 ± 1	4.1 ± 0.2	0.51 ± 0.07
Bacteria ^a	6.6 ± 0.9	5.4 ± 0.3	0.8 ± 0.1
Mouse ^b	5.8 ± 0.6	6 ± 2	0.95 ± 0.33
Lancelet ^a	6 ± 3	7 ± 1	1.2 ± 0.6
Daphnia ^a	7 ± 1	17.5 ± 0.8	2.5 ± 0.4

^{a,b} parameters were reported previously (45, 54).

According to the analysis on all the current available IYD homologs, all the key residues involved in the active site and FMN binding site are well conserved (Figure 1-6) (45). The steady state kinetics parameters presented in this study indicates that IYD from human follow the trend of the catalytic rate of the IYD family for which the k_{cat}/K_M values are clustered between $0.3 \text{ min}^{-1}\mu\text{M}^{-1}$ to

2.5 min⁻¹μM⁻¹ and K_M values ranged from 6 μM to 105 μM for substrate I₂-Tyr (Table 2-1). Among all the homologs, the kinetic parameters of hIYD are most close to the parameters of Honeybee.

2.3.4 Affinity of hIYD for 3-Halotyrosines

Binding of the various halogen-substituted tyrosines (F-Tyr, Cl-Tyr, Br-Tyr, and I-Tyr) to IYD was monitored by the decrease in fluorescence of the active site FMN upon association with these ligands (See Appendices B). As summarized in Table 2-2, I-Tyr also binds very tightly to hIYD as well as to mIYD with K_D values below 1 μM. The K_D of hIYD to I₂-Tyr is 10-fold higher than I-Tyr. Similar trend was found in mIYD, where the K_D to I₂-Tyr is 6-fold higher than I-Tyr (60). hIYD also associates strongly with Br-Tyr and Cl-Tyr

Table 2-2. hIYD affinity for halotyrosines.

halotyrosine derivative	K _D (μM)		pKa ^b (2-halophenol)
	hIYD	mIYD ^a	
I ₂ -Tyr	1.5 ± 0.15	0.49 ± 0.06	6.4
I-Tyr	0.15 ± 0.04	0.090 ± 0.04	8.53
Cl-Tyr	0.14 ± 0.02	0.11 ± 0.03	8.35
Br-Tyr	0.10 ± 0.01	0.15 ± 0.02	8.48
F-Tyr	1.30 ± 0.40	1.30 ± 0.20	8.86
NO ₂ -Tyr		0.12 ± 0.05	7.2
Me-Tyr		>1.5 x 10 ³	10.4
Tyr	>10 ³	>1.4 x 10 ³	10.05

^a Values determined previously (60). ^b From the literature(61) .

which all share K_D values close to 120 nM. Only F-Tyr has a noticeably weaker affinity for hIYD. Still, many orders of magnitude separate the K_D values for all of the halotyrosines versus that for the parent tyrosine.

The halotyrosines with similar pKa display similar binding affinity to hIYD (within an order of magnitude). Tyr, whose pKa is approximately 2 units higher, exhibits a 1000-fold decrease in binding affinity with hIYD. These results support the hypothesis that IYD may prefer binding to the phenolate form of the substrate.

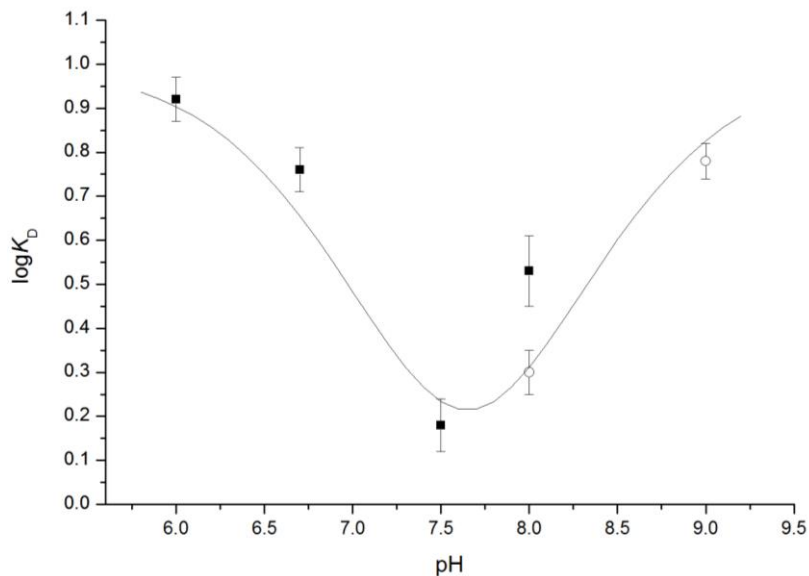


Figure 2-6. The pH dependence of substrate binding to hIYD. The affinity of I₂-Tyr for hIYD (K_D) is reported as the average of three independent measurements in the presence of potassium phosphate (■) and Tris-HCl (○) at the indicated pH values. Error represents the standard deviation from three measurements. Data were fit by non-linear least-squares regression to Equation 2-7 and Equation 2-8.

2.3.5 pH dependence of I₂-Tyr's binding with hIYD

The influence of pH on substrate binding affinity was determined independently by measuring the K_D of I₂-Tyr (Fig. 2-5) over the pH range 6-9 to

test if the phenolate form of substrate is the prefer form for binding. Tightest binding was measured near a neutral pH of 7.5. The affinity of I₂-Tyr increases as pH was increased from 6.0 to 7.5 as measured by the decrease in the dissociation constant K_D (Figure 2-6). Binding affinity of I₂-Tyr weakens as pH increased above 7.5. The importance of two ionizable groups with pK_a values of 6.6 ± 0.2 and 8.7 ± 0.3 was suggested as estimated from non-linear least-squares fitting of the logK_D and pH to Equation 2-7 and 2-8. Deprotonating an acidic group with pK_a ~ 6.6 and protonating a basic group with pK_a ~ 8.7 enhance the binding affinity. The pK_a of the phenolic group of I₂-Tyr has been reported as 6.4 (70) and is similar to the value measured from the pH dependence of binding to IYD. Therefore, the phenolic group of I₂-Tyr may represent the candidate of acidic group with pK_a values of 6.6 as estimated from pH dependent assay. The pH dependent results are consistent with the previous suggestion that the phenolate form of the halotyrosines is the preferential binding form of IYD. Tyr has a high phenolic pK_a of 9.1 (71) and was unable to be deprotonated at pH 7.4, resulting in a 1000-fold poorer binding affinity than I₂-Tyr.

The structure of mIYD•I-Tyr indicates that the phenolate of substrate could have polar contacts with the amide backbone of Ala126 and the 2'-hydroxy group of FMN. These interactions may play an important role in stabilizing the phenolate form of substrate and facilitate the deiodination. Similar interactions between substrate and the 2'-hydroxyl group of FMN has been reported in many acyl CoA dehydrogenases, and were found critical for stabilizing the developing charge (enolate form) of substrate (72, 73). BluB, the most closely structure

homologs of IYD in the nitro-reductase family, was found to form an equivalent hydrogen bond between the 2'-hydroxyl of its FMN and its substrate-molecular oxygen (47). The IYD may function in a similar way as acyl CoA dehydrogenase and BluB by generating non-aromatic keto form of the I₂-Tyr as an electrophilic intermediate to accept reducing equivalents. A non-aromatic pyridine analogue used as the mimic of the intermediate keto was reported with high binding affinity with IYD previously, supporting the current catalytic mechanism (Figure 2-7) that the phenolate form substrate was converted to a keto intermediate for further catalysis.

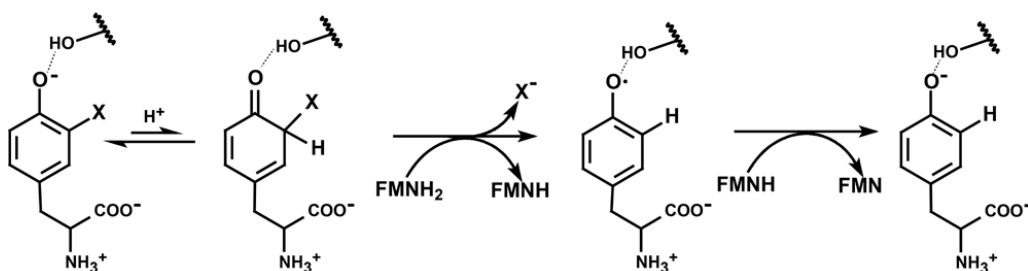


Figure 2-7. Stepwise one-electron transfer catalytic mechanism of IYD.

The proposed basic group that affects binding is likely the α -ammonium group of I₂-Tyr (pK_a of 7.8) (71). According to the crystal structure of mIYD·I₂-Tyr, the α -ammonium group of I₂-Tyr form polar contacts to residues Glu157 and O4 of FMN, and may important for the close of the active site lid and properly position of substrate between IYD and FMN. Another candidate for this basic group might be the N3-H of FMN. Although its pK_a in free solution is reported to be 10 (74), its pK_a inside hIYD may vary and close to 8.7.

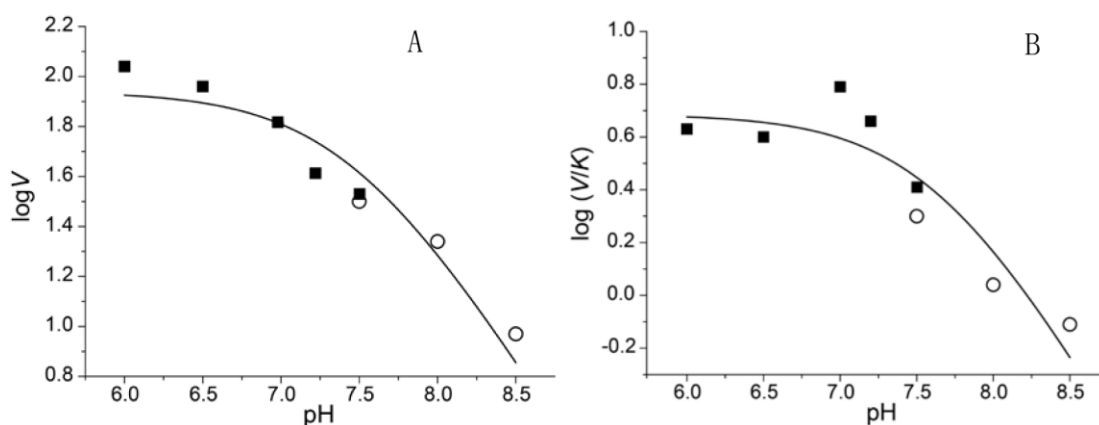


Figure 2-8. The pH dependence for deiodination of I₂-Tyr by hIYD. The pH profile of (A) logV and (B) logV/K were fit by non-linear least-squares regression using Equation 2-7. Each data represents an average of three independent measurements in the presence of potassium phosphate (■) and Tris-HCl (○) at the indicated pH values.

2.3.6 pH dependence of I₂-Tyr deiodination by hIYD

Kinetic analysis of I₂-Tyr deiodination by hIYD was repeated over a pH range of 6.0 - 8.5 (Fig. 2-8) to investigate the ionizable residues that is critical for catalysis. The maximum activity was measured at the lowest pH 6.0. The pH rate profiles of both logV and logV/K illustrate a basic limb with a slope of -1. Their respective pK_a values of 7.5 ± 0.2 and 7.6 ± 0.2 as determined by Equation 2-7 are within experimental error and are consistent with the protonation of a functional group with a pK_a of 7.5 – 7.6. The similarity in the pH dependence of V and V/K indicates that the catalytic parameter k_{cat} dominates the profiles. Few candidates are apparent for this ionizable group other than the α -ammonium group of I₂-Tyr. Its interaction with the O4 of FMN may help orient substrates with regard to the isoalloxazine system and modulate the oxidation-reduction properties of this system and facilitate the deiodination process.

2.4 Conclusion

In this chapter, an efficient expression and purification of hIYD was developed. This system will accelerate the research progress on hIYD due to its simplicity and capability of providing large quantities of protein for further research. The kinetic parameters of hIYD are similar to that for other IYD homologues. The investigation of binding affinity of hIYD with halotyrosine derivatives also showed a similar trend as mIYD in regarding binding affects and pKa of the phenolic group. Both suggest that the phenolate form of the halotyrosines binds preferential to IYD. The pH dependent of bind leads more evidence to this hypothesis. Deprotonating the phenolic group of I₂-Tyr was found critical for its binding. The pheolate form of substrate was thought to be stabilized by the interactions from the 2'-hydroxyl of its FMN. Protonating of another ionizable group with a pKa around 7.6 was found to be important for catalytic. The most likely candidate for this ionizable group was the α -ammonium group of I₂-Tyr, which may participate in position substrates with regard to FMN as well as modulate the redox property of the enzyme.

Chapter 3: The influence of substrate binding on redox property and structure

3.1 Introduction

The redox chemistry of flavin depends on its coordination with its protein environment. Important interactions to FMN redox state include hydrogen-bonding interactions at its N1, O2, N3, O4 and N5, electrostatic interactions, the aromatic stacking of the isoalloxazine ring, solvent accessibility and bend of the isoalloxazine ring (40, 75-78). As observed in structure of mIYD•I-Tyr, substrate binding induces closure of the active site lid and dramatically changes on the coordination of FMN by addition of H-bonding to N3, O4 and N5 of FMN and aromatic stacking (Figure 3-1) (44). Thus, substrate binding is expected to change the redox properties of FMN in IYD and facilitate the deiodination process.

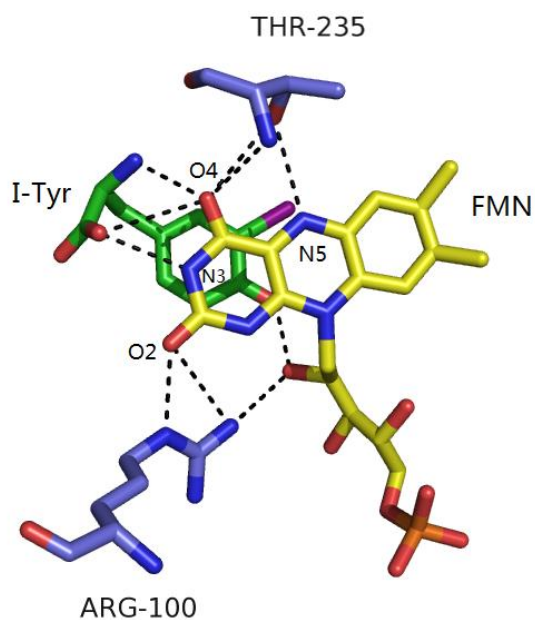


Figure 3-1. Interactions to the isoalloxazine ring of FMN in mIYD•I-Tyr.

Redox potential shows the tendency of a chemical species to acquire electrons. The more negative the potential, the less the species' affinity for electrons and tendency to be oxidized (79). For free FMN in solution, the midpoint redox potential (E_m) for the oxidized/semiquinone couple and semiquinone/reduced couple is -0.314 V and -0.124 V, respectively, at pH 7 (80). Due to the different of protein's ability to stabilize the semiquinone state of FMN, the redox potential of FMN in bound protein vary widely (81). The only report on the redox potential of IYD was published in 1979 using IYD purified from bovine thyroid microsomes (27). Titration of this IYD with dithionite suggested the presence of neutral semiquinone species (absorbance at 585 nm). The midpoint potential of this IYD was reported as -0.190 V and -0.412 V for the oxidized/semiquinone couple and the semiquinone/reduced couple, respectively (27). However, the potentiometric method used was unable to differentiate the kinetically and thermodynamically stable semiquinone. A kinetically semiquinone will dissipate quickly. In contrast, a thermodynamically stable semiquinone will persist in the presence of an electron shuttle, such as the redox dye methyl viologen.

A method using xanthine/xanthine oxidase as reducing system is able to determine the redox potential based on UV/VIS spectra of the thermodynamically stabilized redox state of flavin (32). A low concentration of xanthine oxidase is used to realize the slow reduction to ensure that the redox equilibrium is established between the flavin and a reference dye (32, 79, 82). The redox

potential of flavin can be obtained after calculating its difference with the reference dye of known redox potential by using Nernst equation (32). Reference dyes were selected so that they would be reduced concourse with hIYD, which requires redox potentials within 30 mV of each other. Moreover, the indicator and protein should have distinct absorbance during reduction process to enable the calculation of their concentrations independently.

In this chapter, the crystal structure of hIYD and hIYD•I-Tyr is presented to illustrate structural influence of FMN coordination caused by I-Tyr binding in hIYD. To understand the contribution of structural change on the redox of FMN, the redox property of hIYD in the presence or absence of F-Tyr was investigated by xanthine/xanthine oxidase method. The F-Tyr analog exhibits tight binding to IYD, however, it does not turn over with IYD (68). Replacing the native substrate I-Tyr with F-Tyr is intended to focus the investigation on substrate binding induced change of the redox property of FMN instead of catalytic turnover.

3.2 Materials and Methods

3.2.1 General methods and materials

Protein expression and purification follow the protocols described in Chapter 2. UV/VIS spectra were obtained with a Hewlett-packard 8453 spectrophotometer (Palo Alto, CA). Biochemical reagents including xanthine oxidase were purchased from Sigma Chemicals and used without further purification unless specified. F-Tyr and Nile Blue were obtained from Astatech, Inc. and Santa Cruz Biotechnology, Inc., respectively.

3.2.2 Protein crystallization, structure determination and refinement.

Crystallization trials utilized a Phoenix crystallization robot and sparse matrix screening WizardTM I, II, III and IV (Emerald Biosciences), PEGSuiteTM and CryoSuiteTM (Qiagen) and IndexTM (Hampton Research). After optimization, hIYD crystals grew in approximately 2 days at 20 °C by the hanging drop diffusion method with a ratio of 1 µl hIYD (12 mg/ml, 50 mM sodium phosphate pH 7.4, 100 mM NaCl, 1 mM DTT, 10 % glycerol) and 1 µl precipitant (0.05 M ammonium sulfate, 50 mM BisTris (pH 6.5), and 25 % pentaerythritol ethoxylate. Crystals were cryoprotected in the precipitant supplemented with 15 % glycerol and 1 mM FMN for prior to data collection. To generate co-crystals, hIYD was treated with 1.5 mM I-Tyr overnight at 4 °C and then subject to the same hanging drop procedure using a well solution of 0.15 M sodium acetate, 85 mM Tris-HCl pH 8.5, 25.5 % w/v polyethylene glycol 4,000 and 15 % glycerol at 20 °C. Co-crystals of hIYD·I-Tyr formed within 24 hours and were flash frozen in liquid nitrogen.

X-ray diffraction data were collected at beamline 7-1 at the Stanford Synchrotron Radiation Laboratory. Data were processed using the HKL2000 package (83). The structures of hIYD and hIYD·I-Tyr were solved by molecular replacement using AutoMR in PHENIX by Dr. Watchalee Chuenchor (84). Final refinement statistics for both structures are summarized in Table 3-1. All images were prepared using Pymol (Schrödinger, LLC). Structure factors and coordinates have been deposited with the Protein Data Bank at PDB under accession number 4TTB and 4TTC.

Table 3-1. Data collection and refinement statistics.

Protein	hIYD-FMN	hIYD-FMN-I-Tyr
Ligands	FMN	FMN and I-Tyr
PDB code	4TTB	4TTC
Data collection		
Space group	$P3_1$	$P6_1$
No. Molecule/ASU	2	6
Unit cell parameters (Å, °)	$a = 72.89,$ $b = 72.89,$ $c = 95.51$	$a = 104.75,$ $b = 104.75,$ $c = 303.34$
	$\alpha = 90, \beta = 90, \gamma = 120$	$\alpha = 90, \beta = 90, \gamma = 120$
Resolution range (Å) ^a	50-2.45 (2.54-2.45)	50-2.65 (2.74-2.65)
No. of unique reflections ^a	20957 (2074)	54565 (5465)
No. of observed reflections	172255	522006
Completeness ^a	100 (100)	100 (100)
Redundancy ^a	8.2 (7.6)	9.6 (9.6)
R_{sym} (%) ^a	6.1 (61)	8.8 (55.4)
$I/\sigma I$ ^a	33.8 (2.9)	27.1 (4.9)
Refinement		
Resolution used in refinement (Å)	38.09-2.45	44.86-2.65
No. of reflections used in working set	18749	54432
No. of reflections for R_{free} calculation	1874	2708
R_{work} (%), R_{free} (%)	18.17, 23.64	19.02, 22.14
No. atoms		
Protein	3042 (A-B)	10680 (A-F)
Hetero atoms	62 (FMN)	186/84 (FMN and I-Tyr)
Solvent	42	221
Mean B -factor (Å ²)		
Protein	86.2	52.3
FMN	85.8	37.8
I-Tyr	None	40.1
Solvent	62.7	41.8
RMSD from ideality		
Bond lengths (Å)	0.008	0.008
Bond angles (deg.)	1.142	1.059
Ramachandran analysis		
Favored (%)	98.4	97.4
Allowed (%)	100	100
Outliers	0	0
Coordinate Error	0.28	0.78

^aNumbers in parentheses are outer shell parameters.

3.2.3 Anaerobic Titration

All titrations were performed at 25 °C using xanthine/xanthine oxidase as the reducing system (32, 82). Individual samples within sealable quartz cuvettes contained 10-15 μM hIYD, 900 μM xanthine, 2 μM methyl viologen, 200 mM

potassium chloride and 100 mM potassium phosphate pH 7.4. Molecular oxygen was removed from these solutions by continuously flushing with argon for at least 20 min prior to addition of hIYD. Reaction was initiated by addition of 40 µg/ml xanthine oxidase. Spectra changes were monitored every 2 min. Titrations were also repeated in the presence of F-Tyr (0.6 mM) to investigate the effect of ligand binding on the oxidation-reduction properties of the enzyme-bound FMN.

Redox potential measurement is based on the method described by Massey (32, 82). The following reference dyes were used as indicator: anthraquinone-2,6-disulfonate (AQDS, $E_m = -188$ mV), Nile blue ($E_m = -116$ mV), or safranin O ($E_m = -280$ mV) (85). The UV/VIS spectral changes were recorded every 2 mins for over 2 hours. The concentration of species are determined at a wavelength at which the other redox partner has an isobestic point between the oxidized and reduced forms or has no absorbance at all. The potential at 50 % reduction of flavoenzyme can be calculated by the Nernst equation (82):

$$\text{Equation 3-1. } E_h(\text{dye}) = E_m(\text{dye}) + 2.303(RT/n_{\text{dye}}F)\log(\text{dye}_{\text{ox}}/\text{dye}_{\text{red}})$$

$$\text{Equation 3-2. } E_h(E) = E_m(E) + 2.303(RT/n_E F)\log(E_{\text{ox}}/E_{\text{red}})$$

At equilibrium, $E_h(\text{dye}) = E_h(E)$

$$\text{Equation 3-3.}$$

$$E_m(E) + 2.303(RT/n_E F)\log(E_{\text{ox}}/E_{\text{red}}) = E_m(\text{dye}) + 2.303(RT/n_{\text{dye}} F)\log(\text{dye}_{\text{ox}}/\text{dye}_{\text{red}})$$

$$\text{Equation 3-4.}$$

$$\log(\text{dye}_{\text{ox}}/\text{dye}_{\text{red}}) = (n_{\text{dye}} F / n_E F) \log(E_{\text{ox}}/E_{\text{red}}) + (E_m(E) - E_m(\text{dye})) n_{\text{dye}} F / 2.303RT$$

R is the gas constant ($8.31\text{JK}^{-1}\text{mol}^{-1}$). At 25°C , $n_{\text{dye}}F/2.303RT = n_{\text{dye}}/59\text{ mV}$. After calculate the concentration of each species, plot the $\log(E_{\text{ox}}/E_{\text{red}})$ VS $\log(\text{dye}_{\text{ox}}/\text{dye}_{\text{red}})$ and linear analysis the data by Origin 7. The Y-intercept value was used to calculate the midpoint redox potential of the enzyme. To make the analysis reliable, the first 10 % and last 10 % reaction data was not be included. All mid-point potentials are reported versus the standard hydrogen electrode and represent the average of three independent determinations.

3.3 Results and Discussion

3.3.1 Structural determination of hIYD

The structure of hIYD and hIYD·I-Tyr were solved from different crystal forms by molecular replacement with previously described for mIYD and mIYD·I-Tyr (44, 46). hIYD crystallized with one dimer per asymmetric unit. The hIYD·I-Tyr complex crystallized with three dimers per asymmetric unit. All the parameters were summarized in Table 3-1. Similar to the mouse IYD structure, electron density for the first 39 residues (32-70) representing part of the intermediate domain of hIYD was not observed in either hIYD diffraction patterns. Truncation of this flexible region may help improve the quality of the crystal. However, truncation of the 32-70 residues resulted in 90 % of hIYD insoluble when expressed in *E.coli* and no further deletions were attempted. This intermediate domain likely stabilizes the homodimeric structure or at least aids in its initial folding.

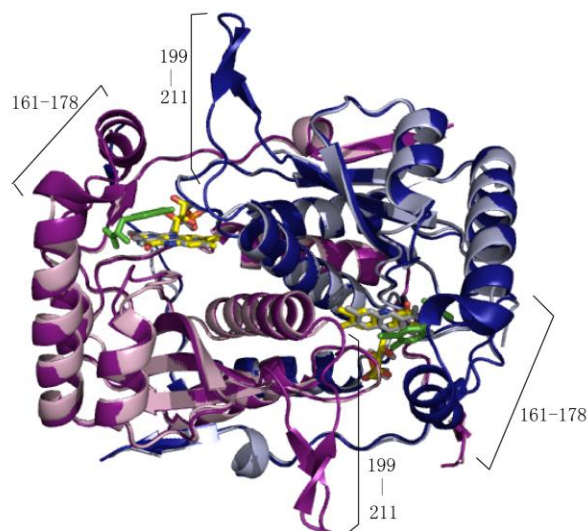


Figure 3-2. Comparison between structures of hIYD and hIYD•I-Tyr. The structure of hIYD•I-Tyr (deep blue and deep purple to indicate the two monomers) is overlaid with the structure of hIYD (light blue and light pink to indicate the two monomers). The active site lid composed of a loop (residues 199-211) and a helix-turn (residues 161-178) are only detected in the hIYD•I-Tyr co-crystal.

hIYD belongs to the nitroreductase superfamily and its structure shares some common feature with all the other members of this family. The two identical subunits of hIYD consist of a typical α - β fold swap (Figure 3-2). The FMN is bound non-covalently to the hIYD at the interface of two helices formed by the two monomers. The FMN is flat (bend angle $< 2^\circ$) and interacts through hydrogen bonds and hydrophobic region to both subunits. The phosphate group of FMN is coordinated by Arg-100, Arg-101 and Arg-279, all from the same subunit (Figure 3-4). The hydroxyl groups of Ser-102 and Ser-128 from different subunits form hydrogen bonds to the ribose group of FMN. Arg 104 maintains hydrogen bond with O² of FMN. The structures of hIYD and its co-crystal with I-Tyr are nearly superimposable (RMSD of 0.226 Å for a 398 atom comparison) (Fig 3-2). However, in the absence of substrate I-Tyr, the electron density of residues of

160-181 and 199-212 was not detected in the structure of hIYD. The presence of bound I-Tyr increases the order of this region, forming as a lid (a helix and loop) in the structure of hIYD·I-Tyr, covering the I-Tyr and FMN active site and sequestering it from solvent out (Fig 3-3).

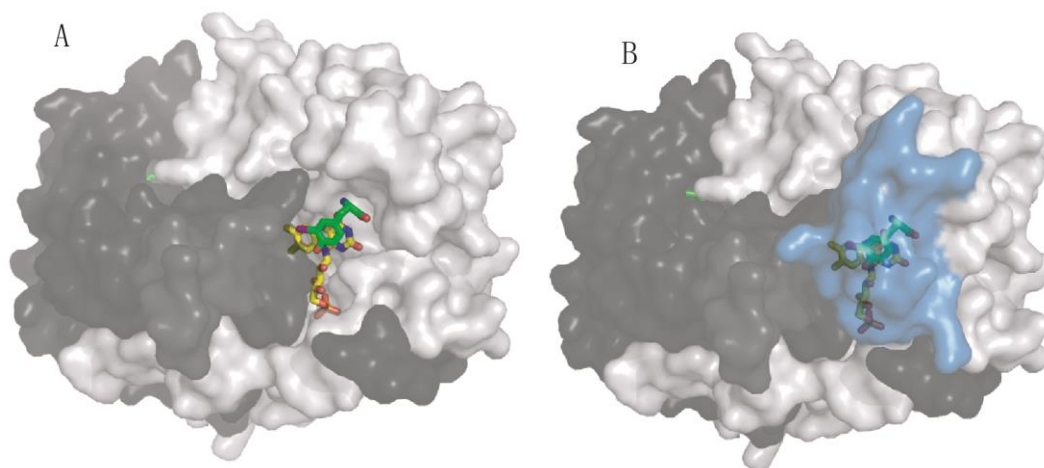


Figure 3-3. The active site lid shields the substrate and FMN from solvent. A) The two identical polypeptides within the hIYD·I-Tyr structure are indicated by shades of grey. FMN and I-Tyr reside in the active site and are depicted in color. Residues 161-178 of one polypeptide are not shown in order to reveal the position of FMN and I-Tyr. B) The surface formed by residues 161-178 of the same polypeptide is highlighted in blue to illustrate their ability to cover the active site.

The FMN forms additional critical interactions to the substrate I-Tyr and active site residues in hIYD as indicated in Figure 3-4. The zwitterionic region of I-Tyr forms H-bonds to the N3 and O4 of the FMN. Thr-239 additionally moves toward to the FMN. The distance between the OH side chain of Thr239 and the N5 of FMN changes from 4.8 Å to 3.1Å and allows the formation of a hydrogen bond. Further contact is made by the aromatic ring of I-Tyr stacking above the FMN with its closest approach between the FMN N10 and the phenolic oxygen of I-Tyr. The C-I bond of I-Tyr orients directly over the C4a-N5 bond of FMN that is crucial during redox cycling of many flavoproteins (81, 86). These substantial

changes in the environment around the isoalloxazine ring of FMN suggested that substrate binding may significantly affect the oxidation-reduction properties of IYD.

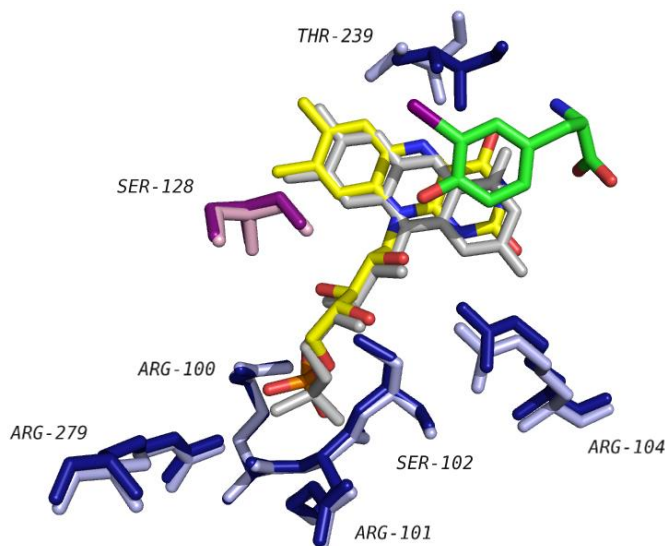


Figure 3-4. Details of the active site interactions around FMN. The surrounding residues from hIYD·I-Tyr (deep blue and deep purple to indicate from two monomers) are overlaid with the residues from hIYD (light blue and light pink to indicate from two monomers). Substrate I-Tyr is illustrated in green. For the structure lacking substrate, the FMN is depicted in grey. For hIYD·I-Tyr, the FMN is depicted in yellow.

hIYD shares 87 % sequence identity with mIYD. The structure of hIYD·I-Tyr and mIYD·I-Tyr are nearly superimposable (Figure 3-5), indicating that the structures of the flavin binding site and the active site in IYD are conserved. In both hIYD·I-Tyr and mIYD·I-Tyr, substrate binding induces the same formation of an active site lids consisting of a loop and helix. The four known human mutations that compromise IYD activity and result in thyroid disease as predicted earlier from the mIYD model map to the hIYD structure (15, 19, 44). One of the

most severe mutations is R101W that effects a key stabilization interaction with the protein and the phosphate group of FMN (Figure 3-4).

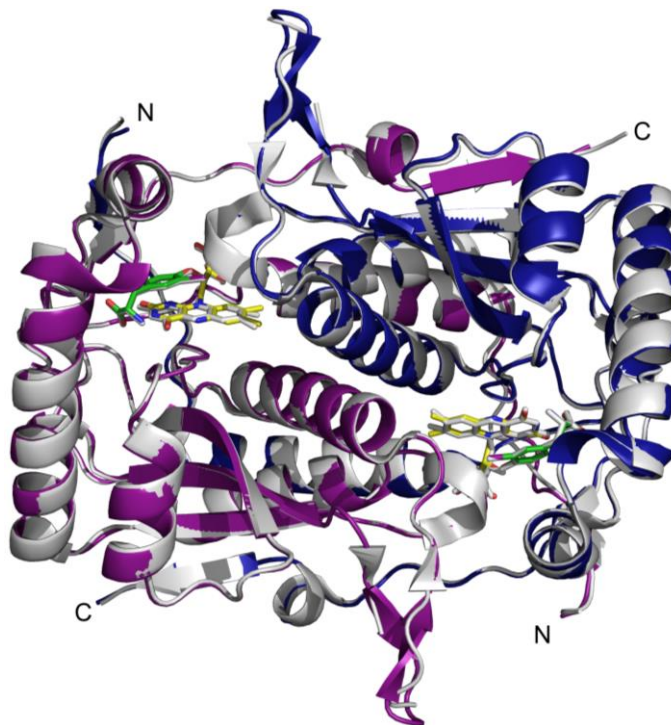


Figure 3-5. Comparison between structures of human and mouse IYD with bound I-Tyr. Individual polypeptides of hIYD•I-Tyr (purple and blue, Protein Data Bank code 4TTC) are overlaid with the corresponding polypeptide structure from mIYD•I-Tyr (gray, Protein Data Bank code 3GFD).

3.3.2 The effect of substrate binding on the reduction of hIYD.

UV visible spectroscopy was used to characterize the bound FMN in hIYD. The absorbance of oxidized hIYD has a maximum at 446 nm and a shoulder around 460 nm. Anaerobic reduction of hIYD by the xanthine and xanthine oxidase system decreases the absorbance at 446 nm rapidly and share an isosbestic point at 325 nm (Figure 3-6 A). The oxidized FMN is reduced to the two-electron reduced FMN without observation of accumulation of one electron

reduced semiquinone. Only oxidized FMN and fully reduced FMN are thermodynamically stable during the course of the titration of hIYD demonstrated the reduction of hIYD exhibits a two-electron transfer process in the absence of ligand.

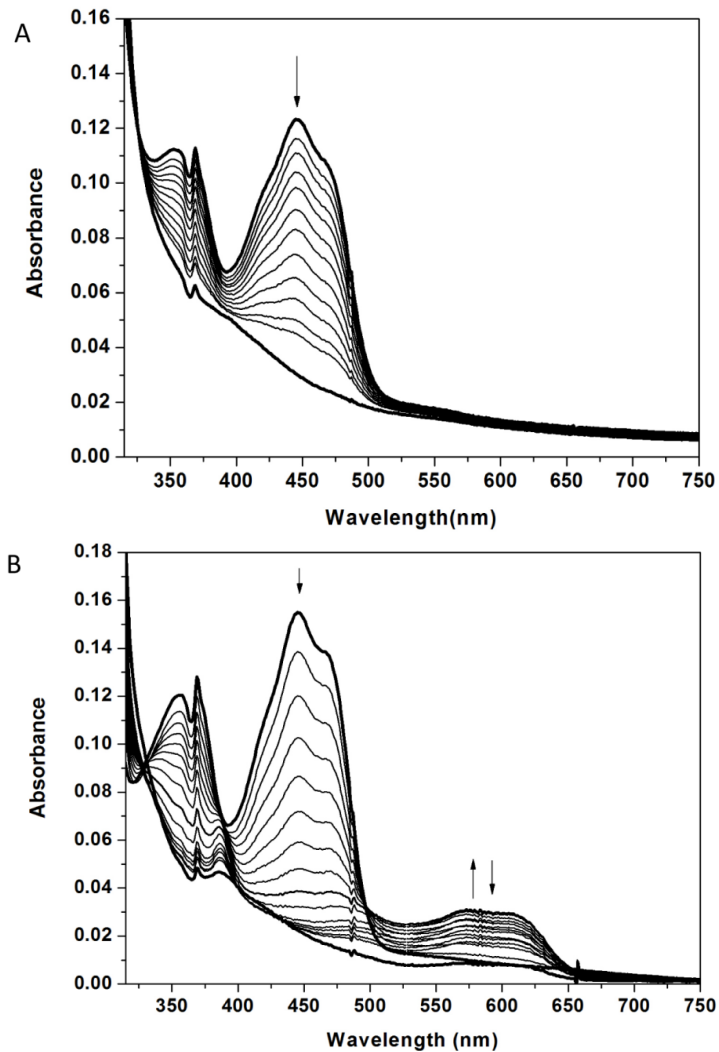


Figure 3-6. Anaerobic reduction of hIYD by xanthine and xanthine oxidase as observed by UV/VIS. A. Arrows at 446 nm indicate direction of absorption change during the reduction process in the absence of F-Tyr; B. Arrows at 590 nm indicate that absorptions were first increase and then followed with decrease in the presence of F-Tyr.

In contrast, in the presence of F-Tyr, spectral changes of hIYD occurring during an equivalent titration indicates the accumulation of neutral semiquinone (Figure 3-6 B) with a peak at 590 nm and a shoulder around 610 nm (32). Accumulation of the neutral semiquinone was observed indicating that the binding of F-Tyr caused a change of the FMN environment significantly enough to stabilize the neutral semiquinone form of FMN (Figure 3-3). Prolonged reduction results in the gradual disappearance of this long wavelength peak and the appearance of the spectrum of fully reduced FMN. As a result, in the presence of F-Tyr, reduction of hIYD leads to two stepwise single electron transfer phases. The first phase is the reduction of oxidized FMN to the neutral semiquinone. The second phase of reduction converts the neutral semiquinone to the fully reduced flavin. Observation of the semiquinone suggests that there is a large separation between the midpoint potentials of the two reduction steps.

3.3.3 The effect of substrate on the redox potential of FMN in hIYD

Redox titration of hIYD was repeated in the presence of suitable redox indicators to determine the redox potential of the FMN cofactor in hIYD. Initial test indicates that the redox potential of anthraquinone-2, 6-disulfonate (AQDS) is comparable to redox potential of $\text{FMN}_{\text{ox/hq}}$ and can be reduced simultaneously with hIYD. This dye was used as the reference dye to measure the midpoint potential of the two electrons couple for $\text{FMN}_{\text{ox/sq}}$. The plot of $\log (\text{FMN}_{\text{ox/hq}})$ versus $\log (\text{AQDS}_{\text{ox/red}})$ gives a slope of 0.96, indicative of two-electron processes for both AQDS and hIYD. A value of - 200 mV for the midpoint redox potential

of $\text{FMN}_{\text{ox/hq}}$ (Figure 3-7) was calculated by Equation 3-4. The E_m of hIYD in the absence of substrate is very similar to the $E_{\text{ox/red}}$ of free FMN (pH 7, - 205 mV) in solution (87).

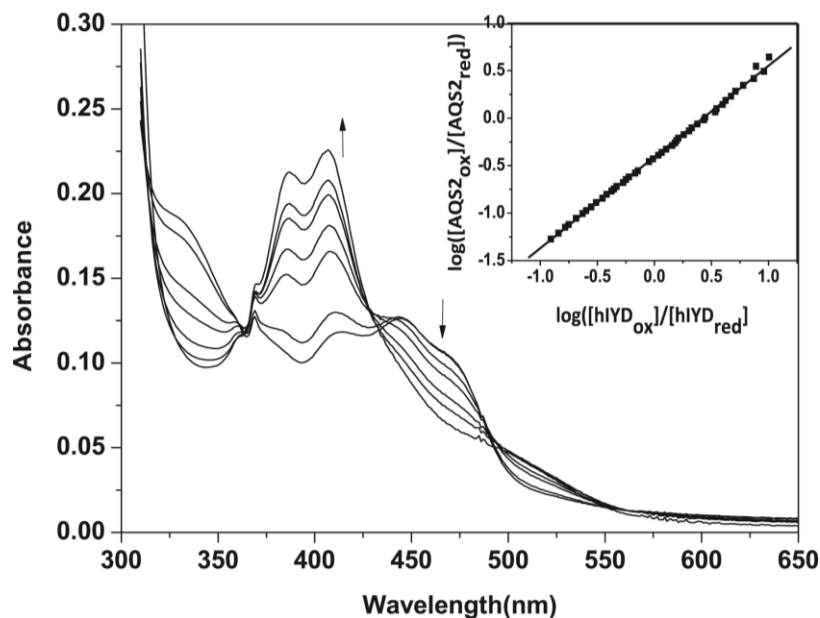


Figure 3-7. Selected spectra for the reduction of hIYD flavin in the presence of AQDS by the xanthine/xanthine oxidase. The reaction was monitored over 120 min. The arrows indicate the direction of the changes in absorbance. Insert: plot of $\log(\text{FMN}_{\text{ox}}/\text{FMN}_{\text{hq}})$ vs $\log(\text{AQDS}_{\text{ox}}/\text{AQDS}_{\text{red}})$. The concentrations of oxidized and reduced AQDS were calculated by the absorbance at 325 nm (the isosbestic point of hIYD). The amount of FMN and FMNH₂ was quantified based on the absorbance at 355 nm (the isosbestic point of AQDS).

As described above, the substrate analogue F-Tyr converts the reduction of hIYD to a stepwise single-electron transfer process. For the reduction of FMN_{ox} to FMN_{sq} , Nile Blue (NB) was observed to be reduced at the same time as the $\text{FMN}_{\text{ox/sq}}$ couple in hIYD. As shown in Figure 3-8, a slope of 1.9 was obtained after plotting the $\log(\text{FMN}_{\text{ox/sq}})$ versus $\log(\text{NB}_{\text{ox/red}})$ indicative of a two-electron process for NB_{ox} to NB_{red} and an one-electron process for FMN_{ox} to FMN_{sq} . The mid-point potential of $\text{FMN}_{\text{ox/sq}}$ was calculated as - 156 mV by Equation 3-4.

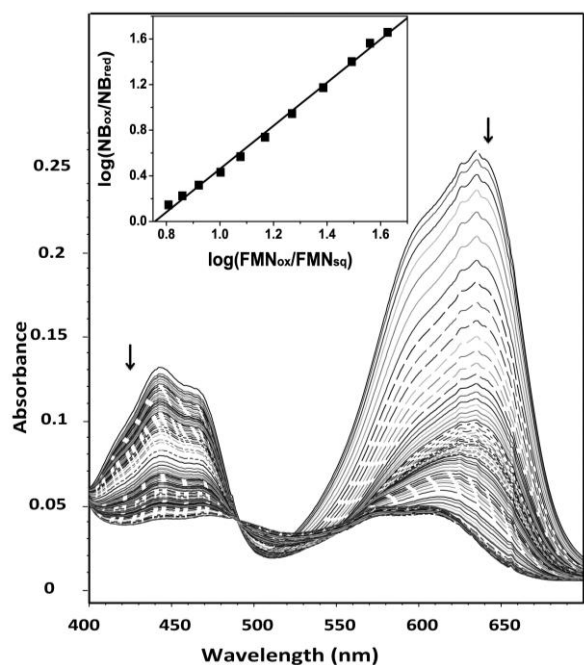


Figure 3-8. Selected spectra showing the reduction of oxidized FMN to neural semiquinone FMN in hIYD in the presence of substrate analogue F-Tyr and NB by xanthine/xanthine oxidase. Insert: plot of $\log(\text{FMN}_{\text{ox}}/\text{FMN}_{\text{sq}})$ vs $\log(\text{NB}_{\text{ox}}/\text{NB}_{\text{red}})$. Concentrations of oxidized forms of dye and flavin were calculated by the absorbance at 450 nm and 650 nm separately.

For FMN_{sq} to FMN_{hq} , Safranin O (SFO) was selected since both FMN_{sq} and dye were reduced concurrently. The plot of $\log(\text{FMN}_{\text{sq/hq}})$ vs $\log(\text{SFO}_{\text{ox/red}})$ should give a slope of 2 since SFO is a two-electron acceptor and FMN_{sq} to FMN_{hq} is a one-electron process. A slope of 1.2 was observed instead (Figure 3-9). A kinetic barrier for the reduction process may lead to this error as reported in other enzyme (88, 89). A value of - 310 mV for the midpoint redox potential of $\text{FMN}_{\text{sq/hq}}$ was obtained after calculation by Equation 3-4.

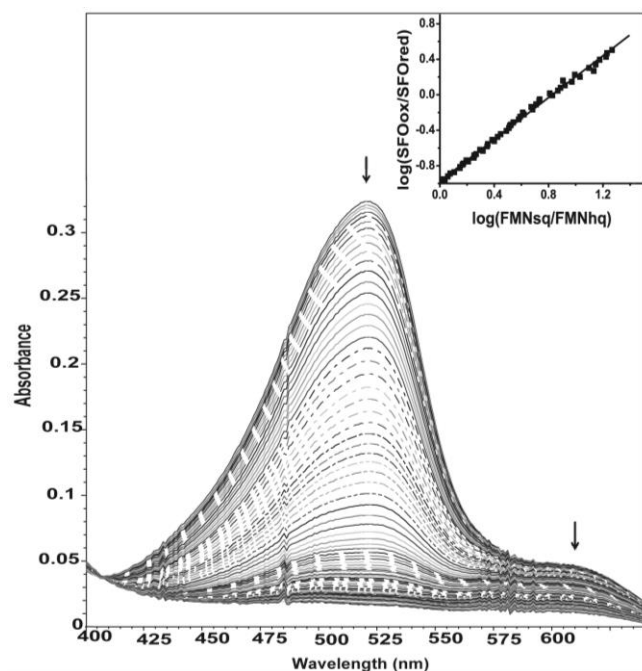


Figure 3-9. Reduction of FMNsq to FMNhq in hIYD in the presence F-Tyr and SFO by xanthine/xanthine oxidase. The arrows indicate the direction of the changes in absorbance. Insert: plot of $\log(\text{FMNsq}/\text{FMNhq})$ vs $\log(\text{SFOox}/\text{SFOred})$. Concentrations of oxidized forms of dye and FMNsq were calculated by the absorbance at 520 nm and 610 nm separately.

The difference between the $E_m(\text{FMN}_{\text{ox/sq}})$ and $E_m(\text{FMN}_{\text{sq/hq}})$ is 154 mV. We could use equation 3-5 and 3-6 to estimate the extent to which semiquinone accumulated before its further reduction (85, 90). K is the semiquinone formation constant, I is the concentration of semiquinone, and S is the total enzyme concentration. According to the calculation, this accumulation corresponds to \approx 99 % FMN_{sq} formation before further reduced to FMN_{hq} .

Equation 3-5.
$$\frac{[I]}{[S]} = \frac{\sqrt{K}}{2+\sqrt{K}}$$

Equation 3-6.
$$E_m(\text{FMN}_{\text{ox/sq}}) - E_m(\text{FMN}_{\text{sq/hq}}) = 2.303 (RT/F) \log K$$

3.3.4 A comparison of the redox properties of hIYD with other flavoprotein

The ability of substrate to promote the stepwise single electron transfer process is consistent with the previous conclusion that BluB and IYD represents a new subfamily of nitro-FMN reductase since BluB are oxygen-insensitive reductase involving a single-electron transfer mechanisms (9, 47). In contrast, all the other members of the nitro-FMN promote a two-electron transfer mechanism. This difference may be caused by the different FMN coordination, especially the difference of N5 H-bonding of FMN as described in chapter 1.

Though unusual in nitro-FMN reductase family, stabilization of the blue neutral form of the flavin semiquinone radical is very common in the flavodoxin family (39). Similar to hIYD, most flavodoxin also establish a very low one-electron reduction potential for the semiquinone-hydroquinone couple and a large separation (>100 mV) between its $E_{\text{ox/sq}}$ and $E_{\text{sq/hq}}$. For example, the midpoint potential for the bounded FMN $E_{\text{ox/sq}}$ and $E_{\text{sq/hq}}$ in the *clostridium beijerinckii* flavodoxin are - 92 mV and - 399 mV at pH 7, respectively (77). For the *Megasphaera elsdenii* flavodoxin, the midpoint potential for the bounded FMN $E_{\text{ox/sq}}$ and $E_{\text{sq/hq}}$ are - 115 mV and - 372 mV at pH 7, respectively (91). For the *Escherichia coli* flavodoxin, the midpoint potential for the bounded FMN $E_{\text{ox/sq}}$ and $E_{\text{sq/hq}}$ are - 244 mV and - 455 mV at pH 7, respectively (39). Large separation (>100 mV) of its two potentials are result from the stabilization and accumulation of the blue semiquinone. A very low redox potential for the $\text{FMN}_{\text{sq/hq}}$ indicates that hydroquinone is unfavorable and does not accumulate. Based on the available structure and mutations in the flavodoxin, unfavorable

electrostatic and aromatic stacking interactions are considered critical for controlling the reduction of flavin. In hIYD, similar π - π stacking between I-Tyr and isoalloxazine ring of FMN are established (Figure 3-10) and may also be necessary for stabilization of FMN_{sq} and destabilization of FMN_{hq}.

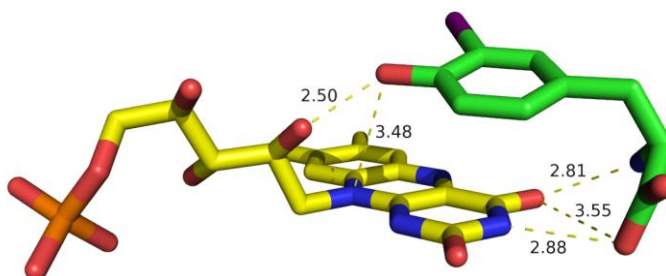


Figure 3-10. Aromatic stacking between I-Tyr and FMN observed in structure of hIYD•I-Tyr. I-Tyr stacks over FMN and establishes numerous polar contacts with FMN in the active site of hIYD. Distances in Å are included.

Ligand binding induces the modulation of the redox property of flavin has also been reported in certain acyl CoA dehydrogenases (72, 73). In these flavoproteins, the electron donating property of reduced flavin was largely affected by the presence of an enoyl CoA product and facilitates the subsequent transfer of its electrons to the electron carrier.

3.4 Conclusion

Solving the crystal structure of hIYD provided the structural base for molecular analysis on hIYD related disease. Association of I-Tyr significantly changes on the coordination surrounding the isoalloxazine ring of FMN. Those changes are similar to those observed in mIYD•I-Tyr including aromatic stacking between I-Tyr and FMN, H-bonding to N5 of FMN, H-bonding interacts between zwitterion region of I-Tyr and the N3 and O4 of the FMN. Those coordination

changes on FMN induced by substrate binding were thought critical for the redox control of FMN.

Redox titration analysis indicates that the substrate binding indeed dramatically affect the redox property of hIYD. The substrate analogue F-Tyr was used in place of I-Tyr in order to observe FMN reduction without catalytic turnover. In the absence of any active site ligand, the midpoint potential is similar to that of FMN in solution and only FMN_{ox} and FMN_{hq} could be observed during reduction. In contrast, a neutral FMN_{sq} became a distinct intermediate during reduction of FMN_{ox} upon F-Tyr binding to hIYD indicating a definitive switch to a stepwise one-electron reduction process. According to our current knowledge, this is the first report of substrate binding inducing stabilization of neutral semiquinone in flavoprotein.

Chapter 4: The role of H-bonding to FMN N5 in hIYD for redox control and deiodination

4.1 Introduction

Electron transfer is essential for the catalytic reactions of most flavoproteins. Protein must tightly control the lifetimes of flavin radical intermediates to facilitate the electron transfer. The N5 atom of the flavin ring is one of the most important positions for redox control since the N5 atom can either be a hydrogen bond donor or acceptor based on its redox state (92). Forming or breaking a N5 H-bond could control of the lifetime of the semiquinone flavin. Moreover, the strength of hydrogen bond to N5 was also shown to have a significant influence on the redox states of flavoprotein (75, 78, 93, 94).

As described in Chapter 3, substrate binding induces the stabilization of the neutral semiquinone form of FMN and converts the reduction of FMN from a single two-electron transfer process to two stepwise single electron transfer processes. Structural comparison of hIYD and hIYD•I-Tyr indicated that substrate binding induces a movement of the OH side chain of Thr239 toward the N5 atom of the FMN allowing the formation of H-bonding between them. As shown in Figure 4-1, the Thr239 is the turn between two helices of the active site lid. Substrate binding causes the rearrangement of the turn, the distance between the OH group of Thr239 and N5 of FMN changed from 4.8 Å to 3.1 Å.

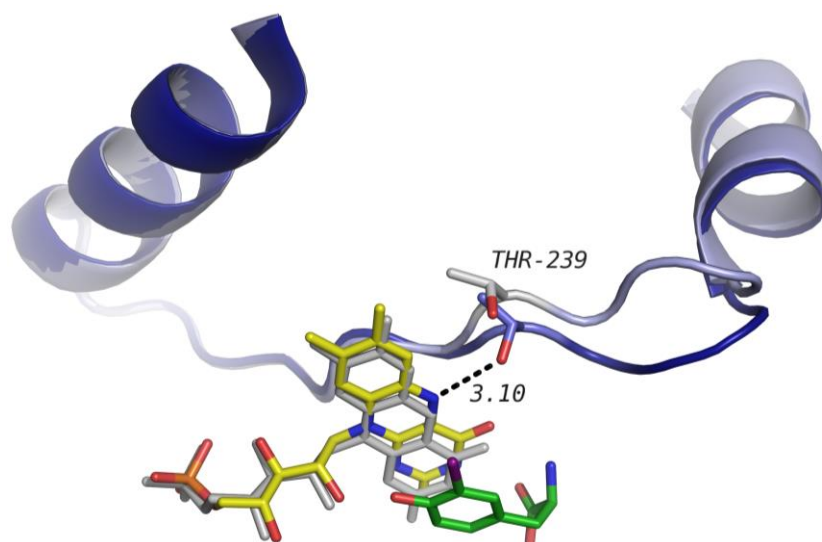


Figure 4-1. Substrate binding induces the movement of Thr239 toward N5 of FMN. For hIYD•I-Tyr (PDB ID: 4TTC), residues are in deep blue, FMN in yellow and I-Tyr in green. In hIYD (PDB ID: 4TTB), residues are shown in light blue and FMN are in gray.

This N5 H-bond of FMN in hIYD is similar to the N5 H-bond of FMN in BluB, its closest member in the nitro-FMN reductase superfamily. In BluB, the N5 H-bond of FMN is also derived from an OH side chain (Ser167). Based on current publications on the nitro-FMN reductase family, hydrogen bonding between protein and the N5 of the isoalloxazine ring is very common but usually derives from the N-H backbone as indicated in Table 4-1. For example, the N5 hydrogen bonds in NTR, FRase 1, FRP, NOX, NfsA and RdxA1 are derived from the backbone N-H and all of them are oxygen-insensitive reductases that supporting only two electron reduction processes. However, BluB is shown oxygen-sensitive and able to promote one electron transfer to activate its substrate, molecular oxygen. This in turns implies a stepwise one electron reduction process. Moreover, the Ser 167 of BluB was also found critical to the catalytic activity, mutation of Ser 167 to Gly reduces the product formation 30-

fold, and mutation to Cys caused complete loss of activity (47). Considering the importance of N5 H-bonding for stabilization of the flavin radical in other flavoproteins and the similarity of N5 H-bonding in IYD and BluB, we assumed that this N5 H-bonding in hIYD•I-Tyr may represent the primary coordination to stabilize of semiquinone.

Table 4-1. The N5 H-bonding of FMN in nitro-FMN reductase superfamily.

Protein	PDB code	To N5	Group	ET process	Reference
hIYD	4TTC	Thr239	OH side chain	1e ?	
BluB	2ISJ	Ser167	OH side chain	1e	(47)
NTR	1DS7	Glu165	NH back bond	2e	(95)
FRase I	1VFR	Glu165	NH back bond	2e	(96)
FRP	2BKJ	Gly130	NH back bond	2e	(49)
NOX	1NOX	Leu158	NH back bond	2e	(48)
NfsA	1F5V	Gly130	NH back bond	2e	(97)
RdxA	3QDL	Gly162	NH back bond	2e	(98)

To understand the significance of N5 H-bond of FMN in semiquinone stabilization and deiodination process of IYD, mutation of Thr239 to Ser and Ala is generated in this chapter. Mutant T239A removes the OH group to eliminate the N5 H-bond between OH of Thr239 and N5. However, N5 may still form a H-bond with H₂O in T239A if there is any water molecule close to the N5 of FMN. To provide more information on the interactions to the N5 of FMN in T239A mutants, a crystal structure of T239A•F-Tyr is also presented. The redox property of the both mutants in the presence and absence of ligand were also investigated and compared with wild type hIYD to illustrate the importance of N5 H-bond in

redox control in hIYD. The kinetics of deiodination was also measured in this chapter to understand the significance of N5 H-bond in catalytic process.

4.2 Materials and Methods

4.2.1 General methods

Proteins were expressed in Rosetta2 DE3 *E.coli* and purified by two steps (Ni²⁺ column and size exclusion column) as described in Chapter 2. Redox titration was performed by the xanthine/xanthine oxidase method as described in Chapter 3. UV measurements were obtained with a Hewlett-Packard 8543 spectrophotometer. Fluorescence titration was used to measure the dissociation constant of ligands as described in Chapter 2. Kinetics parameters were determined by radioactive assay using [¹²⁵I]-diiodotyrosine as substrate and dithionite as reducing reagent as reported previously. Assays were performed in triplicate. The data were averaged and fit to the Michaelis-Menten equation by Origin 7.0 (Northampton, MA). Errors of K_m and V_{max} represent the error of fitting.

4.2.2 Site-directed Mutagenesis

Site-directed mutagenesis was performed on plasmid pETSUMO-hIYD to generate the T239S and T239A mutants. T239S was created by using primer 5'-GGTGACTGTCACCACGAGTCCTCTCAACTGTGGCC-3' and its complement 5'-GGCCACAGTTGAGAGGACTCGTGGTGACAGTCACC-3'. T239A mutant was generated by using a forward primer of 5'-

CTGGTGACTGTCACTACGGCGCCTCTCAACTGTGGCC -3' and its complement 5'-GGCCACAGTTGAGAGGGCGCCGTAGTGACAGTCACCAG-3'. Mutations were confirmed by sequencing. The mutants were transformed to electro-competent cell Rosetta 2(DE3) *E.coli* for expression.

4.2.3 Crystallization of hIYDT239A·F-Tyr

To obtain the hIYDT239A·F-Tyr co-crystal, hIYDT239A was pre-incubated with 3 mM F-Tyr. hIYDT239A·F-Tyr crystallized in approximately 2 days at 20 °C by the hanging drop diffusion method with a ratio of 0.8 μ l hIYDT239A (11.7 mg/ml, 50 mM sodium phosphate (pH 7.4), 100 mM NaCl, 1 mM DTT, 10 % glycerol) to 1 μ l precipitant containing 0.17 M sodium acetate, 85 mM Tris-HCl (pH 8.5), 22.5 % w/v polyethylene glycol 4,000 and 15 % glycerol. The crystals were flash frozen in liquid nitrogen. X-ray diffraction data were collected at National Synchrotron Light Source beamline X-25. All collected data were processed using HKL2000 package (83). Molecular replacement was performed by PHASER within the CCP4 program suite using a dimer of mIYD·I-Tyr (PDB code 3GFD) with all heteroatoms removed and B-factors set to 20.0 (square Angstroms) (44, 99). Three iterations of PHASER were performed to yield a model with six monomers per asymmetric unit, as predicted by Matthews coefficient calculations. Iterative manual model building and addition of water molecules, FMN, and the F-Tyr ligand were performed in COOT and refined by Refmac in CCP4 (100). The final refinement statistics are summarized in Table 4-2. All structure figures were prepared with Pymol.

Table 4-2. Data collection and refinement statistics for hIYDT239A.

Protein	hIYDT239A-FMN-F-Tyr
Ligands	FMN and F-Tyr
Data collection	
Space group	$P6_1$
No. Molecule/ASU	6
Unit cell parameters (Å, °)	$a = 105.079,$ $b = 105.079,$ $c = 300.202$ $\alpha = 90, \beta = 90, \gamma = 120$
Resolution range (Å) ^a	49.59-2.30
No. of observed reflections	661766
No. of unique reflections ^a	82734 (5790)
Completeness ^a	100 (100)
Redundancy ^a	8.0 (8.2)
R_{sym} (%) ^a	9.3 (35.1)
$I/\sigma I$ ^a	41.5 (6.5)
Wilson B factor (Å ²)	37.46
Refinement	
Resolution used in refinement (Å)	46.52-2.30
No. of reflections used in working set	78650
No. of reflections for R_{free} calculation	4144
R_{work} (%), R_{free} (%)	18.30, 22.58
No. atoms	
Protein	11102 (A-F)
Hetero atoms	186/84 (FMN and YOF)
Solvent	386
Mean B -factor (Å ²)	
Protein	48.8
FMN	38.3
F-Tyr	37.7
Solvent	42.7
RMSD from ideality	
Bond lengths (Å)	0.012
Bond angles (deg.)	1.543
Ramachandran analysis	
Favored (%)	97.5
Allowed (%)	2.5
Outliers	0

^a Numbers in parentheses are outer shell parameters.

4.3 Results and Discussion

The H-bond between N5 of FMN and Thr239 in the structure of hIYD·I-Tyr was assumed critical for stabilization of the semiquinone FMN. To understand the importance of N5 H-bond on the redox control of FMN in hIYD, mutants T239S and T239A were generated individually by standard site-directed mutagenesis. The mutants alter or eliminate the hydrogen bond donor to N5 atom of FMN. Both mutants were expressed in *E.coli* in a soluble form. After purification, >95 % pure proteins were obtained. The binding affinities of the mutants with ligands (I-Tyr and F-Tyr) were determined before the redox analysis.

Table 4-3. Characterization of mutants T239S and T239A.

			hIYD	hIYDT239S	hIYDT239A	
K _D	I-Tyr	μM	0.15 ± 0.04	0.37 ± 0.07	0.20 ± 0.05	
	F-Tyr	μM	1.3 ± 0.3	3.3 ± 0.5	1.5 ± 0.2	
Kinetics	K _M	μM	31 ± 6	17 ± 3.9	55 ± 10	
	k _{cat}	min ⁻¹	12.5 ± 1.0	12 ± 1.5	3.4 ± 0.5	
	k _{cat} /K _M	μM ⁻¹ min ⁻¹	0.4 ± 0.1	0.7 ± 0.17	0.06 ± 0.01	
Redox titration	- F-Tyr	E _m (FMN _{ox/hq})	mV	-200 ± 4	-206 ± 3	-215 ± 4
	+ F-Tyr	semiquinone		99 %	55 %	N/D
		E _m (FMN _{ox/sq})	mV	-156 ± 2.3	~ -234	E _m (FMN _{ox/hq}) -272 ± 4
		E _m (FMN _{sq/hq})	mV	-310 ± 3.5	-	

4.3.1 Influence of N5 H-bond on ligand binding property

The K_D values of T239S and T239A for I-Tyr and F-Tyr were measured by fluorescence titration (Appendices D) and summarized in Table 4-3. The binding affinity of the mutants to I-Tyr and F-Tyr are very similar to wild type hIYD. Both mutants exhibit tight binding to native substrate I-Tyr, K_D for T239S

and T239A are 0.37 μM and 0.20 μM , respectively. The K_D of the substrate analogy-F-Tyr for wild type hIYD is 10 fold more than I-Tyr. Similar binding properties of F-Tyr were observed in T239S and T239A, K_D for T239S and T239A are 3.3 μM and 1.5 μM , respectively. The equilibrium binding studies indicated that mutation of T239 to S or A has very little effect on the binding property of substrate. Substrate binding induces the conformational changes in the active site of wild type hIYD. Similar ligand binding property between wild type and mutants may imply a similar overall conformational change induced by substrate binding in mutants and wild type. The major difference in FMN coordination expected between wild type and mutant should be the loss of the N5 H-bond due to the missing OH group in the T239A mutant. However, H-bonding may still possible if there is any H_2O molecule appearing close enough to the N5 atom of FMN.

4.3.2 Crystal structure determination of hIYDT239A•F-Tyr

To provide a clear picture of FMN coordination in hIYDT239A in the presence of ligand, the crystal structure of hIYDT239A•F-Tyr was solved. As shown in Figure 4-2, the overall structure of hIYDT239A•F-Tyr is very similar to the hIYD•I-Tyr (RMSD of 0.192 Å for a 405 atom comparison). F-Tyr binding induces the formation of the active site lid covering the FMN and F-Tyr. A close look at the F-Tyr binding site is shown in Figure 4-2B. All the conformations of the key residues that are critical for substrate binding, including Tyr161, Lys182, Glu157 and Ala130, are very similar in both structures (hIYDT239A•F-Tyr and

hIYD•I-Tyr). The Ala239 is far away from the ligand bound. Mutation Thr239 to Ala was shown to cause negligible effect on the structure of the binding site. This structural information is consistent with the binding affinity results of F-Tyr, in which both T239A mutant and wild type hIYD have similar K_D (1.3 for wild type, 3.3 for T239A).

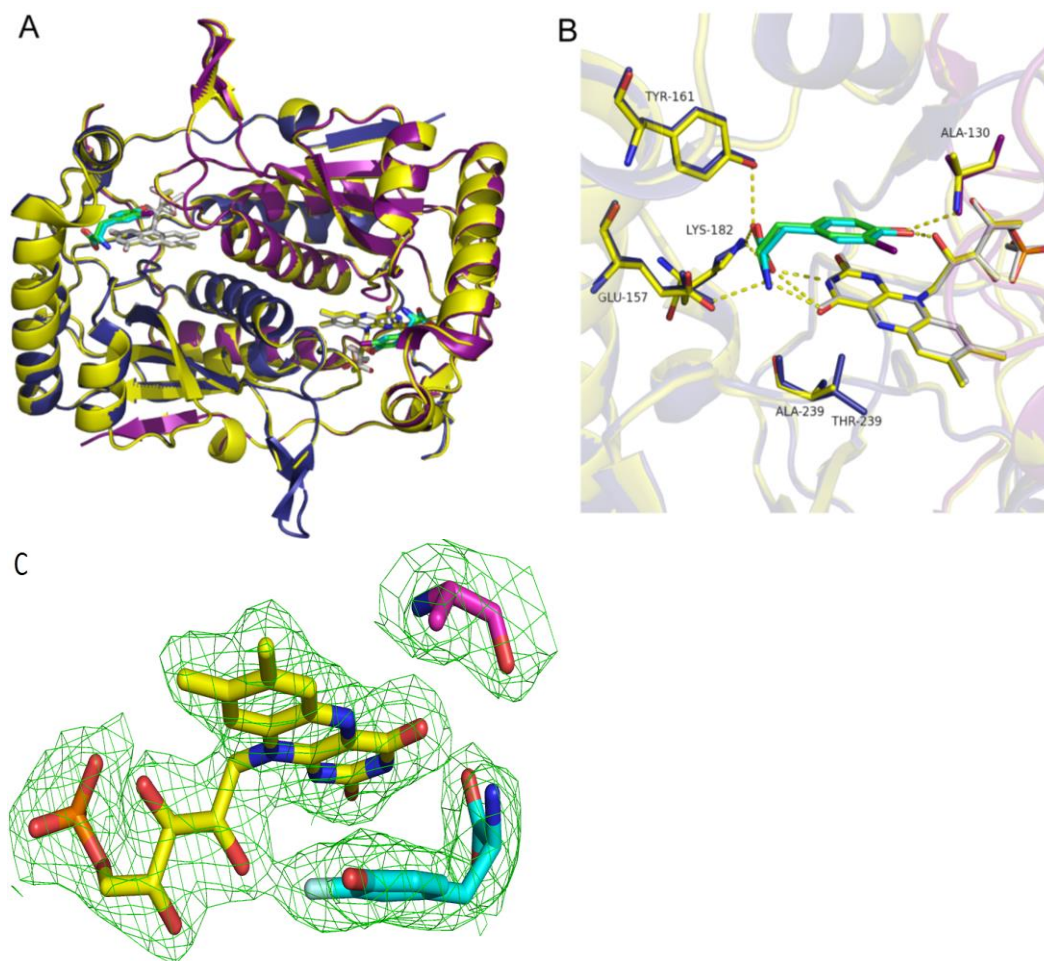


Figure 4-2. A) Structural compare of hIYDT239A•F-Tyr and hIYD•I-Tyr. B) Ligand binding environment in both hIYDT239A•F-Tyr and hIYD•I-Tyr. C) The omit map of Ala239, FMN and F-Tyr (2F0-Fc, contoured at 1 sigma). All the residues from hIYD•I-Tyr are in blue and purple. F-Tyr is in cyan. I-Tyr is in green. FMN from hIYDT239A•F-Tyr is in yellow. FMN from hIYD•I-Tyr is in gray.

Figure 4-3 indicated the comparison of FMN coordination in hIYDT239A•F-Tyr with hIYD•I-Tyr. The notable difference in FMN coordination between them is the interactions between T239/A239 and FMN. As expected, mutation Thr239 to Ala239 eliminates the N5 H-bonding. Moreover, no electron density was detected in structure of hIYDT239A•F-Tyr that may represent a water molecule that could form H-bond with N5 atom of FMN. All the key residues that interact with FMN are superimposable in both structure, including the Ser 102 and 128, Arg 100, 101, 104 and 279.

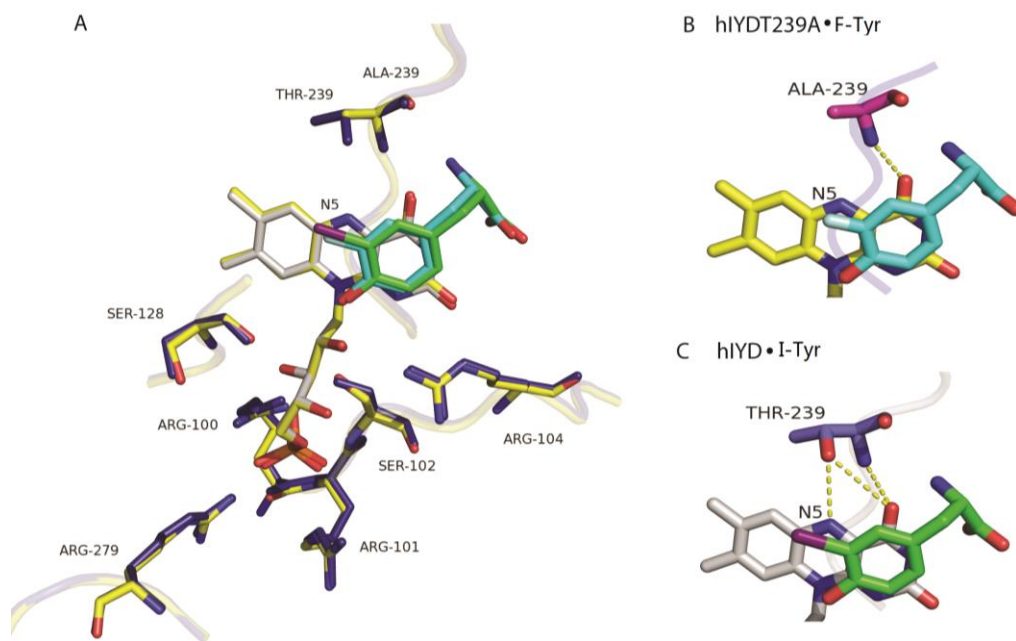


Figure 4-3. FMN coordination in hIYDT239A•F-Tyr and hIYD•I-Tyr. A) overlap the structures of hIYDT239A•F-Tyr and hIYD•I-Tyr. B) and C) show the close look at the FMN and residue 239 interaction. I-Tyr is in green, F-Tyr is in light blue, FMN from hIYDT239A•F-Tyr is in yellow and FMN from hIYD•I-Tyr is in gray. All the residues from hIYD•I-Tyr are shown in blue and purple. Residues from hIYDT239A•F-Tyr are shown in yellow.

4.3.3 Influence of mutation on redox property of FMN

The crystal structure of hIYDT239A•F-Tyr indicated the loss of H-bonding to N5 of FMN. To demonstrate the role of N5 H-bonding in redox control of hIYD, the redox property of FMN in T239S and T239A mutants in the presence and absence of F-Tyr were analyzed by xanthine/xanthine oxidase method as described previously.

4.3.3.1 The redox properties of mutants in the absence of F-Tyr

In the absence of F-Tyr, the oxidized FMN bound to both hIYDT239S and hIYDT239A have an absorbance maximum at 446 nm and a shoulder near 460 nm (Appendices E). This absorbance decreased during reduction by xanthine and xanthine oxidase and ultimately generated a spectrum consistent with the fully reduced FMN_{hq}. The redox titration spectra of both mutants are very similar to the native hIYD as described in chapter 3. Only FMN_{ox} and FMN_{hq} were detected during the titration of hIYDT239S and hIYDT239A, indicating a two-electron transfer process in the absence of F-Tyr (Appendices E). The redox potentials of the FMN_{ox/hq} were then measured to test if there is any change on the redox potential caused by mutation. The anthraquinone-2-sulfonate (AQS, -225mV) was selected as the reference dye for both mutants since AQS and FMN could be reduced simultaneously. The absorbance at 355 nm, an isosbestic point for AQS, was used for calculating the amount of the oxidized and reduced FMN. The absorbance at 330 nm and 328 nm, the isosbestic points for reduction of

hiYDT239S and hiYDT239A, respectively, were used for calculating the amount of the oxidized and reduced dye.

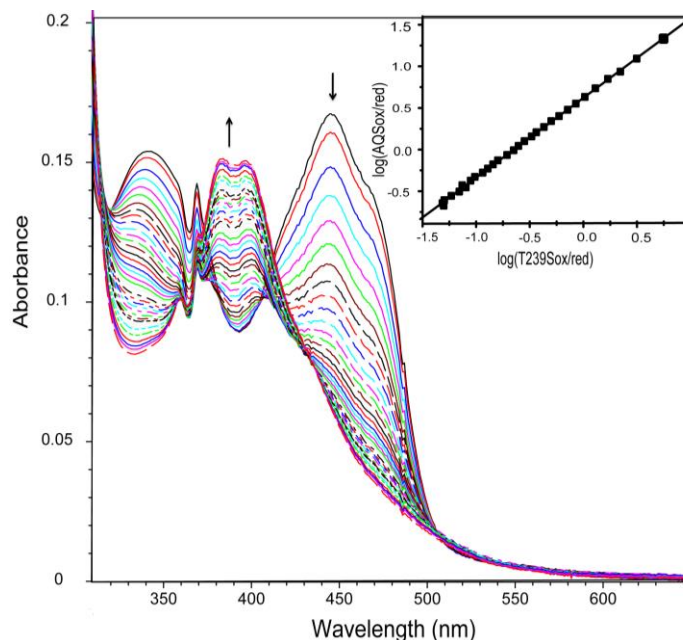


Figure 4-4. Reduction of FMN bound to hiYDT239S and the reference dye AQS by xanthine/xanthine oxidase. Spectral changes were monitored every 2 min over a total of 120 min. Only a selected number of spectra are illustrated for clarity and the arrows indicate the direction of the absorbance change. The concentration of reduced AQS was measured at 330 nm, an isosbestic point for hiYDT239S, and conversely the concentration of reduced hiYD was measured at 355 nm, the isosbestic point of AQS. Insert: the linear best fit of $\log(\text{T239Sox/red})$ versus $\log(\text{AQSox/red})$ was used to calculate the midpoint potential.

As illustrated in figure 4-4, plot of $\log(\text{T239S}_{\text{ox/red}})$ versus $\log(\text{AQS}_{\text{ox/red}})$ gave a slope of 1.03, indicating that T239S was reduced via a two-electron process by xanthine/xanthine oxidase. The midpoint potential calculated from this plot is -206 mV. A plot of $\log(\text{T239A}_{\text{ox/red}})$ versus $\log(\text{AQS}_{\text{ox/red}})$ gave a slope of 0.92, indicating that T239A was also reduced via a two-electron process in the absence of substrate (Figure 4-5). The midpoint potential for $\text{T239A}_{\text{ox/red}}$ was calculated to be -215 mV by method as described in Chapter 3. The midpoint

potential for T239S and T239A (-215 mV) are similar to the wild-type enzyme hIYD (-200 mV) (Table 4-3). In the absence of substrate, the E_m of wild-type hIYD, T239S and T239A mutants are all very close to the $E_{ox/red}$ of free FMN (pH 7, -205 mV) in solution (79). This result is reasonable since the FMN binding site is open to the solvent in the absence of substrate. The distance between the OH side chain of Thr239 and the N5 of FMN ring was measured as 4.8 \AA , which doesn't allow for H-bonding with N5. As a result, the mutation T to S or A did not cause dramatic change of the redox properties of FMN in the absence ligand.

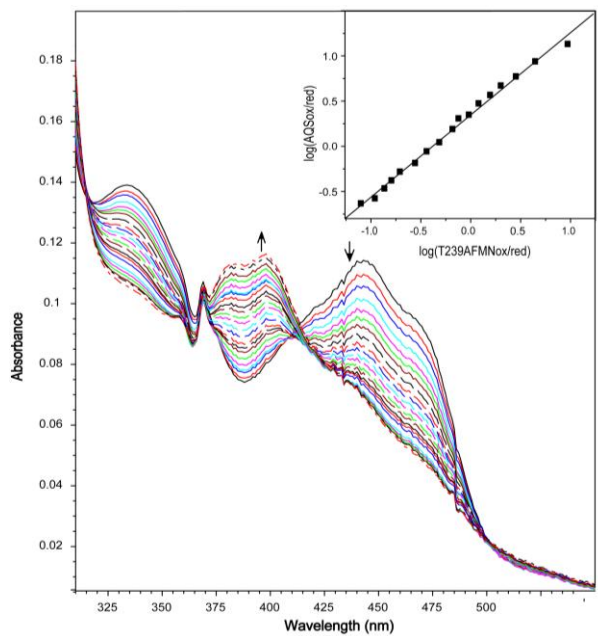


Figure 4-5. Reduction of hIYDT239A and the reference dye AQS by xanthine/xanthine oxidase. The concentration of reduced AQS was measured at 328 nm and 355 nm, the isosbestic point for hIYDT239A and AQS, respectively. Insert: the linear best fit of $\log(T239Aox/red)$ versus $\log(AQSox/red)$ was used to calculate the midpoint potential.

4.3.3.2 Redox titration of T239S and T239A mutants in the presence of F-Tyr

As described in Chapter 3, neutral semiquinone accumulated during the titration of wild type hIYD in the presence of F-Tyr. In contrast, no stable neutral semiquinone FMN could be detected during the reduction of T239A (Figure 4-6 B). According to the structure of hIYDT239A•F-Tyr, mutation T239 to A causes

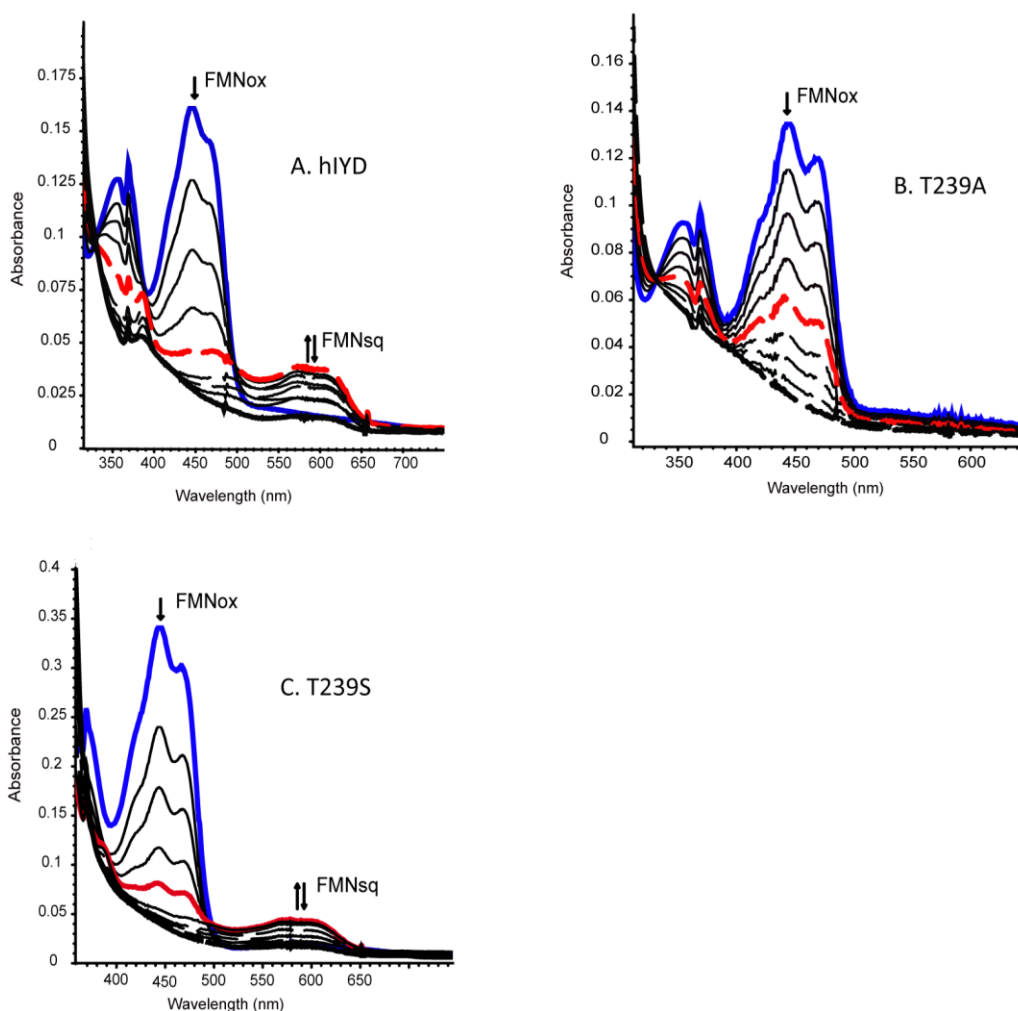


Figure 4-6. Reduction of hIYD (A), hIYDT239A (B) and hIYDT239S (C) in the presence of F-Tyr by xanthine/xanthine oxidase. A spectral intermediate with a λ_{max} of 590 nm was observed in reduction of both hIYDT239S and hIYD (red line-maximum accumulation). In contrast, this intermediate wasn't observed in reduction of hIYDT239A (red line – no 590 nm peak). Blue line represents the starting spectra.

the loss of the OH side chain and its H-bond to N5 atom of FMN. The lack of neutral semiquinone observed in T239A mutant indicates that the H-bond between the OH side chain of T239 and N5 of FMN is very critical to the stabilization of the semiquinone.

As shown in Figure 4-7, safranin O (SFO, -280 mV) was used as the reference dye to measure the redox potential of T239A_{ox/hq}. The absorbance at 520 nm, the maximum absorbance of SFO, and the absorbance at 445 nm after correcting for the SFO absorbance at 445 nm were used for calculating the amount of the SFO and FMN, respectively. A slope of 0.9 was obtained after plotting the $\log(\text{T239AFMN}_{\text{ox/red}})$ versus $\log(\text{SFO}_{\text{ox/red}})$, indicative of the two-electron process for T239A oxidized FMN to hydroquinone FMN. The midpoint redox potential for T239AFMN_{ox/hq} was calculated to be -272 mV.

For hIYD T239S mutant (Figure 4-6 C), in the presence of F-Tyr, an absorption peak was observed at 590 nm regions, suggesting the formation of a neutral semiquinone species during the reduction. However, as indicated by the absorbance at 595 nm, the maximum accumulation of the semiquinone in the T239S mutant is 55 % compared to 99 % from FMN_{ox} to FMN_{sq} for wild type hIYD. This difference may be caused by the missing methyl group, which alters the position of the OH side chain relative to N5 atom. T239S mutants may result in a weaker of hydrogen bond and a decrease in the stabilization of the semiquinone FMN. The redox potential of FMN_{ox/sq} for T239S mutants was close to the dye phenosafranine (PSF, -259 mV). The absorbance at 494 nm, an isosbestic point for reduction of oxidized T239S to semiquinone T239S, was used

for calculating the amount of the dye PSF (Figure 4-8). The absorbance at 445 nm after correcting for the PSF absorbance at 445nm was used for calculating the amount of the oxidized FMN. The plot of $\log(\text{T239SFMN}_{\text{ox/sq}})$ versus $\log(\text{PSF}_{\text{ox/red}})$ should give a slope of 2 since oxidized FMN to semiquinone FMN is a one-electron process. However, a slope of 1.4 was found. The midpoint potential for $\text{T239AFMN}_{\text{ox/sq}}$ was calculated to be -234 mV, which is 80 mV lower than the wild type $\text{hIYD}_{\text{ox/sq}}$ (-156 mV). The redox potential for the second phase $\text{FMN}_{\text{sq/hq}}$ in hIYDT239S wasn't determined due to lack of obvious starting point of reduction from FMN_{sq} to FMN_{hq} .

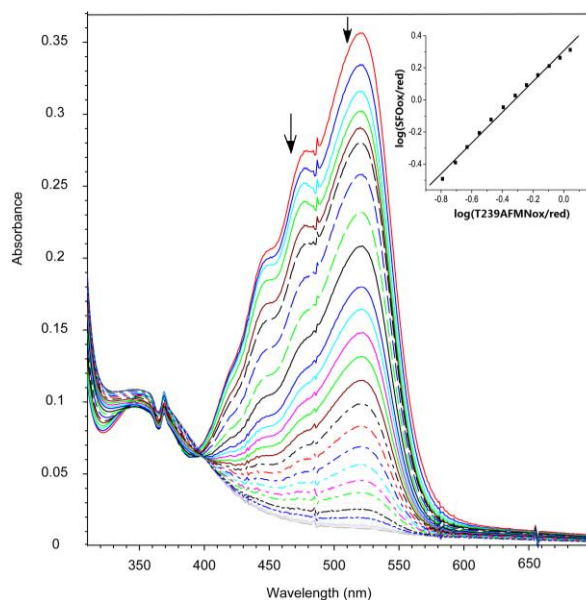


Figure 4-7. Reduction of hIYDT239A in the presence of F-Tyr and the dye SFO by xanthine/xanthine oxidase. Concentration of oxidized FMN_{ox} was measured at 445 nm after correcting for the SFO absorbance. SFO concentration was measured at 520 nm. Insert: the linear best fit of $\log(\text{T239AFMN}_{\text{ox/red}})$ versus $\log(\text{SFO}_{\text{ox/red}})$ was used to calculate the midpoint potential.

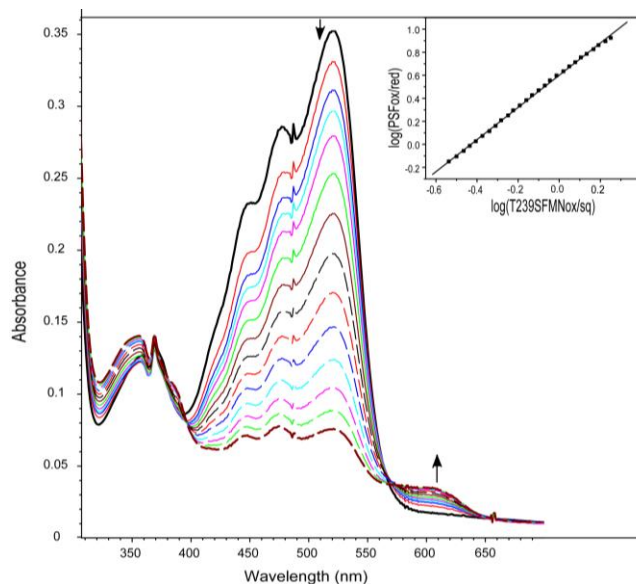


Figure 4-8. Reduction of hIYDT239S in the presence of F-Tyr and the dye PSF by xanthine/xanthine oxidase. Concentration of oxidized FMNox was measured at 445 nm after correcting for the PSF absorbance. PSF concentration was measured at 494 nm, an isosbestic point for reduction of oxidized FMN to semiquinone in T239S. Insert: the linear best fit of $\log(\text{T239SFMNox/sq})$ versus $\log(\text{PSF}_{\text{ox/red}})$ was used to calculate the midpoint potential.

The redox titration of the mutant enzyme indicated that the N5 H-bond induced by ligand binding is very important for the redox property of hIYD. The mutant T239S exhibited a lower $E_{\text{ox/sq}}$ by 90 mV. Accumulation of semiquinone was still presented (55 % compared with 99 % for wild type). However, Mutant T239A significantly alters the redox property of $E_{\text{ox/sq}}$ and largely destabilizes the semiquinone. No semiquinone was observed for the reduction of T239A mutant. Similar N5 H-bonding had been reported in other flavoenzyme and also found critical for the stabilization of the semiquinone. For example, in the electron transfer protein from methylotrophic bacterium W3A1, the N5 of the FMN cofactor is hydrogen bonded to the side-chain OH group of Ser 254. A highly stabilized anionic flavin semiquinone was observed in oxidized W3A1 (78).

Mutations Ser254 to Thr, Cys and Ala were characterized to investigate the effect on the redox potential of $\text{FAD}_{\text{ox/sq}}$. Replacing Ser254 with Thr decreased $E_{\text{ox/sq}}$ by 90 mV. This difference may be caused by additional methyl group, which alter the position of the OH side chain relative to N5 atom. Ser254Cys and Ser254Ala mutants result in a weaker or absence of hydrogen bonding, decreased $E_{\text{ox/sq}}$ by 105 mV and 120 mV, respectively, indicating that the N5 H-bonding is critical for establishing an high $E_{\text{ox/sq}}$ to stabilize the anionic semiquinone.

4.3.4 Influence of an H-bond to FMN N5 on deiodination activity

Redox titration indicated that mutation of Thr239 to Ala significantly affects the stabilization of the FMN semiquinone, which may also affect catalytic. To test this, the deiodination activities of T239S and T239A mutants of hIYD were determined (Appendices C) by radioactive assay as described in Chapter 2.

The kinetic behavior of the hIYD T239S mutant is very similar to the wild type hIYD (Table 4-3). The K_M of T239S is 17 μM for substrate $\text{I}_2\text{-Tyr}$, which is slightly lower than the wild type 31 μM . The k_{cat} (12 min^{-1}) and k_{cat}/K_M (0.7 $\mu\text{M}^{-1}\text{min}^{-1}$) of T239S are also very close to the k_{cat} (12.5 min^{-1}) and k_{cat}/K_M (0.4 $\mu\text{M}^{-1}\text{min}^{-1}$) of wild type. Mutation T239 to S has a slight effect on the deiodination process. The kinetics study on the T239A mutant indicates that T239A is still active. The K_M of T239A is 50 μM for substrate $\text{I}_2\text{-Tyr}$, which is slightly higher than the wild type 31 μM . However, the k_{cat}/K_M of T239A (0.06 $\mu\text{M}^{-1}\text{min}^{-1}$) is around ten-fold less than wild type hIYD. This result is very interesting and leads to an assumption that the semiquinone stabilization is important for the

deiodination process. Disabling the stabilization of the semiquinone could not completely disable the deiodination, however, could largely slow the process.

4.4 Conclusion

Substrate binding induced the formation of N5 H-bond from the OH side chain of Thr239 in hIYD. This H-bond is similar to one found in BluB. Otherwise, this type of H-bonding is very uncommon in nitro-FMN reductase family. The N5 H-bond in hIYD was assumed to be critical for the stabilization of the semiquinone. Mutations T239 to S and A were generated to alter or eliminate the N5-H bond of FMN. Structural analysis indicated that the mutant T239A successfully removed the N5 H-bond but kept all the other FMN interactions. Binding analysis indicated that elimination of N5 H-bond has a negligible effect on the binding of the ligands F-Tyr and I-Tyr. Redox analyses show that N5 H-bond is very important for the stabilization of semiquinone. Mutant T239A was unable to stabilize the semiquinone. Kinetic study illustrated that the k_{cat}/K_M of T239A is 10 fold less than wild type, suggesting that stabilization of the semiquinone is important for the deiodination process of hIYD and providing more evident for the catalytic mechanism of hIYD through stepwise one-electron transfer processes.

Chapter 5: Importance of the zwitterion region of I-Tyr for recognition and catalysis by hIYD

5.1 Introduction

In most flavoproteins, protein side chains and backbone provide direct contacts to the isoalloxazine ring of FMN. For example, in FRP, the O²-N3-O⁴ edge of isoalloxazine is stabilized by H-bonds from backbone of Gly130 and Gly131, and side chains of Gln67, Tyr67 and Arg15 (49). In BluB, the closest member of the nitro-FMN reductase family to IYD, the interactions to O²-N3-O⁴ are much less than FRP and involve only backbone of Ser167 and Leu108 and Arg34 side chain (47). The O²-N3-O⁴ edge coordination of FMN in hIYD is primary from the zwitterion region of substrate instead provided by residues of protein. As shown in Figure 5-1C, only Arg 104 is available to form a polar contact with the isoalloxazine ring of FMN at O2 in the absence of substrate. No polar contact to the N3O4 of the FMN ring was observed from the crystal structure of hIYD. In the presence of substrate (Figure 5-1), the carboxylate group of I-Tyr is H-bonding to N3 atom of FMN (distance is 2.9 Å). Both the α -ammonium and carboxylate groups of I-Tyr are able to form H-bonds to the O4 atom (distance 2.8 Å and 3.5 Å). Thr239 also forms H-bond to the O4 atom of FMN.

The role of N3 H-bonding at FMN for redox control is unclear though the N3 H-bonding is common in flavoproteins. Initially it was suggested that the primary function of N3 H-bond is to facilitate the FMN binding (101). Later

studies suggested that N3 H-bond contributed to the stabilization of the oxidized form FMN. Using N3 methyl derivatives precluding the N3 interactions, a lower midpoint potential for the oxidized to semiquinone couple was created (102). In the flavodoxin from *Closteridium beijerinckii*, the carboxylate group of Glu59 serves as a hydrogen bond acceptor with the N(3)H of FMN. Mutagenesis of Glu to Gln and Ala significantly weakened the stabilization of FMN semiquinone state and has modestly (<45 mV) perturbed the redox couple of FMN in flavodoxin (103). The direct interactions between the zwitterion region of I-Tyr and N3 of FMN in hIYD encouraged our investigation of the role of the N3 H-bond for the redox of FMN and catalysis of hIYD.

I-Tyr binding induces the arrangement of three highly conserved residues of IYD homologs, Glu157, Tyr161 and Lys182 (Figure 5-1A hIYD), providing interactions to the zwitterion region of I-Tyr. The Glu157 forms H-bonds to both NH_3^+ (2.8 Å) and COO^- (3.4 Å) groups of substrate. Both Tyr161 and Lys182 form H-bonds (distance between 2.6 to 2.9 Å) to the COO^- of I-Tyr. Mutagenesis of these three amino acids (E153Q, Y157F and K178Q) in mIYD indicated that they are important for folding and catalysis. The K178Q mutant of mIYD was found insoluble and inactive. The Y157F and E153Q mutants were expressed in a soluble form. The Y157F weakened the binding of I-Tyr by 20 fold and decreased the $k_{\text{cat}}/K_{\text{M}}$ value by 40 % (104). E153Q mutation abolished binding affinity of I-Tyr and led to no detectable deiodination of $\text{I}_2\text{-Tyr}$ (104). The relationship of these residues to the catalysis might be realized through the H-bonding network

between these residues and the zwitterion region of substrate to stabilize the active site lid.

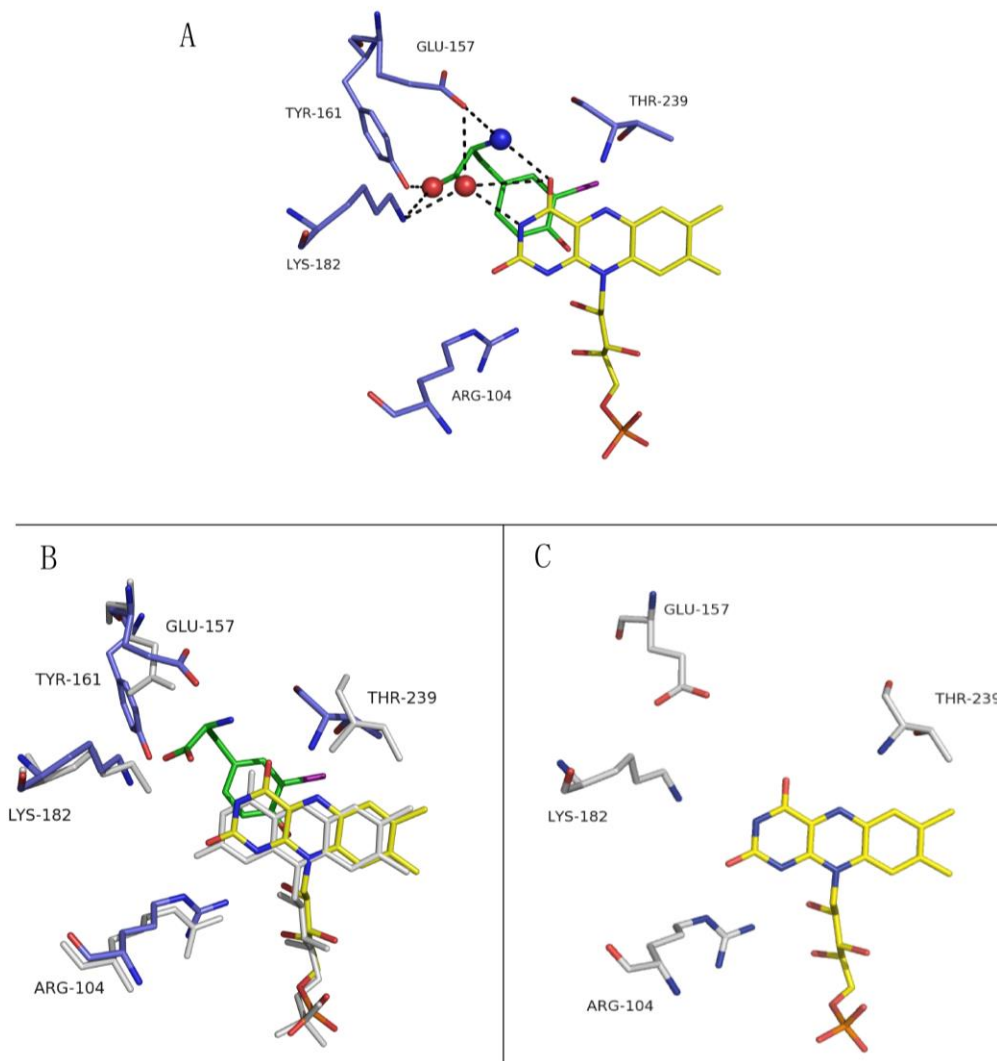


Figure 5-1. Interactions between the zwitterion region of I-Tyr and FMN in hIYD. A) H-bondings among I-Tyr, FMN and protein in hIYD-I-Tyr. B) I-Tyr binding caused arrangement of Glu157, Tyr161, Lys182, Arg104, Thr239 and FMN in hIYD. C) Interactions to isoalloxazine ring of FMN in the structure of hIYD in the absence of I-Tyr. In hIYD-I-Tyr, amino acids are in blue, FMN is in yellow and I-Tyr is in green. In hIYD, amino acids and FMN are all colored in gray. The zwitterion region of I-Tyr was shown as spheres in A.

The role of the zwitterion region of I-Tyr for binding, redox and catalysis is evaluated in this chapter by using a number of substrate analogs with

substituents at the zwitterion region (Figure 5-2). 3-Iodotyrosinamide (I-tyrosinamide) neutralizes the α -carboxyl group of I-Tyr but retains all other polar contacts to the protein and FMN. 3-Iodotyramine (I-tyramine) removes the COO^- group from I-Tyr, precluding the H-bonding to Tyr161, Lys182 and N(3)H of FMN. 4-Hydroxy-3-iodophenyl propionic acid (I-HPPA), removes the NH_3^+ group from I-Tyr, and disrupts the hydrogen bonding interactions to Glu157 and O4 atom of FMN. All the modified substrate analogs are expected to have negatively effect on IYD's binding and catalysis. Moreover, to focus on the coordination instead of turnover influence on the redox, the fluoro-analogs were also generated to investigate the effects of modification on the redox of FMN.

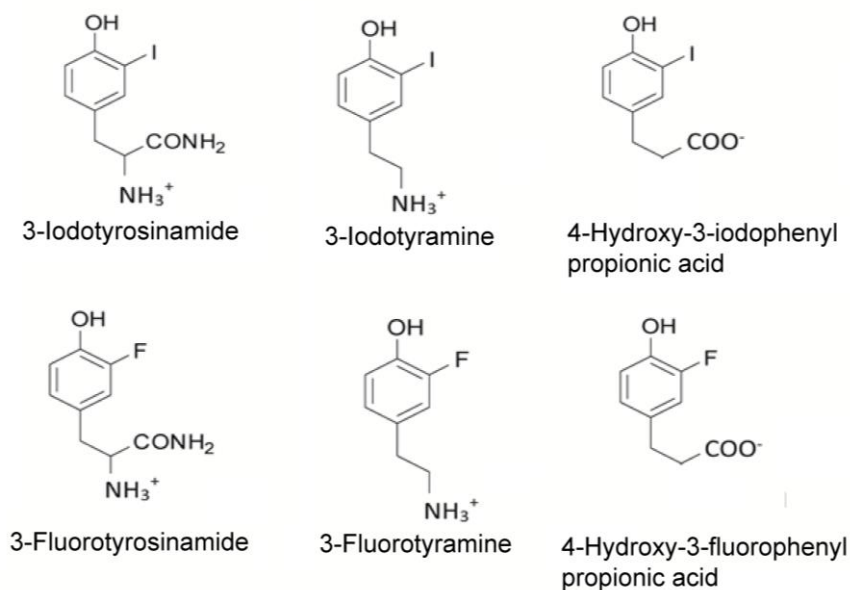


Figure 5-2. Modifications on the zwitterion region of substrate I-Tyr and F-Tyr.

5.2 Materials and Methods

5.2.1 Materials

3-Iodotyrosinamide, 3-fluorotyrosinamide (F-tyrosinamide), 3-iodotyramine, 3-fluorotyramine (F-tyramine), 4-hydroxy-3-iodophenyl propionic acid and 4-hydroxy-3-fluorophenyl propionic acid (F-HPPA) were synthesized by Dr. Fazel Fakhari, a post-doctoral associate in our group. All other reagents were obtained commercially at the highest grade available.

5.2.2 General methods

hIYD was expressed and purified according to the method described in Chapter 2. Protein concentration was determined using an ϵ_{280} of $37,930 \text{ M}^{-1}\text{cm}^{-1}$ after correcting for the contribution from bound FMN ($A_{280}/A_{450} = 1.57$). The ratio of FMN/hIYD monomer is 2. UV measurements were made with a Hewlett-Packard 8453 spectrophotometer (Palo Alto, CA). Fluorescence data were obtained with a Horiba scientific fluoromax-4 spectrophotometer (Tokoyo, Japan). Analytic HPLC employed a reverse-phase Alltech C18 Econosphere semipreparative column with a flow rate of 1 mL/min. High-resolution mass spectra were determined with a Waters Acquity UPLC-MS (Xevo-G2).

5.2.3 Kinetic characterization of hIYD with I-Tyr and I-Tyr analogs by HPLC

Catalytic deiodination of I-Tyr was measured by detecting formation of the deiodinated product by HPLC. The hIYD concentration was 0.08 μM and the reaction was performed at 25 $^{\circ}\text{C}$ with 500 mM NaCl and 100 mM sodium phosphate at pH 7.4. The concentration of I-Tyr was varied from 0 to 70 μM . 0.5 % sodium dithionite was used as the reducing reagent for enzyme turnover. The total volume of the reaction mixture was 1 ml. The reaction was quenched by adding 10 μL formic acid.

The reaction solutions (volume 1.01 ml) were then analyzed by a reverse-phase HPLC using the following method: 0-10 min linear gradient from 0 to 5 % B, 25 min to 60 % B, 30 min to 95 % B, and another 10 min wash with 95 % B (buffer A- 0.1 % formic acid, buffer B-acetonitrile). Detection was carried out at 280 nm. 40 μM m-cresol was included as an internal standard. Each assay was performed in duplicate and the average of their product formation was fit to Michaelis-Menten kinetics using Origin 7.0.

The calibration curve of products was normalized by internal standard. The response factor (RF) of product Tyr with internal standard (m-cresol) is used to calculate the product formation by using the equation 5-1 (105) (C_x = concentration of the analyte, C_{is} = concentration of the internal standard, A_x = peak area of the analyte, A_{is} = peak area of the internal standard).

$$\text{Equation 5-1.} \quad \text{RF} = ((A_x)(C_{is}))/((A_{is})(C_x))$$

Analysis of hIYD activity with the modified substrate followed the same procedures described above. However, determinations of their initial rates were performed at concentrations equal to their K_D . The hIYD concentration was 0.8 μM and the reaction time was varied from 0 min to 5 hours to investigate the product formation vs time. After time-dependent analysis, the product peak was identified. The product was then analyzed by Mass Spec. To quantitate the amount of product, calibration curves normalized by the internal standard were created for each product with commercial tyrosinamide, tyramine or HPPA (concentration in the range of 5-80 μM) and the RF were obtained. The amount of product formation from the reaction mixture was determined by the RF and the peak area of every product as described above. All the reactions were repeated at least twice. The average of the two measurements was plotted as product formation vs time by Origin 7.0. The slope of the linear range of the progress curve represents the initial rate of hIYD.

5.3 Results and Discussion

5.3.1 Importance of the zwitterion region of I-Tyr for its binding affinity to hIYD

The contributions of individual functional groups to the binding of the I-Tyr were compared by determining the K_D of modified substrate analogs by monitor fluorescence properties of bound FMN (Figure 5-3) and summarized in Table 5-1. The protein was found to precipitate under high ligand concentration.

Therefore, titrations were limited by the tolerance of the protein to ligands (~1mM). All the data were collected before protein precipitation was observed.

Modifications of the zwitterion tail of the ligands affected binding significantly (Table 5-1). Although I-tyrosinamide bound most tightly among I-tyrosinamide, I-tyramine and I-HPPA, its K_D is still 500-fold more than the native substrate I-Tyr. The effect of its CONH_2 substitution might prevent the closing of the active cavity and the proper orientation of I-tyrosinamide to the isoalloxazine of FMN and Glu157, Tyr161 and Lys182.

Once the NH_3^+ group from the I-Tyr is removed, the binding property of the subsequent derivative I-HPPA is also significantly impaired. The K_D of I-HPPA is 10-fold more than I-tyrosinamide and 5000-fold more than the native substrate I-Tyr. Removing the NH_3^+ group results a loss of H-bond to O4 of FMN and Glu157. The difference in the binding properties of I-HPPA and I-Tyr suggested the importance of the H-bonds from NH_3^+ group for binding to hIYD.

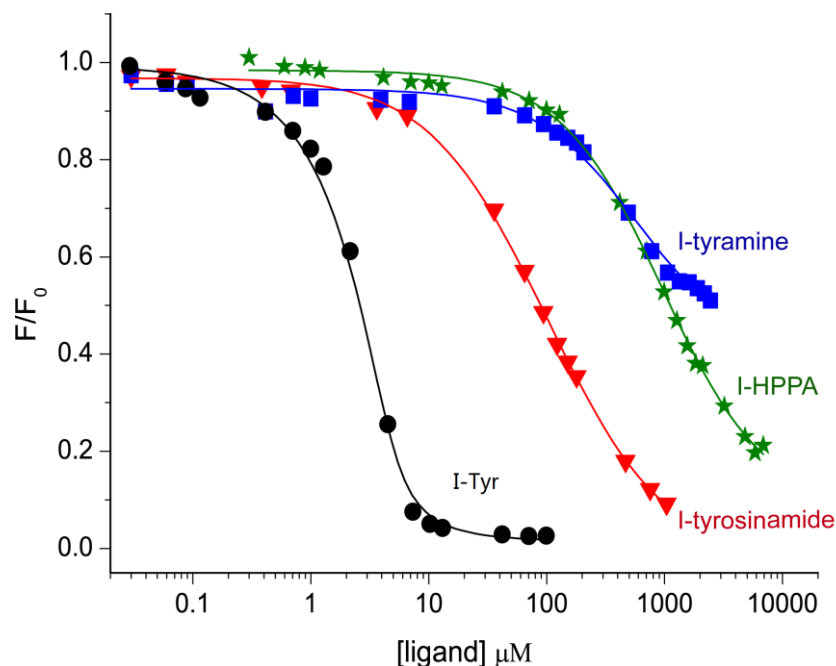


Figure 5-3. Equilibrium binding curves of hIYD with different ligands. Ligand binding was monitored by the change of fluorescence of FMN bound to IYD (4.5 μM). The fluorescence intensities were normalized by dividing the initial fluorescence and plotted against ligand's concentration. The measurement was repeated three times. The dissociation constants were obtained after nonlinear fit by Origin 7.0 as described in chapter 2.

From the crystal structure of hIYD•I-Tyr, we observed that there are more H-bonds contacts to the COO^- group than NH_3^+ group. The COO^- group is H-bonded to Glu157, Tyr161, Lys182 and N3 and O4 atom of FMN, whereas, the α -ammonium group only has H-bonds to O4 and Glu157. Surprisingly, the binding affinity of compounds without a COO^- (I-tyramine) is 3 times tighter than compounds without a NH_3^+ group (I-HPPA). Perhaps the difference of K_D between I-tyramine and I-HPPA indicates that the NH_3^+ group contributes more than the COO^- group to the successful closing of the active site lid.

Table 5-1. The binding properties of substrate analogs to hIYD.

Iodo-ligands	Zwitterion substitution		K_D (μM)
I-Tyr	COO^-	NH_3^+	0.15 ± 0.04
I-tyrosinamide	CONH_2	NH_3^+	80 ± 5^a
I-tyramine	--	NH_3^+	400 ± 45^a
I-HPPA	COO^-	--	1000 ± 120^a
<hr/>			
Fluoro-ligands			
F-Tyr	COO^-	NH_3^+	1.3 ± 0.40
F-tyrosinamide	CONH_2	NH_3^+	>1000
F-tyramine	--	NH_3^+	>1000
F-HPPA	COO^-	--	>1000

^aError represents the standard deviation of K_D from three independent measurements.

Removing or altering the COO^- group and NH_3^+ groups alter the H-bonds network to the N3O4 edge of FMN and may result in a change in the redox property of FMN. To focus on the coordination effects on the redox of FMN rather than the subsequent catalysis, fluoro-analogs were used to measure the effect on the redox property of FMN in hIYD as described in chapter 3 and 4., Thus the binding affinities of the fluoro-analogs were necessary to evaluate the binding of the ligand with the active site for later redox titration characterization. As illustrated in Table 5-1, none of the fluoro-derivatives bound to IYD tightly. The strongest binding fluoro-substitution is F- tyrosinamide whose K_D is more than 1 mM. For the F-tyramine and F-HPPA, the binding constants could not be obtained due to the limitation of protein's tolerance to high concentrations of ligand (1 mM). No fluorescence quench for F-tyramine and F-HPPA observed

before the protein precipitated (Appendices F), indicating that the K_D of F-tyramine and F-HPPA must be higher than the K_D of F-tyrosinamide.

5.3.2 Zwitterion requirement for IYD catalysis

All the activity assays were performed with a substrate concentration that equal to its K_D to provide equal amount of active site occupancy. The reaction mixture was analyzed by HPLC and the product peak was identified by comparing the chromatogram of the reaction with the chromatogram of their mixture at 0 min, followed by UPLC/MS analysis.

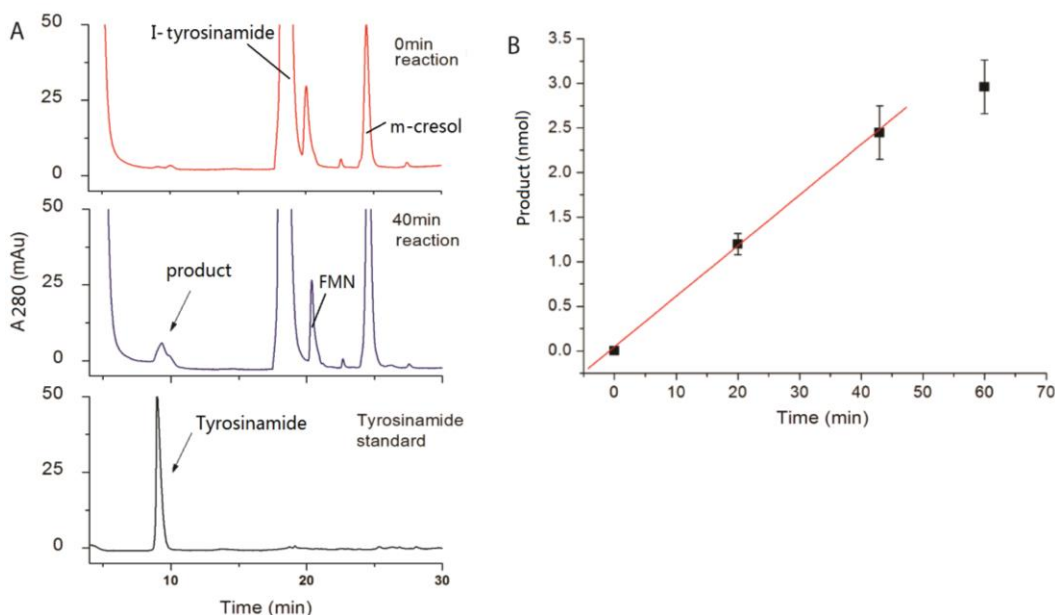


Figure 5-4. Analysis of hIYD's activity with I-tyrosinamide by HPLC. A) Identification of product peak by comparing the chromatography at A280 of sample after 40 min catalysis with 0 min mixture. The product was identified with a retention time of 9.3 min. B) Progress curve of hIYD with I-tyrosinamide. 0.8 μ M hIYD was added to 80 μ M I-tyrosinamide. All the experiment was repeated twice. Error in the figure represents the range. Linear analysis was performed in Origin 7.0 for the 0 min, 20 min and 43 min points.

5.3.2.1 The activity of hIYD with I-tyrosinamide

I-tyrosinamide exhibited the tightest binding to hIYD among all the modified compounds and was selected first for testing as a substrate for hIYD catalysis. As indicated in Figure 5-4, a new compound with a retention time of 9.3 min was observed in the chromatography of the mixture (I-tyrosinamide, hIYD and dithionite) after 40 min incubation when compared to the chromatography of the same mixture with 0 min incubation. The peak area at 9.3 min was found to increase as the reaction time increased from 0 min to 60 min (Figure 5-4 B). This new species was likely the product of deiodination of I-tyrosinamide by hIYD. Considering the function of IYD as a dehalogenase, this product was assumed to be tyrosinamide. To test this, the chromatography of the commercial tyrosinamide was obtained. As we expected, the commercial tyrosinamide also show an A_{280} peak at 9.3 min (Figure 5-4 A, black curve). The mass spectra of the fraction of 9.3 min, revealed the most abundant peaks at m/z 136.08, as the tyrosinamide after fragmentation CONH_2 (therotical m/z 136.07) (Figure 5-5 A). Standard tyrosinamide was also analyzed by LC/MS and was generated the same mass spectra as the product (Figure 5-5 B). Thus the product of the I-tyrosinamide after catalysis by hIYD was identified as tyrosinamide.

To measure the initial rates of I-tyrosinamide catalyzed by hIYD, a progress curve of product formation was created as shown in Figure 5-4 B. The amount of product formation was calculated based on the observed peak area of product (9.3 min) and internal standard by using equation 5-1 and response factor

of 2.29 as observed from calibration analysis of tyrosinamide. The linear region of the reaction was observed within first 40 min. A slope of 0.057 ($\mu\text{M}/\text{min}$) was estimated from the linear region of the progress curve. The activity was performed under 0.8 μM hIYD. Therefore, the turnover number of IYD with I-tyrosinamide was calculated as 4.28 hour^{-1} .

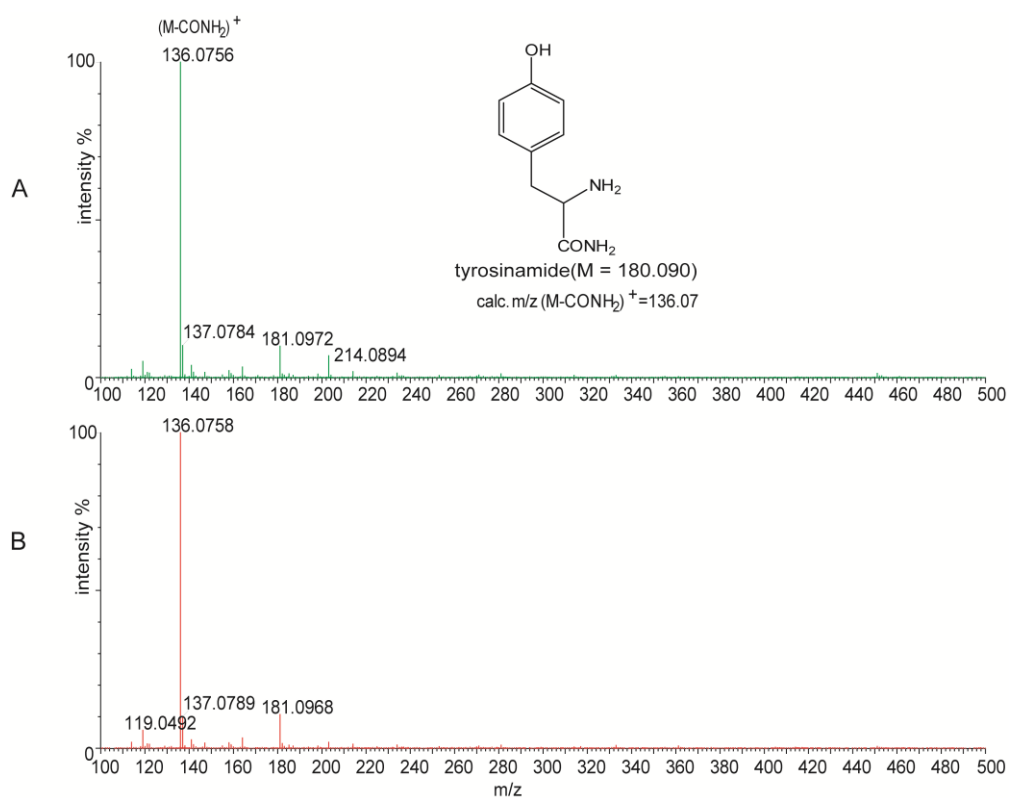


Figure 5-5. Mass spectra of product of I-tyrosinamide catalyzed by hIYD. A) Mass spectra of product fraction (9.3 min HPLC collection) of I-tyrosinamide catalyzed by hIYD. B) Mass spectra of commercial tyrosinamide.

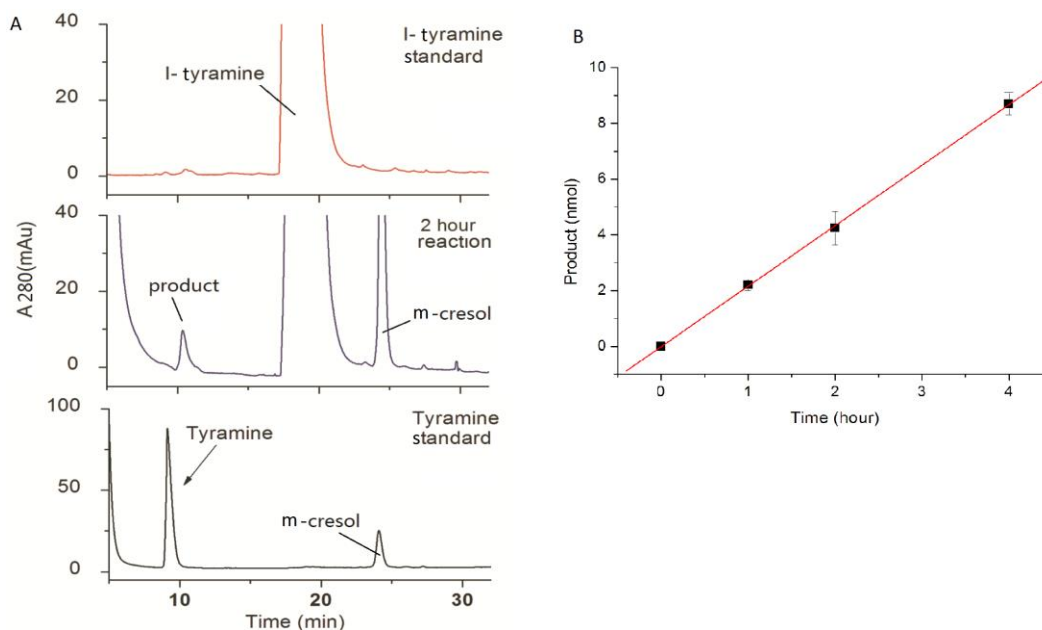


Figure 5-6. Analysis of hIYD's activity with I-tyramine by HPLC. A) Identification of product peak by comparing the chromatography at A280 of 2 hour reaction mixture with the chromatography of substrate. The product was identified with a retention time of 10.2 min. B) Progress curve of hIYD with I-tyramine. 0.8 μ M hIYD was added to 400 μ M I-tyramine. All the experiment was repeated twice. Error in the figure represents the range. Linear analysis was performed in Origin 7.0 for the 0 hour, 1 hour, 2 hour and 4 hour points.

5.3.2.2 The activity of IYD with I- tyramine

The catalytic activity of IYD with I-tyramine was also investigated under the condition that I-tyramine's concentration equals to its K_D value (400 μ M). A new peak at 10.2 min was found to increase as the reaction time increased and as expected for a product. As shown in Figure 5-6 A, the retention time of this product (10.2 min) is close to the retention time of the commercial tyramine (9.8 min). The slightly shift of the retention time may be caused by the dithionite in reaction sample. The UPLC/MS analysis of the 10.2 min fraction revealed the most abundant peaks at m/z 121.06, consistent with tyramine after fragmentation

NH₂ (therotical m/z = 121.06) (Figure 5-7 A). The same mass spec pattern was found for the commercial tyramine (Figure 5-7 B). Thus, as expected, tyramine was the product of I-tyramine catalyzed by hIYD.

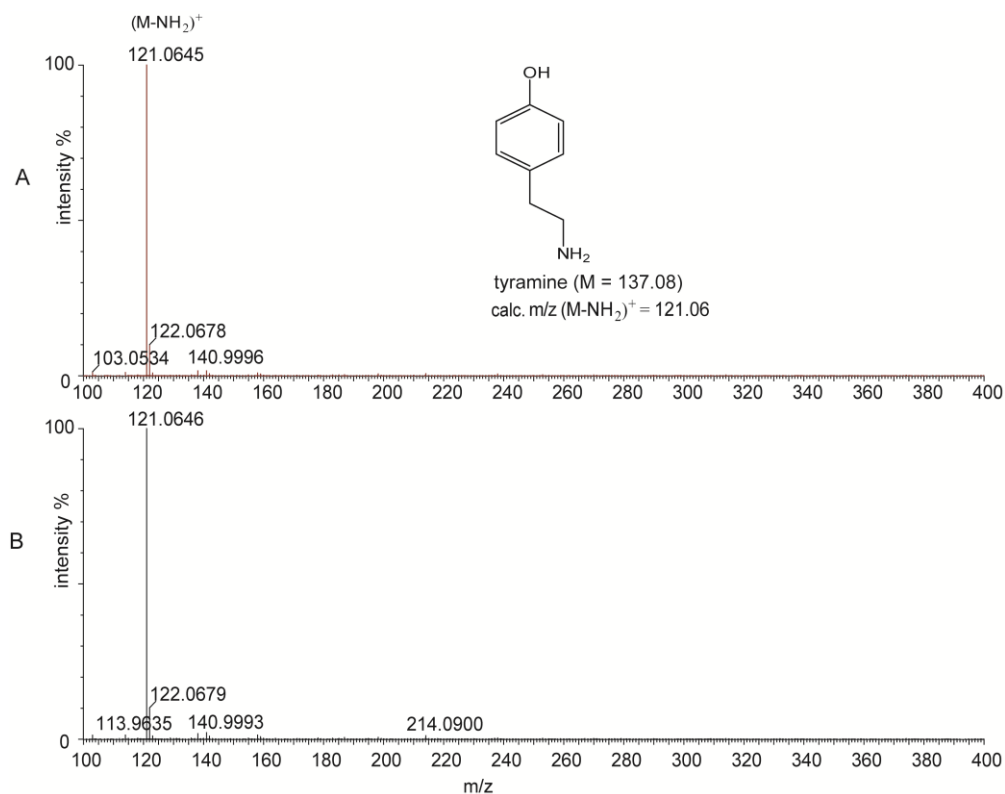


Figure 5-7. Mass spectra of product of I-tyramine catalyzed by hIYD. A) Mass spectra of product fraction (HPLC collection, retention time = 10.2 min) of I-tyramine catalyzed by hIYD. B) Mass spectra of commercial tyramine.

A progress curve for the product of I-tyramine catalyzed by hIYD was performed with reaction times of 4 hours. The product formation was calculated based on the observed peak area of product (10.2 min) and internal standard by using equation 5-1 and response factor of 2.54 for tyramine with m-creasol. As shown in Figure 5-6 B, product formation is linear for the first 4 hours. A slope of 2.17 was estimated from the linear region of the progress curve by Origin 7.0 and

the rate of the IYD catalysis under 400 μM I-tyramine was measured as 2.71 per hour.

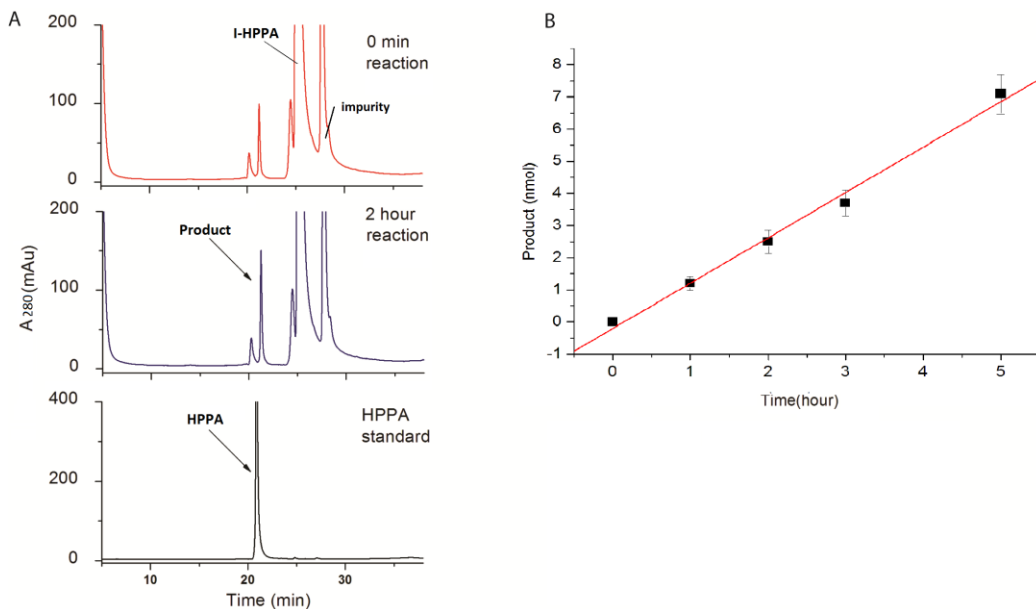


Figure 5-8. Analysis of hIYD's activity with I-HPPA by HPLC. A) Identification of product peak by comparing the chromatography at A₂₈₀ of 2 hour reaction mixture with the chromatography of 0 min mixture. The product was identified with a retention time of 21.8 min. m-cresol is the internal standard. B) Progress curve of hIYD with I-tyramine. 0.8 μM hIYD was added to 1000 μM I-HPPA. All the experiment was repeated twice. Error in the figure represents the range. Linear analysis was performed in Origin 7.0 for reaction mixture with catalysis of 0 hour, 1 hour, 2 hour and 3 hour points and 5 hour.

5.3.2.3 The activity of hIYD with I- HPPA

The activity of hIYD with I-HPPA was also analyzed at the concentration of I-HPPA equal to its K_D (1000 μM). Mixture (I-HPPA, hIYD and dithionite) after 2 hours incubation was analyzed by HPLC. Comparing the chromatography of the mixture with 2 hour incubation with chromatography of the same mixture with 0 min incubation, a peak area at 21.8 min was found to increase with the reaction time (Figure 5-8 A), and was expected to be the product of I-HPPA

catalyzed by hIYD. Commercial HPPA was analyzed under the same HPLC condition and exhibited a retention time at 21.4 min. The suggested product (21.8 min fraction) was collected and analyzed by mass spec. The most abundant peak of the product was m/z 165.05, as the HPPA anion (therotical m/z = 165.06) (Figure 5-9 A). The same mass spec pattern was observed with the commercial HPPA (Figure 5-9 B). Based on the HPLC and LC/MS analysis, HPPA was identified as the product of I-HPPA after hIYD catalysis.

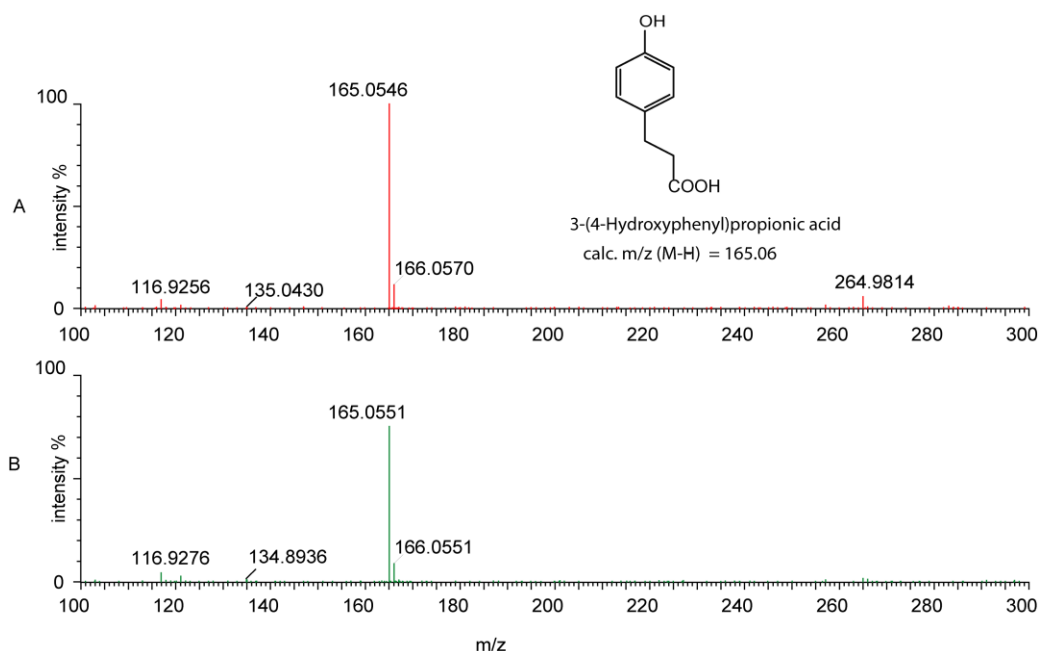


Figure 5-9. Mass spectra of product of I-HPPA catalyzed by hIYD. A) Mass spectra analysis of expected product (HPLC collection of 21.8 min fraction) of I-HPPA catalyzed by hIYD. B) Mass spectra of commercial HPPA.

The progress curve of hIYD (0.8 μM) with I-HPPA (1000 μM) was generated to obtain the initial rate. The response factor of HPPA with *m*-creosol was observed as 2.14 after calibration analysis. The product formation was then calculated based on the observed peak area of product (21.8 min) and internal

standard by using equation 5-1. As shown in Figure 5-8 B, the product formation of I-HPPA deiodination is linear increase up to 5 hours. A slope of 1.41 was estimated from the linear region of the production formation curve by Origin 7.0 and the rate of the hIYD catalysis under 1000 μM I-HPPA was measured as 1.76 per hour.

5.3.2.4 The kinetics parameter of IYD with native substrate I-Tyr

The kinetic property of hIYD with native substrate (I-Tyr) under a concentration equal to its K_D was characterized to provide a direct comparison to the catalytic property of hIYD with modified substrates. The binding of I-Tyr to hIYD is very tight, K_D is 0.15 μM . Measuring the initial rate of deiodination at such low concentrations was not possible by the HPLC assay since the signal would be too low to be detected. The initial rate under 0.15 μM I-Tyr was extrapolated by creating the Michaelis-Menten curve over an I-Tyr concentration range of 5 μM to 60 μM . The amount of product under each [S] was calculated based on the response factor and the area of product and internal standard as described in method. For every [S] by using equation 5-1, the experiment was repeated twice. The average of the product formation was fitted into Michaelis-Menten equation by Origin 7.0 (Figure 5-10). The K_M and k_{cat} of I-Tyr deiodination obtained from fitting analysis are $12 \pm 2.5 \mu\text{M}$ and $7.3 \pm 1.0 \text{ min}^{-1}$, respectively. The k_{cat}/K_M (0.6 $\mu\text{M}/\text{min}$) of I-Tyr from this HPLC analysis is very close to the k_{cat}/K_M of another native substrate I₂-Tyr measured by radioactive

deiodination assay (0.4 $\mu\text{M}/\text{min}$). The initial rate of the hIYD catalysis with 0.15 μM I-Tyr is estimated to be 4.9 hour^{-1} from the Michaelis-Menten curve.

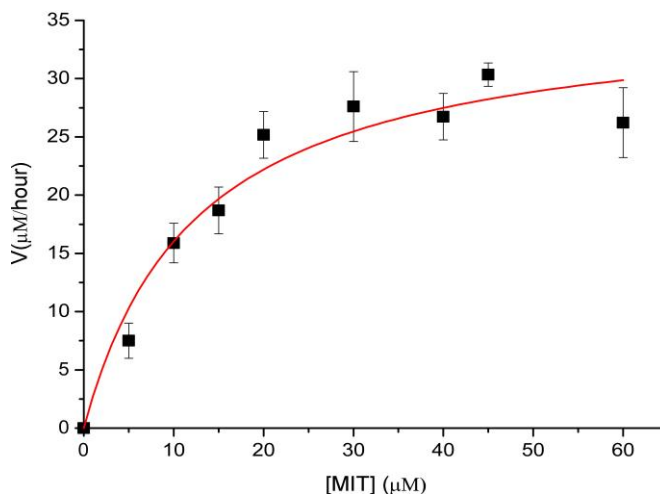


Figure 5-10. Michaelis-Menten curve of I-Tyr deiodination by hIYD. Data points are an average of two repeats. Error is the range of data. Kinetic parameters were obtained after Michaelis-Menten analysis by Origin 7.0. The initial rate of I-Tyr deiodination at the concentration of I-Tyr equals to K_D value (0.15 μM) was estimated from the curve.

Table 5-2. Initial catalytic rates of hIYD with native and modified substrate.

Substrate	[substrate] μM	Rate (hour^{-1})
I-tyrosinamide	80	4.28 ± 0.04^a
I-tyramine	400	2.71 ± 0.03^a
I-HPPA	1000	1.76 ± 0.09^a
I-Tyr	0.15	4.9^b

^a Error represents the linear fitting error of the average of two repeats..

^b Estimated from the Michaelis-Menten curve of hIYD with I-Tyr.

5.3.2.5 Comparison of the catalytic rates of native and modified substrate.

Table 5-2 summarized the deiodination rate of IYD with its native substrate I-Tyr and the modified substrates under $[S] = K_D$. IYD deiodinated all

the modified iodo-ligands, and all of the rates are within one order of magnitude the rate of the native substrate I-Tyr. The rate of deiodination of I-HPPA is 2-fold less than the catalysis of I-Tyr. Considering the modification of zwitterion region caused at least 500 fold decrease in binding with IYD, the zwitterion region seems very critical for the affinity of ligand to IYD but not for activity. One possible explanation is that the zwitterion regions as well as the H-bond networks are very helpful for orienting the ligands in the active site but not directly involved in the catalytic process of IYD.

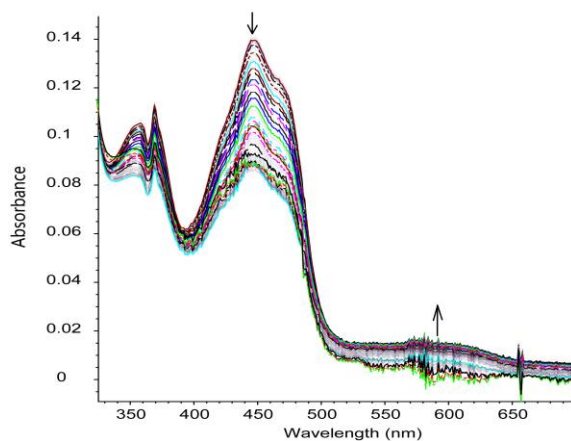


Figure 5-11. Anaerobic reduction of hIYD in the presence of I-tyrosinamide by xanthine/xanthine oxidase. The absorbance at 445 nm was decrease while the absorbance around 590 nm was observed to increase during the reduction of hIYD in the presence of I-tyrosinamide. The absorptions at 446 nm later stop changing due reached steady-state of catalysis of hIYD with I-tyrosinamide.

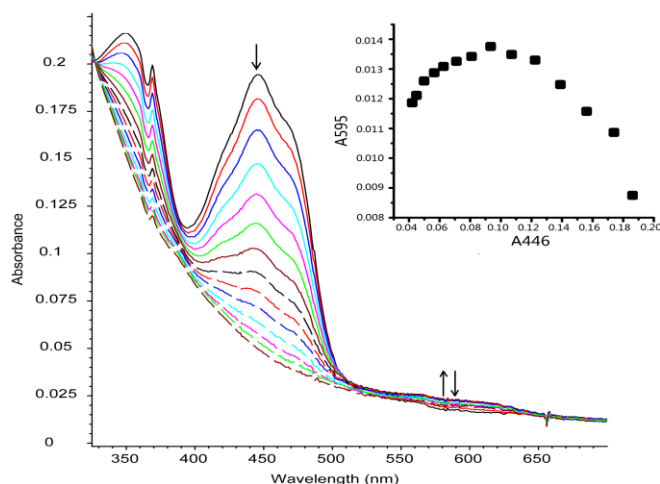


Figure 5-12. Selected spectra for the reduction of hIYD in the presence of F-tyrosinamide by xanthine/xanthine oxidase. The reaction was monitored over 120 min. The arrows indicate the direction of the changes in absorbance. Insert: A446 vs A595 (A446 and A595 indicate the absorbance at 446 nm and 595 nm, respectively).

5.3.3 Redox chemistry of IYD affected by the of H-bond interactions between the zwitterion region of substrates and N3 and O4 of the FMN ring

To investigate the redox effect of the zwitterion interaction with FMN in hIYD, redox titrations were performed in the presence of I-tyrosinamide by xanthine/xanthine oxidase as described in chapter 2. As shown in Figure 5-11, a small absorbance peak was observed around 595-610 nm and was suggested as the neutral semiquinone peak. During the reduction of hIYD in the presence of I-tyrosinamide, this 595 nm peak was found to increase in the beginning and last for 2 hours without decrease for doing turn over with enzyme. To focus on the coordination effects rather than the catalytic effects, 1 mM of F-tyrosinamide was added as the ligand to investigate the redox property of IYD. Again, a small A_{595} peak was observed during the reduction of hIYD. Analysis the absorbance at 595

demonstrated that the absorbance first increase and then decrease indicating the FMN was first reduced to one-electron reduced semiquinone form and then reduced to two-electron reduced hydroquinone form (Figure 5-12). These observations are very similar to the observation of redox titration in the presence of F-Tyr with the native zwitterion region. F-Tyr binding induced the stabilization of semiquinone converts the reduction of hIYD to a stepwise single-electron transfer process. The observation of the semiquinone indicated that the F-tyrosinamide is still able to convert the electron transfer of hIYD from a two-electron to a stepwise single-electron process. The observed semiquinone in the presence of F-tyrosinamide is much less (20 % vs 99 %) than that observed for hIYD in the presence of F-Tyr. Decrease of the semiquinone formation may be

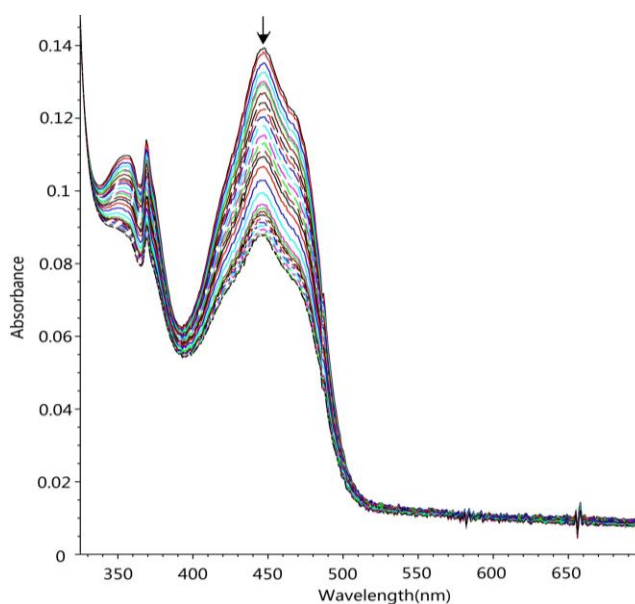


Figure 5-13. Reduction of hIYD in the presence of 1mM I-tyramine by xanthine/xanthine oxidase and monitored by UV/VIS. The data was recorded every 2 min for over 120 min. The arrows indicate the direction of the changes in absorbance.

due to the poor binding affinity of the modified ligand or the change of the redox potential of the FMN in hIYD.

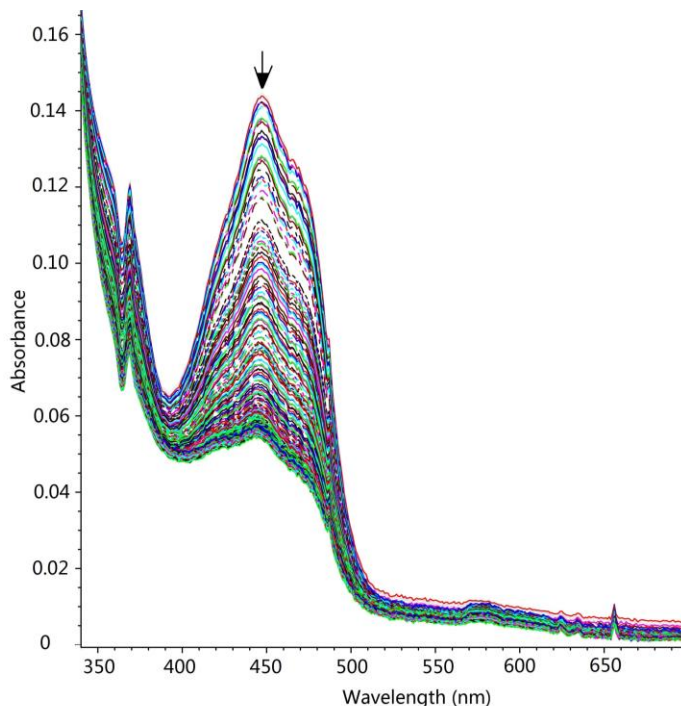


Figure 5-14. Redox titration of hIYD in the presence of 1mM I-HPPA by xanthine/xanthine oxidase. The data was recorded every 2 min for over 120 min. The arrows indicate the direction of the changes in absorbance.

The FMN Semiquinone was not detected during the redox titration of hIYD in the presence of 1 mM of I-tyramine and I-HPPA (2-fold K_D of I-tyramine, 1-fold K_D of I-HPPA) (Figure 5-13 and 5-14). There are several possibilities regarding to this observation. First, the semiquinone signal may be too low to be detected due to the low active site occupancy at 1 mM of I-tyramine and I-HPPA. Second, H-bondings to the N3O4 edge might affect the redox of FMN since removing the H-bonding to the N3O4 edge results the semiquinone unable to be stabilized. Another possibility is related to the N5 H-bonding of the FMN. Removing the NH_3^+ or COO^- group disrupted the interactions of substrate

with the key residues of the active site lid. As a result, the OH side chain of the Thr239 may be unable to move toward the N5 and H-bonding to the N5 of the isoalloxazine ring of FMN. Consequently, considering the critical role of N5 H-bonding for stabilization of semiquinone in hIYD as described in Chapter 4, the loss of the N5 H-bonding result in the loss of the ability of hIYD to stabilize the semiquinone FMN in the presence of modified substrate.

5.4 Conclusion

The zwitterion region of substrate makes direct contacts to the key residue of protein (Glu157, Tyr161 and Lys182) and the N3O4 edge of FMN. The role of this zwitterion region in binding, redox control and catalysis were investigated by using ligands with modified zwitterionic regions. This region was found critical for proper binding of the ligand to the active site of the enzyme. Altering the COO^- group to CONH_2 or removing the COO^- group or NH_3^+ group caused at least a 500-fold decrease in binding affinity. hIYD was able to turn over all the modified ligands and release iodide from I-tyrosinamide, I-tyramine and I-HPPA. With equal occupancy to the active sites of hIYD, initial rates of deiodination of native and modified substrates were similar and within one order of magnitude, implying the zwitterion region of substrate is not critical for the catalysis of IYD. Modifications on the substrate certainly altered the H-bond network on the N3O4 edge of FMN in IYD and might have contributed to the redox properties. Stabilized neutral semiquinone was observed during the redox titration of IYD in the presence of I-tyrosinamide and F-tyrosinamide, suggesting that these modified

substrates are still able to induce the stepwise single-electron transfer process for IYD's catalysis. No semiquinone signal was detected by UV/VIS during titration of hIYD in the presence of 1 mM I-tyramine or 1mM I-HPPA. This observation either caused by the low occupancy of the enzyme active site or the change of the redox property of FMN in hIYD.

Chapter 6: Conclusion

Despite the physiological importance of hIYD for thyroid hormone, hIYD remained poorly characterized. Previous discovery of the cDNA of hIYD allowed for limited expression of hIYD in HEK293. Characterization of hIYD was hampered by a lack of a convenient source of high quality active protein. Prior studies on mIYD indicated IYD consists of an N-terminal membrane domain, an intermediate domain and a catalytic domain that is common to the nitro-FMN reductase family. Removing the N-terminal domain previously allowed expression of soluble mIYD in insect cells (sf9) and more recently a sumo fusion of IYD allowed for heterologous expression in *E.coli*.

The strategy of fusion to sumo and expression in *E.coli* has now been applied to hIYD and provide a large scale of highly pure hIYD (> 95 %, ~ 10 mg of hIYD per 1 L of culture). This provided sufficient quantities of hIYD for structural and mechanistic studies. Kinetics characterization indicated that the ability of hIYD to promote deiodination of I₂-Tyr with similar kinetic parameters as homoenzymes from a wide range of organism. Crystallographic studies of hIYD indicated that the structure of hIYD and mIYD are nearly superimposable. Previous crystallographic studies with mIYD demonstrated that the substrate I-Tyr coordinates directly to the isoalloxazine ring of FMN and induces closure of an active site lid. Similar interactions with the isoalloxazine ring are also induced by substrate in the structure of hIYD•I-Tyr, including the formation of H-bonds between the zwitterionic region of I-Tyr and the N³ and O⁴ of the isoalloxazine

ring. The OH side chain of Thr239 moves close to the N⁵ of FMN and allows for an H-bond. After substrate binds, the aromatic ring of I-Tyr additionally stacks above the FMN. All the key residues (Thr239, Glu157, Tyr161 and Lys182) involved in these interactions are conserved in IYD homologs, implying their significance for catalysis.

Consistent with previous proposals, IYD may promote catalysis through single electron transfer steps. In this thesis, accumulation of a neutral semiquinone FMN was observed during the reduction of hIYD in the presence of substrate. In the absence of substrate, only oxidized FMN and two-electron reduced FMN were observed during the reduction of hIYD by xanthine/xanthine oxidase. These observations indicate that substrate binding converts a two-electron transfer process to a stepwise single-electron transfer process. The difference between the midpoint potentials of FMN_{ox/sq} and FMN_{sq/hq} is 154 mV in the presence of F-Tyr; suggesting 99 % of FMN was reduced to FMN_{sq} before further reduction. In contrast to the stabilization of the semiquinone, the hydroquinone was destabilized. The reduction of FMN_{sq} to FMN_{hq} in hIYD in the presence of F-Tyr was lowered to -310 mV versus -124 mV for free in solution. The ability of substrate to destabilize the FMN_{hq} may facilitate its initial one electron reduction to initiate deiodination.

The pH dependence of I₂-Tyr binding with hIYD suggests that the phenolate form of substrate is the preferential form for IYD binding. Together with the observation of a semiquinone during redox titration, these findings improve our understanding about the catalytic mechanism and suggest that the phenolate form

of substrate binds to IYD, tautomerization to a keto intermediate and subsequent injection of a single electron into the carbonyl of the keto group to promote the deiodination process. However, fully understanding the catalytic mechanism of IYD awaits further investigation that is capable of trapping the keto intermediate.

H-bonding to the isoalloxazine ring is crucial for redox control of many flavoproteins. Direct interaction between substrate and the isoalloxazine ring of FMN is rare in flavoproteins. Using hIYD as model, the investigation performed in this dissertation describes the significance of these interactions in stabilizing the active site lid, controlling the redox chemistry of FMN and promoting the catalysis. The N5 H-bonding between FMN and the OH side chain of Thr239 in hIYD was identified as the most important redox control of FMN among all the substrate induced interactions with FMN. Mutagenesis of Thr239 to Ala239 removed the N5 H-bonding as confirmed by a crystal structure of hIYDT239A•F-Tyr and no stable semiquinone was detected during the titration of T239A mutant in the presence of F-Tyr. Kinetic characterization of T239A with I₂-Tyr illustrated that its k_{cat}/K_M is 10-fold lower than wild type, suggesting that the deiodination was affected by removing N5 H-bond of FMN.

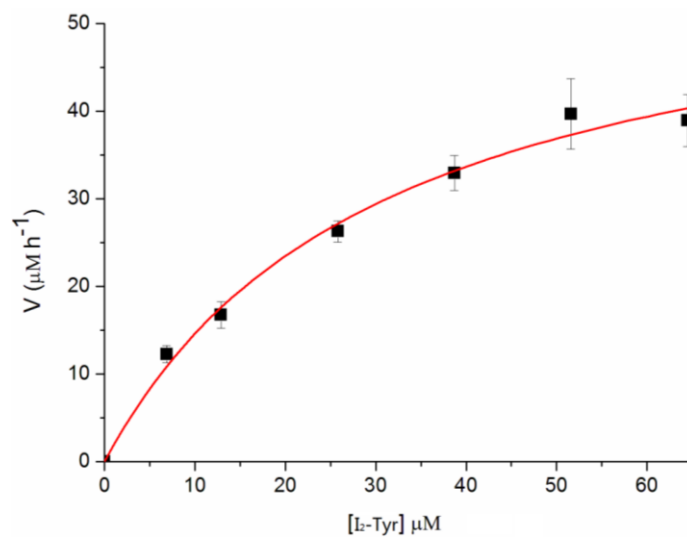
Moreover, the zwitterion region of substrate appeared to be critical for binding to IYD to stabilize the active site lid as indicated by the binding affinity of substrate analogs modified in their zwitterion region. Altering the COO⁻ to CONH₂, removing the NH₃⁺ or COO⁻ group of I-Tyr caused at least a 500-fold decrease in binding affinity to hIYD. However, the interactions between this zwitterion region and FMN has little effects on the catalytic activity since all the

modified substrates exhibit similar initial rates of deiodination (within a order of magnitude) under ligands concentration equals to their K_D .

Appendices

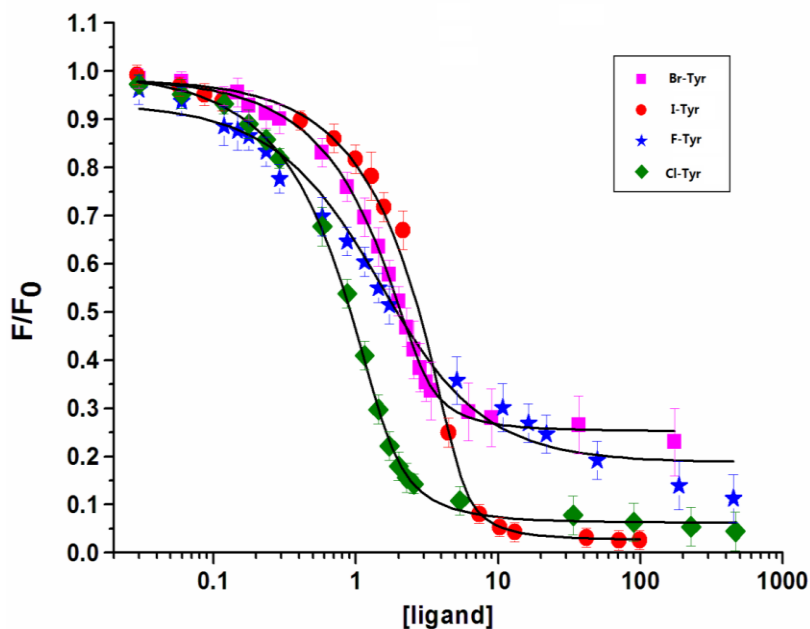
A. Rate of deiodination of hIYD with I₂-Tyr.

The activity of hIYD with I₂-Tyr was determined using the standard [¹²⁵I]-iodide release assays. Assays were performed in triplicate. The average of the three independent measurements was fit to the Michaelis-Menten equation using Origin 7.0. Error represents the standard derivation of three measurements. Red line was the fitting curve. The kinetic parameter obtained from fitting was a K_M of $31 \pm 6 \mu\text{M}$ and a k_{cat} of $12.5 \pm 1 \text{ min}^{-1}$.



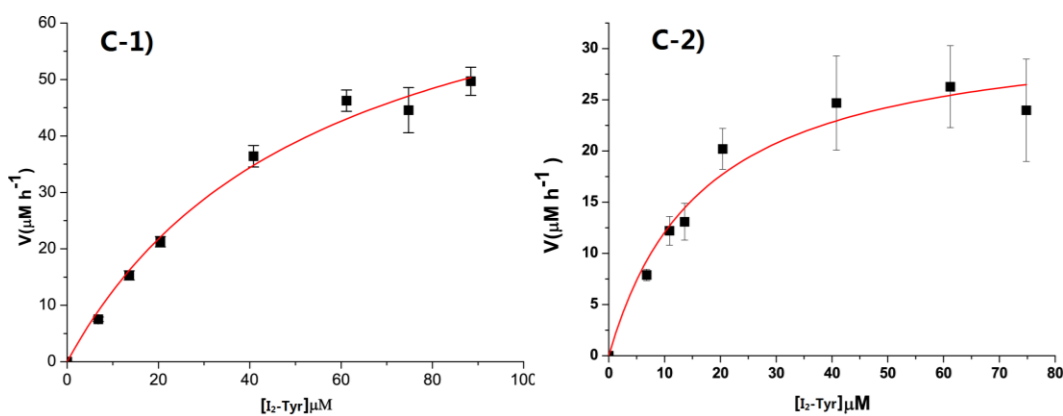
B. Fluorescence titration assay to measure hIYD affinity for Tyr-derivatives.

Ligand (I-Tyr, Cl-Tyr, Br-Tyr and F-Tyr) binding was monitored by the change of fluorescence ($\lambda_{\text{ex}} = 450$ and $\lambda_{\text{em}} = 527$) of FMN bound to hIYD (4.5 μM). The measurement was repeated three times. The average fluorescence intensities were normalized by dividing the initial fluorescence and plotted against ligand's concentration. Error represents the standard derivation of three measurements. The dissociation constants were obtained after nonlinear fit by Origin 7.0 as described in chapter 2. Black lines are the fitting curves.



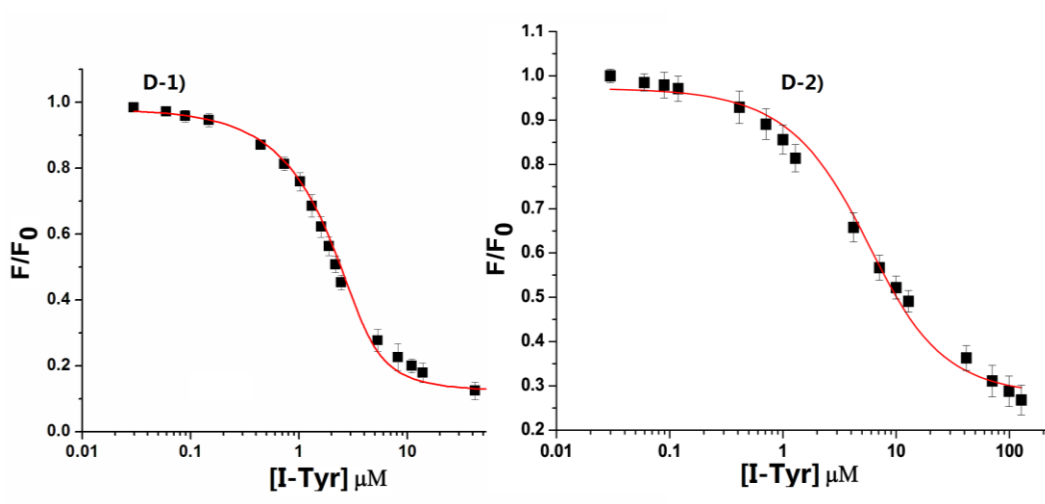
C. Rate of I₂-Tyr deiodination of hIYDT239A and hIYDT239S

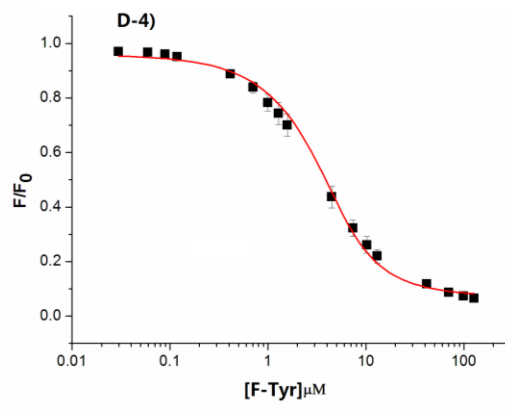
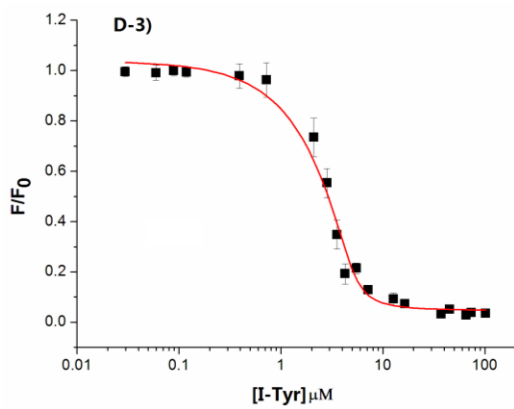
Deiodinase activity of hIYDT239A (C-1) and hIYDT239S (C-2) with substrate I₂-Tyr was determined using the standard [¹²⁵I]-iodide release assays. The [hIYDT239A] = 0.4 μM. The [hIYDT239S] = 0.08 μM. Assays were performed in triplicate. The average of the three independent measurements was fit to the Michaelis-Menten equation using Origin 7.0. Error represents the standard derivation of three measurements. Red lines represent the fitting curves.



D. Fluorescence titration assay to measure hIYDT239S and hIYDT239A affinity for I-Tyr and F-Tyr.

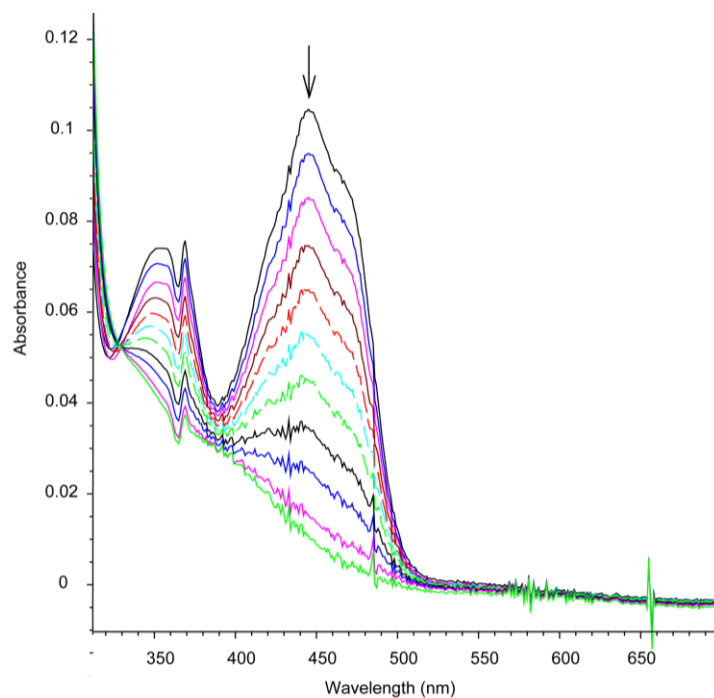
The binding of ligand I-Tyr (D-1) and F-Tyr (D-2) to hIYDT239S (4.5 μM) and the binding of ligand I-Tyr (D-3) and F-Tyr (D-4) to hIYDT239A (4.5 μM) were monitored by the change of fluorescence ($\lambda_{\text{ex}} = 450$ and $\lambda_{\text{em}} = 527$) of FMN bound to protein. The measurement was repeated three times. The average fluorescence intensities were normalized by dividing the initial fluorescence and plotted against ligand's concentration. The dissociation constants were obtained after nonlinear fit by Origin 7.0 as described in chapter 2. Error represents the standard derivation of three measurements. Red lines represent the fitting curves.





E. Selected spectra of reduction of hIYDT239A by xanthine/xanthine oxidase.

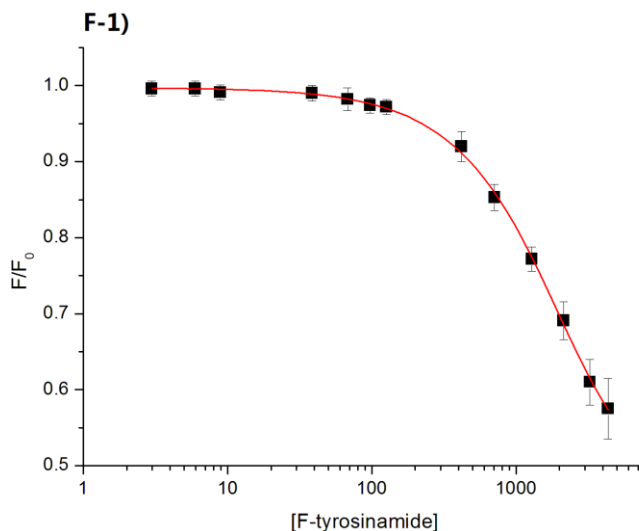
Reduction of hIYDT239A by xanthine/xanthine oxidase as observed by UV/VIS. Arrows at 446 nm indicate direction of absorption change during the reduction process.

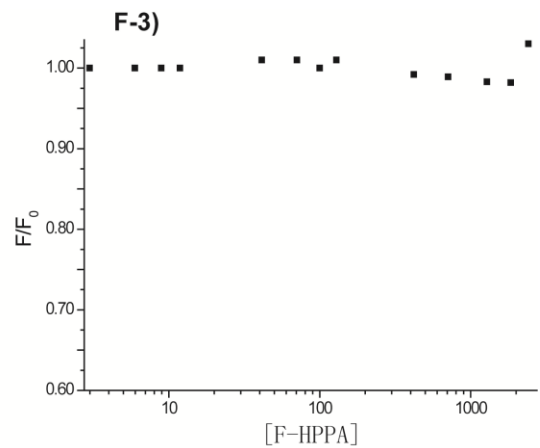
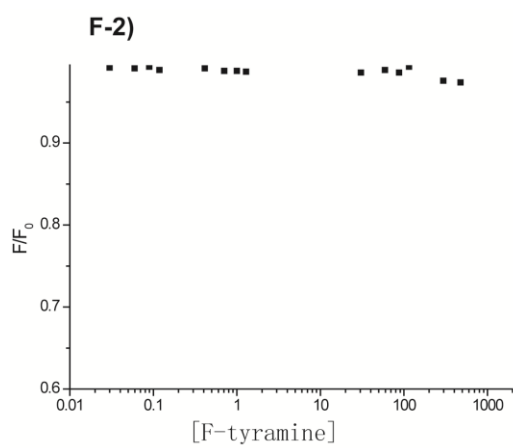


F. Fluorescence titration assay to measure hIYD affinity for fluoro-analogs

The binding of ligand F-tyrosinamide (F-1), F-tyramine (F-2) and F-HPPA (F-3) to hIYD (4.5 μM) were monitored by the change of fluorescence ($\lambda_{\text{ex}} = 450$ and $\lambda_{\text{em}} = 527$) of FMN bound to protein. For F-tyrosinamide, the measurement was repeated three times. The average fluorescence intensities were normalized by dividing the initial fluorescence and plotted against ligand's concentration. The dissociation constants were obtained after nonlinear fit by Origin 7.0 as described in chapter 2.

For F-tyramine and F-HPPA, The average fluorescence intensities of three repeats were normalized by dividing the initial fluorescence and plotted against ligand's concentration. No fluorescence quenching was observed. The titration was limited by the tolerance of hIYD with high concentration of ligands (~ 1 mM). Error represents the standard derivation of three measurements. Red line represent the fitting curve.





References

- (1) Yen, P. M. (2001) Physiological and molecular basis of thyroid hormone action. *Physiol Rev* 81, 1097-142.
- (2) Zimmermann, M. B. (2011) The role of iodine in human growth and development. *Semin Cell Dev Biol* 22, 645-52.
- (3) Zimmermann, M. B. (2009) Iodine deficiency. *Endocr Rev* 30, 376-408.
- (4) de Escobar, G. M., Obregon, M. J., and del Rey, F. E. (2007) Iodine deficiency and brain development in the first half of pregnancy. *Public Health Nutr* 10, 1554-70.
- (5) Zimmermann, M. B. (2013) Iodine deficiency and excess in children: worldwide status in 2013. *Endocr Pract* 19, 839-46.
- (6) Zimmermann, M. B., Jooste, P. L., and Pandav, C. S. (2008) Iodine-deficiency disorders. *Lancet* 372, 1251-62.
- (7) Pearce, E. N., Andersson, M., and Zimmermann, M. B. (2013) Global iodine nutrition: Where do we stand in 2013? *Thyroid* 23, 523-8.
- (8) Dohan, O., De la Vieja, A., Paroder, V., Riedel, C., Artani, M., Reed, M., Ginter, C. S., and Carrasco, N. (2003) The sodium/iodide Symporter (NIS): characterization, regulation, and medical significance. *Endocr Rev* 24, 48-77.
- (9) Rokita, S. E., Adler, J. M., McTamney, P. M., and Watson, J. A., Jr. (2010) Efficient use and recycling of the micronutrient iodide in mammals. *Biochimie* 92, 1227-35.

- (10) Stanbury, J. B., Meijer, J. W., and Kassenaar, A. A. (1956) The metabolism of iodotyrosines. II. The metabolism of mono- and diiodotyrosine in certain patients with familial goiter. *J Clin Endocrinol Metab* 16, 848-68.
- (11) Gaupale, T. C., Mathi, A. A., Ravikumar, A., and Bhargava, S. Y. (2009) Localization and enzyme activity of iodotyrosine dehalogenase 1 during metamorphosis of frog *Microhyala ornata*. *Ann N Y Acad Sci* 1163, 402-6.
- (12) McGirr, E. M., and Hutchison, J. H. (1953) Radioactive-iodine studies in non-endemic goitrous cretinism. *Lancet* 1, 1117-20.
- (13) Hubble, D. (1953) Familial cretinism. *Lancet* 1, 1112-7.
- (14) Stanbury, J. B., Kassenaar, A. A., Meijer, J. W., and Terpstra, J. (1955) The occurrence of mono- and di-iodotyrosine in the blood of a patient with congenital goiter. *J Clin Endocrinol Metab* 15, 1216-27.
- (15) Iglesias, A., Garcia-Nimo, L., Cocho de Juan, J. A., and Moreno, J. C. (2014) Towards the pre-clinical diagnosis of hypothyroidism caused by iodotyrosine deiodinase (DEHAL1) defects. *Best Pract Res Clin Endocrinol Metab* 28, 151-9.
- (16) Moreno, J. C. (2003) Identification of novel genes involved in congenital hypothyroidism using serial analysis of gene expression. *Horm Res* 60 Suppl 3, 96-102.
- (17) Gnidehou, S., Caillou, B., Talbot, M., Ohayon, R., Kaniewski, J., Noel-Hudson, M. S., Morand, S., Agnangji, D., Sezan, A., Courtin, F., Virion, A., and Dupuy, C. (2004) Iodotyrosine dehalogenase 1 (DEHAL1) is a

transmembrane protein involved in the recycling of iodide close to the thyroglobulin iodination site. *Faseb J* 18, 1574-6.

- (18) Gnidehou, S., Lacroix, L., Sezan, A., Ohayon, R., Noel-Hudson, M. S., Morand, S., Francon, J., Courtin, F., Virion, A., and Dupuy, C. (2006) Cloning and characterization of a novel isoform of iodotyrosine dehalogenase 1 (DEHAL1) DEHAL1C from human thyroid: comparisons with DEHAL1 and DEHAL1B. *Thyroid* 16, 715-24.
- (19) Moreno, J. C., Klootwijk, W., van Toor, H., Pinto, G., D'Alessandro, M., Leger, A., Goudie, D., Polak, M., Gruters, A., and Visser, T. J. (2008) Mutations in the iodotyrosine deiodinase gene and hypothyroidism. *N Engl J Med* 358, 1811-8.
- (20) Afink, G., Kulik, W., Overmars, H., de Randamie, J., Veenboer, T., van Cruchten, A., Craen, M., and Ris-Stalpers, C. (2008) Molecular characterization of iodotyrosine dehalogenase deficiency in patients with hypothyroidism. *J Clin Endocrinol Metab* 93, 4894-901.
- (21) Thienpont, L. M., Van Uytvanghe, K., Poppe, K., and Velkeniers, B. (2013) Determination of free thyroid hormones. *Best Pract Res Clin Endocrinol Metab* 27, 689-700.
- (22) Phatarphekar, A., Buss, J. M., and Rokita, S. E. (2014) Iodotyrosine deiodinase: a unique flavoprotein present in organisms of diverse phyla. *Mol Biosyst* 10, 86-92.

- (23) Mathi, A. A., Gaupale, T. C., Dupuy, C., Subhedar, N., and Bhargava, S. (2010) Expression pattern of iodotyrosine dehalogenase 1 (DEHAL1) during chick ontogeny. *Int J Dev Biol* 54, 1503-8.
- (24) de la Cruz, I. P., Ma, L., and Horvitz, H. R. (2014) The *Caenorhabditis elegans* iodotyrosine deiodinase ortholog SUP-18 functions through a conserved channel SC-box to regulate the muscle two-pore domain potassium channel SUP-9. *PLoS Genet* 10, e1004175.
- (25) Rosenberg, I. N., and Ahn, C. S. (1969) Enzymatic deiodination of diiodotyrosine; possible mediation by reduced flavin nucleotide. *Endocrinology* 84, 727-37.
- (26) Rosenberg, I. N., and Goswami, A. (1984) Iodotyrosine deiodinase from bovine thyroid. *Methods Enzymol* 107, 488-500.
- (27) Goswami, A., and Rosenberg, I. N. (1979) Characterization of a flavoprotein iodotyrosine deiodinase from bovine thyroid. Flavin nucleotide binding and oxidation-reduction properties. *J Biol Chem* 254, 12326-30.
- (28) Massey, V. (2000) The chemical and biological versatility of riboflavin. *Biochem Soc Trans* 28, 283-96.
- (29) Joosten, V., and van Berkel, W. J. (2007) Flavoenzymes. *Curr Opin Chem Biol* 11, 195-202.
- (30) Lienhart, W. D., Gudipati, V., and Macheroux, P. (2013) The human flavoproteome. *Arch Biochem Biophys* 535, 150-62.

- (31) Calvo, S. E., Tucker, E. J., Compton, A. G., Kirby, D. M., Crawford, G., Burt, N. P., Rivas, M., Guiducci, C., Bruno, D. L., Goldberger, O. A., Redman, M. C., Wiltshire, E., Wilson, C. J., Altshuler, D., Gabriel, S. B., Daly, M. J., Thorburn, D. R., and Mootha, V. K. (2010) High-throughput, pooled sequencing identifies mutations in NUBPL and FOXRED1 in human complex I deficiency. *Nat Genet* 42, 851-8.
- (32) Massey, V. (1991) *Flavins and Flavoproteins* Walter de Gruyter, Berlin.
- (33) Massey, V., and Palmer, G. (1966) On the existence of spectrally distinct classes of flavoprotein semiquinones. A new method for the quantitative production of flavoprotein semiquinones. *Biochemistry* 5, 3181-9.
- (34) Senda, T., Senda, M., Kimura, S., and Ishida, T. (2009) Redox control of protein conformation in flavoproteins. *Antioxid Redox Signal* 11, 1741-66.
- (35) Lennon, B. W., Williams, C. H., Jr., and Ludwig, M. L. (1999) Crystal structure of reduced thioredoxin reductase from *Escherichia coli*: structural flexibility in the isoalloxazine ring of the flavin adenine dinucleotide cofactor. *Protein Sci* 8, 2366-79.
- (36) Moonen, C. T., Vervoort, J., and Muller, F. (1984) Reinvestigation of the structure of oxidized and reduced flavin: carbon-13 and nitrogen-15 nuclear magnetic resonance study. *Biochemistry* 23, 4859-67.
- (37) Zhang, W., Zhang, M., Zhu, W., Zhou, Y., Wanduragala, S., Rewinkel, D., Tanner, J. J., and Becker, D. F. (2007) Redox-induced changes in flavin structure and roles of flavin N(5) and the ribityl 2'-OH group in regulating PutA--membrane binding. *Biochemistry* 46, 483-91.

- (38) Senda, M., Kishigami, S., Kimura, S., Fukuda, M., Ishida, T., and Senda, T. (2007) Molecular mechanism of the redox-dependent interaction between NADH-dependent ferredoxin reductase and Rieske-type [2Fe-2S] ferredoxin. *J Mol Biol* 373, 382-400.
- (39) Watt, W., Tulinsky, A., Swenson, R. P., and Watenpaugh, K. D. (1991) Comparison of the crystal structures of a flavodoxin in its three oxidation states at cryogenic temperatures. *J Mol Biol* 218, 195-208.
- (40) Zhou, Z., and Swenson, R. P. (1996) The cumulative electrostatic effect of aromatic stacking interactions and the negative electrostatic environment of the flavin mononucleotide binding site is a major determinant of the reduction potential for the flavodoxin from *Desulfovibrio vulgaris* [Hildenborough]. *Biochemistry* 35, 15980-8.
- (41) Warman, A. J., Roitel, O., Neeli, R., Girvan, H. M., Seward, H. E., Murray, S. A., McLean, K. J., Joyce, M. G., Toogood, H., Holt, R. A., Leys, D., Scrutton, N. S., and Munro, A. W. (2005) Flavocytochrome P450 BM3: an update on structure and mechanism of a biotechnologically important enzyme. *Biochem Soc Trans* 33, 747-53.
- (42) Neeli, R., Roitel, O., Scrutton, N. S., and Munro, A. W. (2005) Switching pyridine nucleotide specificity in P450 BM3: mechanistic analysis of the W1046H and W1046A enzymes. *J Biol Chem* 280, 17634-44.
- (43) Friedman, J. E., Watson, J. A., Jr., Lam, D. W., and Rokita, S. E. (2006) Iodotyrosine deiodinase is the first mammalian member of the NADH oxidase/flavin reductase superfamily. *J Biol Chem* 281, 2812-9.

- (44) Thomas, S. R., McTamney, P. M., Adler, J. M., Laronde-Leblanc, N., and Rokita, S. E. (2009) Crystal structure of iodotyrosine deiodinase, a novel flavoprotein responsible for iodide salvage in thyroid glands. *J Biol Chem* 284, 19659-67.
- (45) Phatarphekar, A., Buss, J. M., and Rokita, S. E. (2013) Iodotyrosine deiodinase: a unique flavoprotein present in organisms of diverse phyla. *Mol Biosyst* 10, 86-92.
- (46) Buss, J. M., McTamney, P. M., and Rokita, T. E. (2011) Expression of a soluble form of iodotyrosine deiodinase for active site characterization by engineering the native membrane protein from mus musculus. *Protein Sci* 21, 351-61.
- (47) Taga, M. E., Larsen, N. A., Howard-Jones, A. R., Walsh, C. T., and Walker, G. C. (2007) BluB cannibalizes flavin to form the lower ligand of vitamin B12. *Nature* 446, 449-53.
- (48) Hecht, H. J., Erdmann, H., Park, H. J., Sprinzl, M., and Schmid, R. D. (1995) Crystal structure of NADH oxidase from *Thermus thermophilus*. *Nat Struct Biol* 2, 1109-14.
- (49) Tanner, J. J., Lei, B., Tu, S. C., and Krause, K. L. (1996) Flavin reductase P: structure of a dimeric enzyme that reduces flavin. *Biochemistry* 35, 13531-9.
- (50) Roldan, M. D., Perez-Reinado, E., Castillo, F., and Moreno-Vivian, C. (2008) Reduction of polynitroaromatic compounds: the bacterial nitroreductases. *FEMS Microbiol Rev* 32, 474-500.

- (51) Warner, J. R., and Copley, S. D. (2007) Pre-steady-state kinetic studies of the reductive dehalogenation catalyzed by tetrachlorohydroquinone dehalogenase. *Biochemistry* 46, 13211-22.
- (52) Larsen, P. R. (1997) Update on the human iodothyronine selenodeiodinases, the enzymes regulating the activation and inactivation of thyroid hormone. *Biochem Soc Trans* 25, 588-92.
- (53) Kunishima, M., Friedman, J. E., and Rokita, S. E. (1999) Transition-state stabilization by a mammalian reductive dehalogenase. *J Am Chem Soc* 121, 4722-4723.
- (54) Watson, J. A., Jr., McTamney, P. M., Adler, J. M., and Rokita, S. E. (2008) Flavoprotein iodotyrosine deiodinase functions without cysteine residues. *Chembiochem* 9, 504-6.
- (55) Hilgarth, R. S., and Sarge, K. D. (2005) Detection of sumoylated proteins. *Methods Mol Biol* 301, 329-38.
- (56) Butt, T. R., Edavettal, S. C., Hall, J. P., and Mattern, M. R. (2005) SUMO fusion technology for difficult-to-express proteins. *Protein Expr Purif* 43, 1-9.
- (57) Lee, C. D., Sun, H. C., Hu, S. M., Chiu, C. F., Homhuan, A., Liang, S. M., Leng, C. H., and Wang, T. F. (2008) An improved SUMO fusion protein system for effective production of native proteins. *Protein Sci* 17, 1241-8.
- (58) Marblestone, J. G., Edavettal, S. C., Lim, Y., Lim, P., Zuo, X., and Butt, T. R. (2006) Comparison of SUMO fusion technology with traditional gene

- fusion systems: enhanced expression and solubility with SUMO. *Protein Sci* 15, 182-9.
- (59) Malakhov, M. P., Mattern, M. R., Malakhova, O. A., Drinker, M., Weeks, S. D., and Butt, T. R. (2004) SUMO fusions and SUMO-specific protease for efficient expression and purification of proteins. *J Struct Funct Genomics* 5, 75-86.
- (60) McTamney, P. M. (2009) in *Department of Chemistry and Biochemistry*, University of Maryland, College Park.
- (61) Janis, S., and Beibala, H. (1993) Anodic Voltammetry of phenol and benzenethiol derivatives.: Part 1. Influence of pH on electro-oxidation potentials of substituted phenols and evaluation of pKa from anodic voltammetry data. *J Electroanal Chem* 353, 57-69.
- (62) Green, W. L. (1968) Inhibition of thyroidal iodotyrosine deiodination by tyrosine analogues. *Endocrinology* 83, 336-47.
- (63) Ausubel, M. F., Brent, R., Kingston, E. R., Moore, D. D., Seidman, J. G., Smith, A. J., and Struhl, K. (2002) *Short protocols in molecular biology*, 5th. ed., Wiley.
- (64) Roskams, J., and Rodgers, L. (2002) *Lab Ref: A handbook of recips, reagents and other reference tools for use at the bench*, Cold Spring Laboratory Press, Cold Spring Harbor, NY.
- (65) Pace, C. N., Vajdos, F., Fee, L., Grimsley, G., and Gray, T. (1995) How to measure and predict the molar absorption coefficient of a protein. *Protein Sci* 4, 2411-23.

- (66) Koziol, J. (1971) Fluorometric analyses of riboflavin and its coenzymes. *Methods Enzymol.* 18, 235-285.
- (67) Munro, A. W., Kelly, S. M., and Price, N. C. (1999) Circular dichroism studies of flavoproteins. *Methods Mol Biol* 131, 111-23.
- (68) McTamney, P. M., and Rokita, S. E. (2009) A mammalian reductive deiodinase has broad power to dehalogenate chlorinated and brominated substrates. *J Am Chem Soc* 131, 14212-3.
- (69) Cook, P. F., and Cleland, W. W. (2007) *Enzyme kinetics and mechanism*, Garland Science, New York.
- (70) Gemmill, C. L. (1955) The apparent ionization constants of the phenolic hydroxyl groups of thyroxine and related compounds. *Arch Biochem Biophys* 54, 359-67.
- (71) Greenstein., J. P., and Winitz., M. (1961) *Chemistry of the amino acids*, John Wiley & Sons, New York.
- (72) Thorpe, C., and Kim, J. J. (1995) Structure and mechanism of action of the acyl-CoA dehydrogenases. *Faseb J* 9, 718-25.
- (73) Engst, S., Vock, P., Wang, M., Kim, J. J., and Ghisla, S. (1999) Mechanism of activation of acyl-CoA substrates by medium chain acyl-CoA dehydrogenase: interaction of the thioester carbonyl with the flavin adenine dinucleotide ribityl side chain. *Biochemistry* 38, 257-67.
- (74) Fagan., R. L., and Palfey., A. B. (2010) *Ch. 3 in comprehensive natural products II*, Elsevier, Oxford.

- (75) Chang, F. C., and Swenson, R. P. (1999) The midpoint potentials for the oxidized-semiquinone couple for Gly57 mutants of the *Clostridium beijerinckii* flavodoxin correlate with changes in the hydrogen-bonding interaction with the proton on N(5) of the reduced flavin mononucleotide cofactor as measured by NMR chemical shift temperature dependencies. *Biochemistry* 38, 7168-76.
- (76) Dwyer, T. M., Mortl, S., Kemter, K., Bacher, A., Fauq, A., and Frerman, F. E. (1999) The intraflavin hydrogen bond in human electron transfer flavoprotein modulates redox potentials and may participate in electron transfer. *Biochemistry* 38, 9735-45.
- (77) Zhou, Z., and Swenson, R. P. (1995) Electrostatic effects of surface acidic amino acid residues on the oxidation-reduction potentials of the flavodoxin from *Desulfovibrio vulgaris* (Hildenborough). *Biochemistry* 34, 3183-92.
- (78) Yang, K. Y., and Swenson, R. P. (2007) Modulation of the redox properties of the flavin cofactor through hydrogen-bonding interactions with the N(5) atom: role of alphaSer254 in the electron-transfer flavoprotein from the methylotrophic bacterium W3A1. *Biochemistry* 46, 2289-97.
- (79) Chapman, S. K., and Reid, G. A. (1999) *Flavoprotein protocols* Vol. 131, Human Press.

- (80) Anderson, R. F. (1983) Energetics of the one-electron reduction steps of riboflavin, FMN and FAD to their fully reduced forms. *Biochim Biophys Acta* 722, 158-62.
- (81) Fraaije, M. W., and Mattevi, A. (2000) Flavoenzymes: diverse catalysts with recurrent features. *Trends Biochem Sci* 25, 126-32.
- (82) Van den Heuvel, R. H., Fraaije, M. W., and van Berkel, W. J. (2002) Redox properties of vanillyl-alcohol oxidase. *Methods Enzymol* 353, 177-86.
- (83) Otwinowski, Z., and Minor, W. (1997) Processing of X-ray diffraction data collected in oscillation mode. *Methods Enzymol* 276, 307-26.
- (84) Adams, P. D., Afonine, P. V., Bunkoczi, G., Chen, V. B., Davis, I. W., Echols, N., Headd, J. J., Hung, L. W., Kapral, G. J., Grosse-Kunstleve, R. W., McCoy, A. J., Moriarty, N. W., Oeffner, R., Read, R. J., Richardson, D. C., Richardson, J. S., Terwilliger, T. C., and Zwart, P. H. (2010) PHENIX: a comprehensive Python-based system for macromolecular structure solution. *Acta Crystallogr D Biol Crystallogr* 66, 213-21.
- (85) Clark, W. M. (1960) *Oxidation-Reduction Potentials of Organic Systems*, Williams & Wilkins, Baltimore.
- (86) Mansoorabadi, S. O., Thibodeaux, C. J., and Liu, H. W. (2007) The diverse roles of flavin coenzymes--nature's most versatile thespians. *J Org Chem* 72, 6329-42.
- (87) Draper, R. D., and Ingraham, L. L. (1968) A potentiometric study of the flavin semiquinone equilibrium. *Arch Biochem Biophys* 125, 802-8.

- (88) Byron, C. M., Stankovich, M. T., Husain, M., and Davidson, V. L. (1989) Unusual redox properties of electron-transfer flavoprotein from *Methylophilus methylotrophus*. *Biochemistry* 28, 8582-7.
- (89) Van den Heuvel, R. H., Fraaije, M. W., Mattevi, A., and van Berkel, W. J. (2000) Asp-170 is crucial for the redox properties of vanillyl-alcohol oxidase. *J Biol Chem* 275, 14799-808.
- (90) Hamill, M. J., Jost, M., Wong, C., Bene, N. C., Drennan, C. L., and Elliott, S. J. (2012) Electrochemical characterization of *Escherichia coli* adaptive response protein AidB. *Int J Mol Sci* 13, 16899-915.
- (91) Geoghegan, S. M., Mayhew, S. G., Yalloway, G. N., and Butler, G. (2000) Cloning, sequencing and expression of the gene for flavodoxin from *Megasphaera elsdenii* and the effects of removing the protein negative charge that is closest to N(1) of the bound FMN. *Eur J Biochem* 267, 4434-44.
- (92) Becker, D. F., Zhu, W., and Moxley, M. A. (2011) Flavin redox switching of protein functions. *Antioxid Redox Signal* 14, 1079-91.
- (93) Xu, L., Mu, W., Ding, Y., Luo, Z., Han, Q., Bi, F., Wang, Y., and Song, Q. (2008) Active site of *Escherichia coli* DNA photolyase: Asn378 is crucial both for stabilizing the neutral flavin radical cofactor and for DNA repair. *Biochemistry* 47, 8736-43.
- (94) Pitsawong, W., Sucharitakul, J., Prongjit, M., Tan, T. C., Spadiut, O., Haltrich, D., Divne, C., and Chaiyen, P. (2010) A conserved active-site

- threonine is important for both sugar and flavin oxidations of pyranose 2-oxidase. *J Biol Chem* 285, 9697-705.
- (95) Parkinson, G. N., Skelly, J. V., and Neidle, S. (2000) Crystal structure of FMN-dependent nitroreductase from *Escherichia coli* B: a prodrug-activating enzyme. *J Med Chem* 43, 3624-31.
- (96) Koike, H., Sasaki, H., Kobori, T., Zenno, S., Saigo, K., Murphy, M. E., Adman, E. T., and Tanokura, M. (1998) 1.8 Å crystal structure of the major NAD(P)H:FMN oxidoreductase of a bioluminescent bacterium, *Vibrio fischeri*: overall structure, cofactor and substrate-analog binding, and comparison with related flavoproteins. *J Mol Biol* 280, 259-73.
- (97) Kobori, T., Sasaki, H., Lee, W. C., Zenno, S., Saigo, K., Murphy, M. E., and Tanokura, M. (2001) Structure and site-directed mutagenesis of a flavoprotein from *Escherichia coli* that reduces nitrocompounds: alteration of pyridine nucleotide binding by a single amino acid substitution. *J Biol Chem* 276, 2816-23.
- (98) Martinez-Julvez, M., Rojas, A. L., Olekhovich, I., Espinosa Angarica, V., Hoffman, P. S., and Sancho, J. (2012) Structure of RdxA--an oxygen-insensitive nitroreductase essential for metronidazole activation in *Helicobacter pylori*. *Febs J* 279, 4306-17.
- (99) McCoy, A. J., Grosse-Kunstleve, R. W., Adams, P. D., Winn, M. D., Storoni, L. C., and Read, R. J. (2007) Phaser crystallographic software. *J Appl Crystallogr* 40, 658-674.

- (100) Emsley, P., and Cowtan, K. (2004) Coot: model-building tools for molecular graphics. *Acta Crystallogr D Biol Crystallogr* 60, 2126-32.
- (101) Hall, L. H., Bowers, M. L., and Durfor, C. N. (1987) Further consideration of flavin coenzyme biochemistry afforded by geometry-optimized molecular orbital calculations. *Biochemistry* 26, 7401-9.
- (102) Cuello, A. O., McIntosh, C. M., and Rotello, V. M. (2000) Model systems for flavoenzyme activity. The role of N(3)H hydrogen bonding in flavin redox processes. *J Am Chem Soc* 122, 3517-21.
- (103) Bradley, L. H., and Swenson, R. P. (2001) Role of hydrogen bonding interactions to N(3)H of the flavin mononucleotide cofactor in the modulation of the redox potentials of the *Clostridium beijerinckii* flavodoxin. *Biochemistry* 40, 8686-95.
- (104) Buss, J. M., McTamney, P. M., and Rokita, S. E. (2012) Expression of a soluble form of iodotyrosine deiodinase for active site characterization by engineering the native membrane protein from *Mus musculus*. *Protein Sci* 21, 351-61.
- (105) Moldoveanu, S. C., and David, V. (2002) *Sample preparation in chromatography*, Vol. 65, Elsevier Science.